VOLTAGE AND FREQUENCY CONTROL OF A STAND-ALONE SYNCHRONOUS GENERATOR USING PLC

2021
MASTER THESIS
ELECTRICAL&ELECTRONICS ENGINEERING

MASOUD MOHAMED MASOUD ELHAWAT

Thesis Advisor
Assist.Prof.Dr. Hüseyin ALTINKAYA

VOLTAGE AND FREQUENCY CONTROL OF A STAND-ALONE SYNCHRONOUS GENERATOR USING PLC

Masoud Mohamed Masoud ELHAWAT

T.C.

Karabuk University

Institute of Graduate Programs

Department of Electrical&Electronics Engineering

Prepared as

Master Thesis

Thesis Advisor

Assist.Prof.Dr. Hüseyin ALTINKAYA

KARABUK

June 2021

I certify that in my opinion the thesis submitted by Masoud Mohamed Masoud ELHAWAT titled "VOLTAGE AND FREQUENCY CONTROL OF A STAND-ALONE SYNCHRONOUS GENERATOR USING PLC" is fully adequate in scope and in quality as a thesis for the degree of Master of Science.

Assist.Prof.Dr. Hüseyin ALTINKAYA .....
Thesis Advisor, Department of Electrical&Electronics Engineering

This thesis is accepted by the examining committee with a unanimous vote in the Department of Electrical&Electronics Engineering as a Master of Science thesis. June 25, 2021

Examining Committee Members (Institutions)	Signature
Chairman : Assoc.Prof.Dr. Selim ÖNCÜ (KBU)	.....
Member : Assist.Prof.Dr. Hüseyin ALTINKAYA (KBU)	.....
Member : Assist.Prof.Dr. Adem DALCALI (BANU)	.....

The degree of Master of Science by the thesis submitted is approved by the Administrative Board of the Institute of Graduate Programs, Karabuk University.

Prof. Dr. Hasan SOLMAZ .....
Director of the Institute of Graduate Programs

"I declare that all the information within this thesis has been gathered and presented in accordance with academic regulations and ethical principles and I have according to the requirements of these regulations and principles cited all those which do not originate in this work as well."

Masoud Mohamed Masoud ELHAWAT

ABSTRACT

M. Sc. Thesis

VOLTAGE AND FREQUENCY CONTROL OF A STAND-ALONE SYNCHRONOUS GENERATOR USING PLC

Masoud Mohamed Masoud ELHAWAT
Karabük University
Institute of Graduate Programs
The Department of Electrical and Electronics Engineering

Thesis Advisor:
Assist. Prof. Dr. Hüseyin ALTINKAYA
June 2021, 85 pages

In hydroelectric and thermal type power plants, mechanical energy is converted into electrical energy using synchronous generators. One of the most important issues for both the large and medium sized synchronous generators in such power plants, and the smaller synchronous generators found in diesel or gasoline powered generator sets is to keep the frequency and voltage constant according to the changing load because it is very important to keep the voltage and frequency constant for stabilization of the grid. In this thesis, an automatic speed and voltage control of a 1 kW standalone synchronous generator was aimed to be conducted in accordance with the changing load conditions and therefore, an experimental setup was prepared. The experimental setup consists of a synchronous generator, an asynchronous (induction) motor, a frequency converter driving this asynchronous motor, load groups and other equipment necessary for the control of the system. The system is controlled using PLC (Programmable Logic Controller) and it is possible to control and monitor the system

through a designed SCADA screen. PID and PI controller methods were performed individually for frequency and voltage control in different load conditions and the results obtained from these two methods were compared with each other accordingly.

Key Words : Stand alone SG, PLC, SCADA, PID.

Science Code : 90514, 90526

ÖZET

Yüksek Lisans Tezi

TEK BAŞINA ÇALIŞAN BİR SENKRON GENERATÖRÜN PLC İLE GERİLİM VE FREKANS KONTROLÜ

Masoud Mohamed Masoud ELHAWAT

Karabük Üniversitesi
Lisansüstü Eğitim Enstitüsü
Elektrik-Elektronik Mühendisliği Anabilim Dalı

Tez Danışmanı:
Dr. Öğr. Üyesi Hüseyin ALTINKAYA
Haziran 2021, 85 sayfa

Hidroelektrik, termik vb. tip enerji santrallerinde, mekanik enerji elektrik enerjisine senkron generatörler ile dönüştürlür. Hem bu tür enerji santrallerinde bulunan büyük ve orta büyüklükteki senkron generatörler hem de dizel veya benzin ile çalışan generatör setlerinde bulunan daha küçük güçlerdeki senkron generatörler için en önemli konulardan biri değişen yük durumlarına göre frekans (devir sayısı) ve gerilimin sabit tutulmasıdır. Çünkü şebeke stabilizasyonu için gerilim ve frekansın sabit tutulması çok önemlidir. Bu tezde 1 kW tek başına çalışan bir senkron generatörün değişen yük durumlarına göre otomatik olarak hız ve gerilim kontrolü yapılmıştır. Bunun için bir deney düzeneği hazırlanmıştır. Deney düzeneği bir senkron generator, bir asenkron motor, bu asenkron motoru süren bir frekans konvertöründen, yük gruplarından ve sistemin kontrolu için gerekli diğer ekipmanlardan oluşmaktadır. Sistemin kontrolü PLC (Programmable Logic Controller) ile yapılmıştır. Oluşturulan

SCADA ekranı üzerinden sistemin kontrolü ve izlenmesi yapılabilmektedir. Farklı yük durumlarıda frekans ve gerilim kontrolü için PID ve PI kontrolör yöntemleri ayrı ayrı uygulanmış ve bu iki yöntemden elde edilen sonuçlar birbiriyle kıyaslanmıştır.

Anahtar Kelimeler : Tek başına çalışan SG, PLC, SCADA, PID.
Bilim Kodu **:** 90514, 90526

ACKNOWLEDGMENT

I sincerely thank and acknowledge the support of my supervisor Assist.Prof.Dr. Hüseyin ALTINKAYA. I am deeply indebted to him for his kind guideline during the accomplishment of my thesis. I appreciate his valuable knowledge, his keenness about the research process, and willingness to support.

I acknowledge the efforts of my parents, brothers, sisters and my friends offer my sincerest love to my family especially to My Mother and My wife who has always been with me with their moral support throughout my academic studies. They really have endless contributions to my education and career.

I recognize the efforts of the university employees, support staff, and my coursemates. I am also thankful to the university administration, the Turkish Government, and the people for their kindness and cooperation.

CONTENTS

Page

Page

Page

LIST OF FIGURES

Page

Page

Page

LIST OF TABLES

Page

SYMBOLS AND ABBREVIATIONS INDEX

SYMBOLS

B_{net} : net magnetic field

B_R *:* rotor magnetic field

B_S *:* stator magnetic field

E_A : internally generator voltage

E_{stat} : stator voltage

f_e : electrical frequency(Hz)

I_A *:* load current

L_A *:* coile self-inductance

n_m *:* revolution per minute (r/min)

P : pole number

R_A : coil resistance

U : terminal voltage

VØ : output voltage of per phase

X_S : armature reactance

Φ *:* magnetic flux

ω *:* rotor speed

ABBREVIATIONS

AI : Analog Input

AO : Analog Output

CT : Current Transformer

DI : Digital Input

DO : Digital Output

FC : Frequency Converter

IM : Induction Motor

PID : Proportional Integral Derivative

PLC : Programmable Logic Controller

SCADA : Supervisory Control and Data Acquisition

SG : Synchronous Generator

CHAPTER 1

INTRODUCTION

Frequency and voltage are two of the most important parameters used in determining the reliability of electrical networks. In order for a network to be considered reliable, frequency and voltage need to be kept constant under different operating conditions (between certain limits).

Synchronous generators (SGs) are electrical machines that convert mechanical energy into electrical energy. The mechanical energy obtained in the water turbine of a hydroelectric power plant by using water, the mechanical energy obtained in the steam turbine using coal, natural gas etc. in a thermal power plant and the mechanical energy obtained using gasoline or diesel in generator sets is converted into electricity by a SG mechanically connected to these turbines or the motor. The power of SGs can range from a few kVA to several thousand MVA.

The frequency can be adjusted by changing the mechanical power supplied to the synchronous generator. As the mechanical power supplied to the synchronous generator increases, the speed increases, and similarly, as the mechanical power decreases, the speed decreases. If the mechanical power of a SG working synchronously with other synchronous generators (connected in parallel) is increased, the active power rate which is to be obtained will increase (it takes more active load on it). On the other hand, the terminal voltage of the SGs is adjusted by changing the excitation current. As the excitation current increases, the voltage increases, and as the excitation current decreases, the voltage decreases. If the excitation current of a SG working in synchronization (connected in parallel) with other synchronous generators is increased, the rate of reactive power to be obtained will increase accordingly.

The governor that adjusts the mechanical power given to the SGs and the AVR

(Automatic Voltage Regulator) that adjusts the voltage play a vital role in power stability. Governor and AVR systems are closed loop systems that keep the frequency and voltage of synchronous generators within certain limits. Taking into account the steady and transient states of frequency and terminal voltage, various controller architectures have been proposed so far. Although several new algorithms have been proposed to control the frequency and terminal voltage of the synchronous generator, conventional PID based governor and AVR systems are widely used in industrial systems due to their simple structure and easy application.

Since SGs are structurally non-linear, complex and time varying dynamic systems, artificial intelligence-based studies are carried out in addition to conventional PID. In the literature, there are many different algorithms such as fuzzy-PID, ANN, GA etc. which have been studied and suggestions have been made in order to get better results than classical PID.

In this thesis, the frequency and voltage of a 1 kW SG have been controlled using PID and PI controller types for different load conditions.

A summary of the literature has been presented in Chapter 2. In Chapter 3, concise and precise information regarding SGs has been provided. In Chapter 4, the experimental setup was explained in detail and the results of the experiments were interpreted and the conclusions and suggestions have been given in Chapter 5 respectively.

CHAPTER 2

LITERATURE REVIEW

The conventional fossil energy stocks are on the verge of depletion and are unable to meet the utmost needs of sustainable development of the human society. The pros of distributed generation based on renewable energy resources can be described as pollution-free, flexible and widely distributed. The distributed generation is a suitable form of generation that conforms to the known concept of sustainable development [1].

The distributed generations (DGs) consisting of photovoltaic systems have no rotary part for the inertial response, and these can easily participate in frequency support using virtual inertia through inverters. However, SG can provide the frequency support in case of disturbances using its rotary mass in conventional power generating units. On the other hand, the DGs that are interfaced electronically with power system or grid, show different characteristics when compared with the conventional power generating units. In these electronically interfaced DGs, the generated power at the primary side can be regulated using inverters, however, they cannot supply the required damping and inertia to the power grid [2].

As a result, improvements in the system stability cannot be expected from electronically interfaced DGs. The solution to solve this problem can be developed using appropriate control techniques for the grids that are connected to the inverter and also controlling the switching pattern in order to make it work as a synchronous SG through mimicking the SG behavior. The inverters that are connected to the grid, thus mimicking the transient and the steady-state characteristics of SG, are called virtual synchronous generators (VSGs). It has been predicted that integrated systems with VSG will be at some point the inevitable element of power system networks [3].

The basic idea of VSG with different approaches is presented, which can make the grid connected to the inverter to mimic the operating characteristics of SG. Moreover, the operational characteristics of conventional SG and VSG can also be compared [4].

The use of voltage-controlled techniques in VSG can simulate system frequency modulation and the rotor inertia characteristics of SGs during frequency control in order to improve the system's frequency stability. Simultaneously, reactive voltage relationship is considered to carrying out the function of controlling the stability of voltage output during voltage control [5].

The voltage frequency controller and power controller can make VSG perform the functions of frequency modulation as well as power control [6].

The concerns related to energy challenges and global warming has accelerated the fame and popularity of renewable energy resources namely solar energy, wind energy etc. When some specific characteristics of RES such as prime mover intermittency, voltage level, and lack of intrinsic inertia are considered, some stability challenges might be caused [7].

In a study conducted on VSG, small signal modeling as well as parameter design for VSG was proposed. In order to have proper reactive power that is to be shared in, the virtual impedance was recommended to be added to the structure of VSG. VSG with a multi-loop structure was proposed which included a pre-synchronization unit that was to be activated prior to connecting VSG in order to have a smooth transition between grid connection [8].

In another study, the parameters of VSG were optimized using Particle Swarm Optimization (PSO) by evaluating the stability region of conventional synchroverters. To adjust the damping coefficient values and inertia and consequently have fewer oscillations in frequency characteristic, a control strategy which was adaptive in nature was proposed. When compared to conventional VSG, fuzzy secondary controller present in the VSG structure has an aim of improving the dynamic performance of VSG. The local VSG control is proposed so that the multi-terminal HVDC systems are enabled in order to attenuate the power oscillations in the system [9].

There are some approaches being implemented in different fields. The ANN approach being one of them is implemented in industries or even in medical fields. For modelling linear, nonlinear and practical systems, different neural network types have been implemented successfully so far. The technique namely long short-term memory, derived from neural networks that are known to be recurrent, is used for nonlinear system modelling. A comparative study has already proven this technique's superiority over other techniques by implementing it in two nonlinear systems which were completely different [10].

The system can also be modelled using incremental neural activity that is based on some radial based neural network. In this system, local field potential is applied in order to measure hidden layer's neural activity. The main objective in the utilization of neural activity function can be described as to speed up the conversion process, thus improving generalization process [11].

In another study, the load cells were absent and artificial neural network was applied in the prediction of static load of wing rib. Based on the approach of finite element, the wing rib was first modelled and then calibrated using real collected experimental data. The data and a random strain were acquired using static load variables to perform this process [12].

Fuzzy system and modified neural network approaches have been used in the classification of blood pressure diagnosis and hypertension risk. Different learning strategies and structures determine the learning method and suitable structure in neural networks, whereas, fuzzy inference systems detect the ideal membership function for case study. This can be granted as an indication of advantages in getting good performance through the application of hybrid intelligent systems in order to solve the complex problems, in achieving excellent learning in each case for the neural network, and in the signification of uncertainty caused by fuzzy system [13].

The model designed can utilize the raw mixed frequency data directly without requiring the involvement of latent processes in order to execute data before feeding them to the neural network. The obtained results from such a system show the system's ability for handling the broad application prospect and the mixed frequency data [14].

The approach known to be sparse representation was implemented to develop an algorithm for neural network feedforward training process. The afore-mentioned algorithm has the advantage of training the initial network and optimizing the network structure simultaneously [15].

Thanks to the improvements and developments made in control system and power electronics, PMSG has recently been able to attract the attention of wind turbine (WT) manufactures. Comparatively, variable speed wind turbines provide more effective power than constant speed wind turbines. Hence, the wind turbines are modified so to operate at variable speed and the control system is enhanced in order to cope with the available maximum power being supplied from the WT. Furthermore, the supply of required voltage and fixed frequency for the grid is carried out by the control system. Therefore, PMSG can be used for controllability and high efficiency in WT systems with variable speed. The PMSG are connected to electrical grid using GSC systems but for electrical grids, these electronic converters may cause some sort of harmonic distortion [16].

Owing to the advancement of power electronics and control systems, permanent magnet synchronous generators have recently been able to attract the attention of wind turbine manufactures. In the study, machine side converter and grid side converter were proposed for PMSG that is based on 3 level NPC thus using fuzzy PI. According to the study, the DC link neutral point control system might be applied more easily as compared to two level control systems. Considering the results obtained from Matlab/Simulink, it was seen that the DC link's voltage balance is controlled well enough during the variable speed of PMSG. In this study, the performance of PMSG system is investigated in detail under varying load condition effects. The PMSG performances were analyzed using MSC and GSC which are based on 3 level NPC that uses fuzzy PI. For the NPC topology, the electrical grid voltage known to be THD is calculated to be 1.45% approximately. This is verified by performed analysis indicating that the proposed model may be operated stably using varying load conditions [17].

Voltage stability has been investigated and studied for many years, as this is a vital problem concerning power system which has greatly affected the reliability and stability of the power systems. The active power demand and the frequency value may

be regulated depending on transient and steady states by altering force input (mechanical) of synchronous generators. While by altering the excitation current, the amount of reactive power generator and terminal voltage supplied to the grid may be controlled. Depending on this, the excitation system of synchronous generators has a crucial role to be played on stability of the power system. In order to control and keep the synchronous generators' terminal voltage between defined limit ranges, a closed loop control system known to be AVR is designed. So far, various controller structures have been introduced in the studies conducted to date, which rely on transient and steady-state characteristics of the terminal voltage [18].

In addition to studies conducted using classical methods for the determination of AVR parameter values, there are numerous optimization algorithms designed in the literature based on artificial intelligence [19].

In the above-mentioned study, AVR structure based on artificial neural networks has been proposed in order to solve the problem of voltage stability in a power system. The values of excitation current were estimated using AVR system based on ANN for 3 learning algorithms which were totally different by maintaining the terminal voltage at a desired set point value. Lastly, the results that were obtained using 3 completely different learning algorithms were evaluated to examine the learning algorithm effects on the performance of artificial neural network.

It was concluded that considering the average results, the best learning method was Levenberg- Marquardt method giving a value very close to the average of R2.

The relationship between the data was found to be very high. The RMSE and MSE averages have shown it to be much lower as compared to other learning methods. Referring to those results, it may be confirmed that the Levenberg-Marquardt learning method elaborated and used in the study was the best learning method. In contrast, the learning method known to be Variable Learning Rate Backpropagation was found to be the worst learning method in the list. Meanwhile, the RMSE and MSE averages were found to be significantly higher as compared to other learning methods in the list. Hence, it was concluded that a change in the excitation current could affect synchronous generator's output voltage greatly [20].

In a study, the auto-tuning proportional-integral controller is used to control the speed of a switched reluctance motor. The control algorithm is executed by the programmable logic controller. The proportional integral gains are determined via fuzzy logic. The fuzzy proportional integral control algorithm is compared with the conventional proportional integral controller. With the proposed method, the engine reached the reference speed value in a short time and the overshoots were eliminated in variable conditions such as different load and different speed conditions [21].

In a study by Hadziselimovic et al., a novel construction of synchronous generator was designed in order to be used in free-piston. In their study, short displacement in linear movement and high oscillation frequency presented a challenge for their design on linear oscillatory generator, and they proposed a modular linear construction of synchronous generator [22].

In their study, Shengji et al. proposed a fuzzy-PID control algorithm which was based on fuzzy model, thus obtained by combining conventional PID control law with fuzzy theory. They modified the PID control parameters and used the fuzzy interface for converting the fuzzy set to a more precise output value and the comparison was made through MATLAB simulation example [23].

Hirase et al. proposed a control approach towards an appropriate solution for the implementation of renewable energy into already existing power grids. Their results of analysis were verified through experiments and simulations [24].

In a paper presented by Geraldi et al., a new method was proposed to estimate the parameters of SG by using measurements which were taken during operating conditions. The new method introduced was based on combination of UKF (Unscented Kalman Filter) application with TST (Trajectory Sensitivity techniques) [25].

The study conducted by Huda et al. aimed to determine the changes in electricity and the excitation current in three phase synchronous generators. According to the results,

the output voltage of synchronous generators were highly influenced by current excitation values [26].

Sudjoko conducted a study based on a system consisting of a buck converter controlling the dc excitation voltage via adjustments in duty cycle. The simulation results were obtained accordingly and showed generator output voltage to be 387V and buck converter to be 84.5V [27].

In a study, Munoz-Aguilar et al. presented a sliding mode controller to be used in stator voltage amplitude of synchronous generator's wound rotor. They obtained a standard model of electrical machine that was connected to inductive load which was isolated [28].

The concept proposed by Sophia et al. in their paper represented frequency control using PID controller, fuzzy logic controller, conventional PID and fuzzy PI controller. They carried out the simulation studies using SIMULINK [29].

In a study by Sanampudi et al., ELC (Electronic Load Controller) was modelled with SG by using a uncontrolled three-phase bridge rectifier along with IGBT chopper used as switch in MATLAB Simulink in order to control the voltage in hydro-power plants [30].

In a paper presented by Silva et al., the participation of virtual inertia during wind generation was proposed in load frequency control and oscillation damping in inter-connected lines. Their approach proposed a high penetration of WFPP (Wind Farm Power Plant) which was connected to a large hydro generation area [31].

In their study, Wang et al. proposed a voltage regulation method which was implemented in their simulation over a specified speed range varying between 10.000 to 24.000 rpm and their results showed that the system could respond in no time as well as remain stable during sudden changes in the load [32].

In a study by Fogli et al., the control, design and modelling steps of static conversion structure, which was used as interface, was presented in order to integrate diesel generator into second distribution network. A boost converter was used in their system to increase DC voltage level [33].

Park et al. proposed the output voltage control of SG for the ships through digital AVR. At generator terminal, field current of SG was controlled using digital AVR to have a constant output voltage [34].

The study conducted by Mocanu et al. presented voltage control strategy using three-phase inverter that was connected to PMSG (Permanent Magnet Synchronous Generator) for a DC load [35].

The paper by ShangGuan et al. proposed an approach- based on a switching system- to a multi-area power system which was resilient to some denial-of-service attacks (DoS). After modelling load frequency control under the DoS attacks in terms of switching subsystems which were based on DoS attack duration, the stability criterion for frequency and duration of DoS attacks was achieved [36].

In a study conducted by Kassem, an adaptive control was presented for frequency and voltage regulation of wind-diesel stand-alone hybrid power system which was based on a linear MPC (model predictive control) [37].

In their study, Chang et al. developed a permanent magnet generator having a power of 4.5 kW in order to convert AC output to DC micro-grid. The proposed generator was driven by a permanent-magnet motor so that the wind turbine might be simulated [38].

In a study performed by Bevrani, an updated review for one of the most important stability concerns regarding frequency was provided, and they applied some modern control strategies, as well as existing challenges for integrating renewable energy sources. They also discussed the recent achievements, current trends and the new upcoming research directions [39].

CHAPTER 3

SYNCHRONOUS GENERATORS

A synchronous generator can be defined as an electrical machine that produces alternating or changing electromotive force or voltage having a constant frequency. Depending on the supplied power, the generated AC voltages can be either in single phase or in 3-phase. The single-phase generators are found to be preferable for the low power applications.

3.1. CONSTRUCTION OF SGs

The rotor winding in a synchronous generator is supplied with a DC current that produces rotor magnetic field. Then a prime mover turns the rotor of the synchronous generator, thus producing a rotating magnetic field inside the machine. After the production of a rotating magnetic field, a three-phase voltage set is induced within stator windings of synchronous generator.

There are two terms which are commonly used to describe a machine’s windings namely armature windings and field windings. Generally, the term "armature windings" refers to windings in which main voltage is induced, whereas the term "field windings" refers to windings in which magnetic field is produced in the machine. As the field windings are located on the rotor for synchronous machines, the terms "field windings" and "rotor windings" can be used interchangeably. In the same way, the terms "armature windings" and "stator windings" can be used interchangeably.

The rotor inside synchronous generator can be described as a comparatively large electromagnet. The poles of the magnet can be of two type of construction namely; salient construction or non-salient construction.

A prominent difference between two types of magnetic pole rotors is that the non-salient-pole rotors are generally used for two-pole and for four-pole rotors; however, the salient-pole rotors are used for four-pole rotors or more. Since the rotors of generators are subjected to continuously fluctuating magnetic fields, thin laminations are used in their constructions in order to reduce the losses caused by eddy current.

The field circuit present on the rotor must have a dc current supply. Because there is a rotating rotor, a special type of arrangement is needed to receive the DC power to rotor's respective field windings.

The DC current applied to the rotor windings is supplied using different ways; however, there are two common approaches that can be used to supply it to field circuits present on the rotating rotor efficiently. Two common approaches used in order to supply the afore-mentioned DC power have been mentioned below:

- Using slip rings and brushes, the DC power from an external DC source can be supplied to the rotor.
- DC power can be supplied using a special DC power source that is mounted on the synchronous generator's shaft directly.

3.2. WORKING PRINCIPLE OF SGs

Some basic principles which are involved in the functioning of synchronous generators and the details regarding the components used in the proper functioning of these generators have been discussed below [40,41];

- Synchronous machines can be described as AC machines with a field circuit that is supplied by some external DC source.
- The DC current in synchronous generators is applied to rotor winding thus producing magnetic field in the rotor known as Rotor Magnetic Field. With the applied DC current, a rotating phenomenon is observed in the rotor that induces 3-phase voltage in stator winding.

- The 3-phase stator currents in the synchronous motors produce magnetic field thus causing it to align with the rotor magnetic field.
- The windings which produce the main magnetic field i.e. in the rotor windings are known as Field windings. Whereas, the windings in which main voltage is induced are known as Armature windings i.e. stator windings.
- The rotor in the synchronous machine is known to be a large electromagnet whose magnetic poles' construction can be rendered as either salient, which means protruding out of the rotor surface, or non-salient.

The rotor of synchronous generator consists of electromagnet where direct current is known to be supplied. The magnetic field of the rotor points towards the direction of rotation of rotor. In the machine, the rate of rotation under magnetic fields is related to electrical frequency of stator. The equation can be written as follows;

$$f_e = \frac{n_m P}{120} \tag{3.1}$$

Where, f_e is electrical frequency (Hz), n_m is magnetic field mechanical speed, P is pole number.

As the rotor and the magnetic field rotate at the same speed, the above-mentioned equation shows the relationship between the rotor rotation speed to the electrical frequency denoted as f_e. Since electrical power is generated at a frequency of 50 or 60 Hz, the generator turns at a constant speed thus depending on the number of poles, denoted as P, on the machine.

3.3. TYPES OF SYNCHRONOUS GENERATORS

3.3.1. According to Shape of Poles

Based on the shape of poles used in the synchronous machines, SGs can be classified as follows;

3.3.1.1. Synchronous Machines with Salient Pole Rotor

Salient synchronous machines are rotated in water turbines or low speed diesel machines. Pole heads are made up of metal sheets with insulated surfaces. The pole legs can be made up of cast iron.

The windings in the rotor are connected among themselves in order to form N-S-N-S poles. Salient pole alternators are made multipole. Their rotor diameters are quite large and rotor lengths are small. These alternators are not used at high speed because the centrifugal effect, great noise and wind losses caused by the construction of the rotor cannot be avoided. Rotor mounting patterns can also be varied. Umbrella type vertical axis mounting pattern for alternators that obtain their mechanical energy from Kaplan turbines, Francis turbine driven alternators designed in vertical axis, and Pelton turbines driven alternators designed in horizontal axis are the mounting patterns used.

3.3.1.2. Synchronous Machines with Cylindrical Pole Rotor

Cylindrical pole synchronous machines are used in high speed turbines (steam turbines). In general, cylindrical inductors are long and have smaller diameters. Such alternators are also called turbo alternators. In cylindrical inductors, the pole windings are placed in grooves which are opened parallel to the shaft. The pole winding ends are connected to the collars on the rotor shaft. Wind losses in such alternators are very low. They are made up of 2 or 4 poles and work horizontally. The field windings in the rotor of the round pole synchronous machines are not wound on the poles as in salient pole rotors but placed in the empty spaces. The ends are connected to the rings on the rotor. In large powerful machines, the conductors are copper blades bent in a unique way, thus, providing better cooling and mechanical durability.

The main advantages of having the stator in the stationary part are as follows:

- Not using brushes for the external circuit of the voltage
- Easier to isolate the windings in the stationary part
- No centrifugal effect in the windings

- Easier cooling of the windings

Therefore, making large powerful synchronous generators with stationary armature and rotating inductor have many advantages.

3.3.2. According to Excitation Systems

The loads of the alternators feeding the networks are not the same at all times of the day. On the other hand, while the terminal voltages of alternators decrease in loaded operating conditions (especially in inductive load), there are increases in the terminal voltage of the alternator which is unloaded. However, a constant voltage is always desired in electrical networks, not a variable voltage according to the load. This is achieved by adjusting the terminal voltages of the alternators according to different load conditions. The voltage in alternators can be described as follows;

- Number of revolutions (rpm)
- Depends on variables such as magnetic flux in poles

Since the change in the number of revolutions also changes the frequency (F=P.n/120), the magnetic flux (Φ) in the poles must be changed for voltage adjustment. Hence, it is sufficient to change the excitation current.
The excitation of the alternator is carried out with direct current.

The excitation current of alternators is mainly provided in three ways as free excitation, special excitation and self-excitation.

3.3.2.1. Free Excitation

The excitation machine is completely isolated from the main machine. There is only an electrical connection between them. In free excitation, the energy is supplied using an accumulator battery or a direct current dynamo. With this energy, other machines in the power plant can be excited.

3.3.2.2. Special Excitation

In this system, an excitation dynamo is placed on the shaft of the synchronous machine. Thus, the required excitation current is provided. The power of the dynamo providing the excitation current is at most 5% of the power of the synchronous machine. For example, 10-12.5 kW excitation dynamo is sufficient for a 250 kVA alternator. In some alternators, 2 dynamos are used for good voltage adjustment and stable operation. The second one is used for stimulating the poles of the excitation dynamo.

3.3.2.3. Self Excitation

Recently, self-excitation has been used a lot in synchronous machines. They use the residual magnetic field of the alternator, just like in self-excited dynamos. The alternating voltage produced by the alternator is rectified by the rectifiers and the poles are excited.

The main reason behind the coupling of excitation dynamo to the alternator shaft is to ensure that the required excitation power is always available. For instance; in a short circuit in the network, the alternator output voltage drops strongly. In order to increase the voltage to its normal value, a large direct current power must be applied to the poles of the alternator by the dynamo [40,41].

3.4. MEASURING SYNCHRONOUS GENERATOR PARAMETERS

Some short-circuit and open-circuit tests need to be conducted in order to obtain characteristics of magnetization as well as the generator's synchronous reactance.

- Open-circuit test: All the loads are disconnected first and the generator is run at rated speed. Then, the terminal voltage needs to be measured when the field current varies.
- Short-circuit test: The Armature terminals need to be shorted and generator is run at a rated speed. The armature current needs to be measured when the field current varies.

- In order to obtain the armature resistance, DC voltage test is required to be conducted.

3.5. PARALLEL OPERATION

In synchronous generators, the parallel operations can be carried out with the following requirements:

- SGs must have similar or even same voltage magnitude.
- SGs frequencies should be equal. Frequency of oncoming generator needs to be higher as compared to the running generator's frequency.
- Phase angles to be calculated from two phases must be same.
- The phase sequences of generators to be used must be same.
- Waveforms of SGs must be same.

3.6. EQUIVALENT CIRCUIT OF A SG

The induced voltage E_A can be defined as the internally generated voltage observed in one phase of SG. But, this voltage is not generally the voltage which is seen at the terminal ends of generator. Actually, the internal voltage E_A can only be the same as output voltage (V_Φ) of a phase when no armature current is flowing in generator. The questions that arise here is why the output voltage (V_Φ) and input voltage (E_A) are not equal, and how can the relationship between them be explained? The responses to such questions may yield the synchronous generator model.

A number of factors causing the difference between E_A and V_Φ are presented as follows:

- Air-gap magnetic field distortion produced by stator current, called as the armature reaction
- Armature coils' self-inductance
- Armature coils' resistances
- Rotor shapes' effect of salient-pole rotors

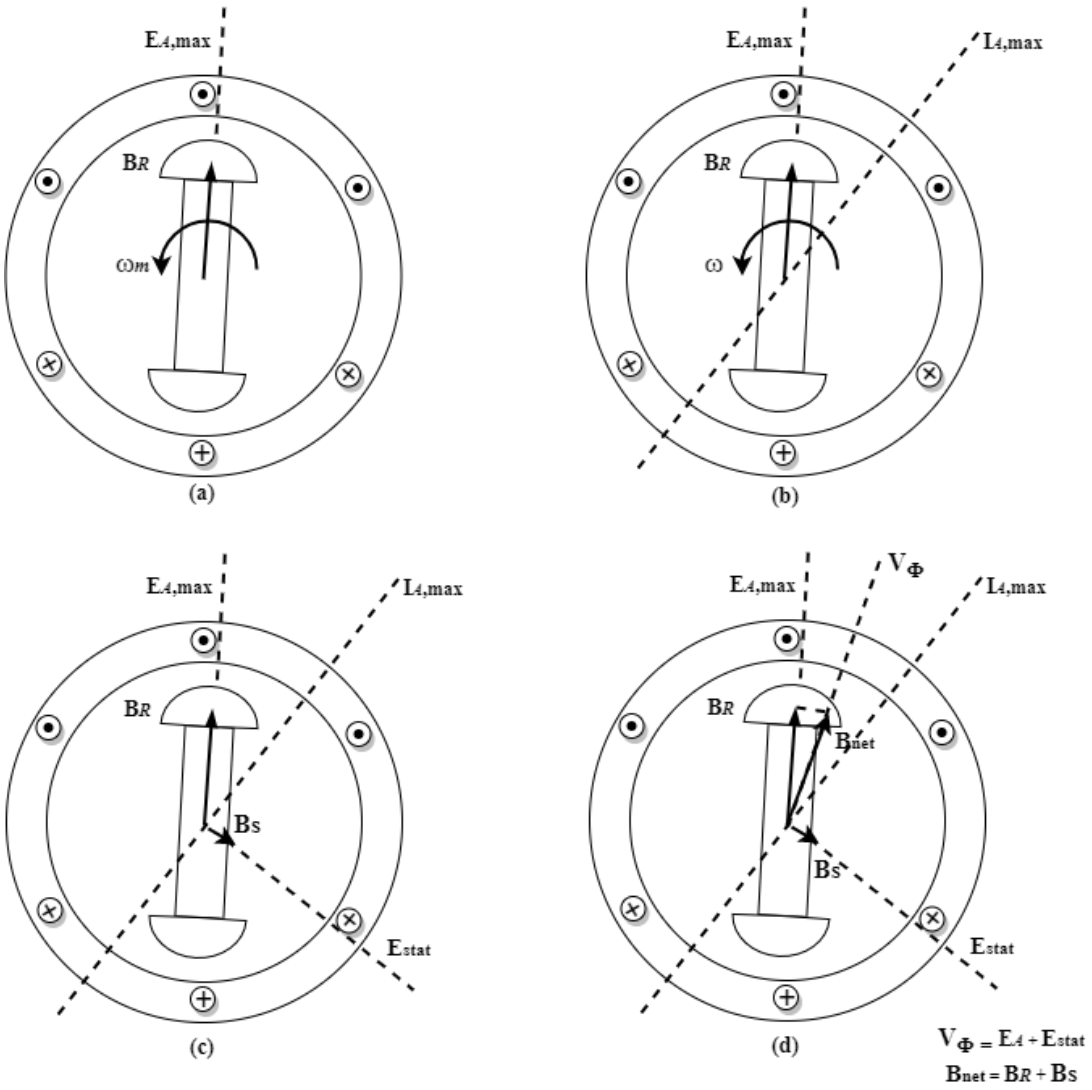

Figure 3.1. Development of a model for armature reaction [40].

In the Figure given above, (a) A rotating magnetic field produces the internal generated voltage $\mathbf{E_A}$'. (b) The resulting voltage produces a lagging currentflow whenconnected to a lagging load. (c) The stator current produces its own magnetic field $\mathbf{B_S}$, which produces its own voltage $\mathbf{E_{stat}}$ in the stator windings of the machine. (d) The field $\mathbf{B_S}$ adds to $\mathbf{B_R}$ distorting it into $\mathbf{B_{net}}$. The voltage $\mathbf{E_{stat}}$ adds to $\mathbf{E_A}$, producing $\mathbf{V_\Phi}$ at the output of the phase [40].

If there is a load attached to generator's terminals, a current will flow. However, the current flow of a 3-phase stator produces its own magnetic field in the machine, thus, distorting the rotor magnetic field, and the resultant phase voltage changes.

This effect is known as armature reaction since the magnetic field is affected by armature current. In order to better understand the armature reaction, Figure 3.1 has

been given above. The figure shows a 2-pole rotor present and rotating inside a 3-phase stator. In this case, no load is connected to stator. The magnetic field of the rotor (B_R) produces voltage E_A having a peak value which coincides with B_R direction. The voltage is observed to be positive outside the conductors present at the top whereas the voltage is observed to be negative inside the conductors present at the bottom. If the generator is not loaded, no armature current flows, which means that the E_A and V_Φ will be equal.

Let us assume that SG is connected to lagging load. Since there is a load lagging, the current will be observed at a particular angle behind peak voltage. Figure 3.1 (b) given above shows this effect. A magnetic field is produced by current which flows in stator windings. The produced magnetic field is known as B_s and the direction of this magnetic field can be given using the right hand rule as shown in Figure 3.1 (c). The magnetic field of the stator denoted as B_s produces a voltage itself in the stator, and the produced voltage is thus called E_{stat}. The sum of the stator reaction voltage E_{stat} and the internally generated voltage E_A present in stator windings yields the total voltage present in a phase as follows:

$$V_\Phi = E_{stat} + E_A \tag{3.2}$$

The net magnetic field denoted as B_{net} is the sum of stator and rotor magnetic field.

$$B_{net} = B_R + B_S \tag{3.3}$$

As the angles of E_{stat} and B_S, and the angles of E_A and B_R are the same, the resultant magnetic field denoted as B_{net} coincides with V_Φ as shown in Figure 3.1 (d). If X is rendered as the proportionality constant, then we may express armature reaction voltage as

$$E_{stat} = -jXI_A \tag{3.4}$$

The voltage observed on this phase is:

$$V_{\emptyset} = E_A - jXI_A \tag{3.5}$$

The armature reaction voltage is modeled as series inductor connected with internally generated voltage. There are effects of armature reaction, and in addition to that the coils have their own resistance and self-inductance. The self-inductance is denoted as L_A whereas the resistance denoted as R_A. The difference between V_Φ and E_A is given as:

$$V_{\emptyset} = E_A - jXI_A - jX_AI_A - R_AI_A \tag{3.6}$$

Self-inductance and armature reaction can be represented as reactance and we may combine them in one equation and name them as synchronous reactance.

$$X_S = X + X_S \tag{3.7}$$

The final equation for V_Φ can be derived as follows:

$$V_{\emptyset} = E_A - jX_SI_S - R_AI_A \tag{3.8}$$

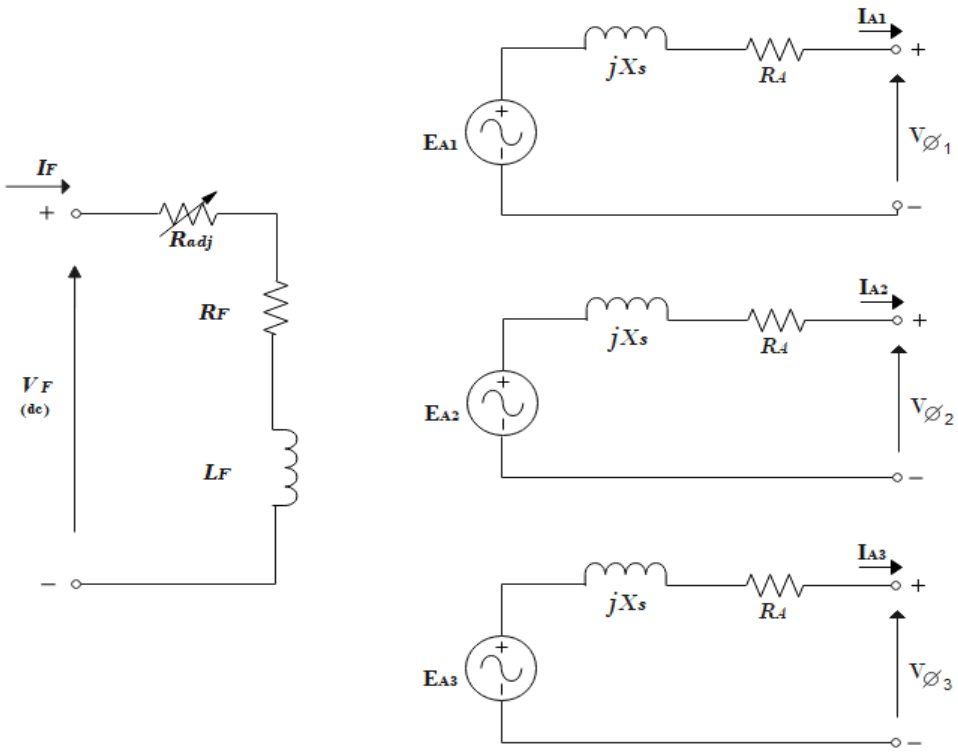

Figure 3.2. The three-phase equivalent circuit of a synchronous generator [40].

The equivalent circuit of the above-mentioned generator has been shown in Figure 3.2 above and the figure depicts a power source (dc) supplying field circuit of the rotor, thus modeled by resistance and inductance of the coil in series.

As a matter of fact the three phases of a synchronous generator are identical in all directions except the phase angle allows one equivalent circuit to be used nominally per phase. The equivalent circuit per phase of this machine is shown in Figure 3.3. [40].

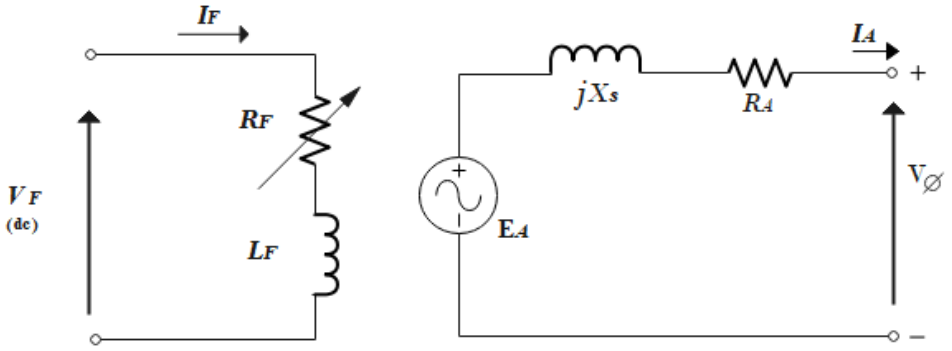

Figure 3.3. The per-phase equivalent circuit of a synchronous generator [40].

3.7. PHASOR DIAGRAM OF A SG

Since the voltages are ac voltages in synchronous generators, they can be expressed as phasors. Phasors have both an angle as well as a magnitude. The relationship ought to be expressed by two-dimensional (2D) plot. Within a phase, when the voltages denoted as V_{Φ}, E_A, R_AI_A and jX_SI_A, and the current denoted as I_A are plotted in a phase in such a manner showing the relationship between the voltage and the current, the plot obtained is known as the phasor diagram.

For instance, Figure 3.4 shows the afore-mentioned relationship in case of a generator supplying the load, which is purely resistive, at unity power factor.

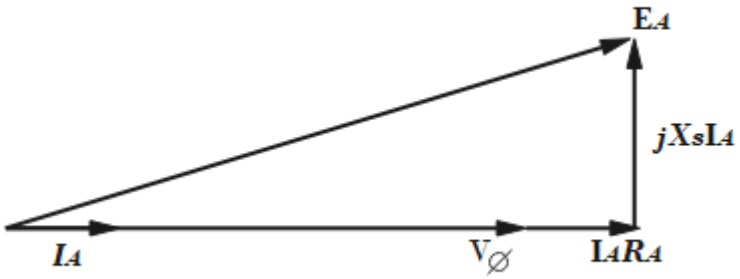

Figure 3.4. Phasor diagram of a synchronous generator at unity power factor.

As we know that the total voltage denoted as E_A differs from phase terminal voltage denoted as V_Φ by the inductive and resistive voltage drops. The currents and voltages in the phasor diagram are referenced to the terminal voltage (V_Φ), assumed to be arbitrarily at 0° angle.

The comparison of the above-mentioned phasor diagram can be made to generators' phasor diagrams operating at leading and lagging power factors. Figure 3.5 shows such phasor diagrams [40].

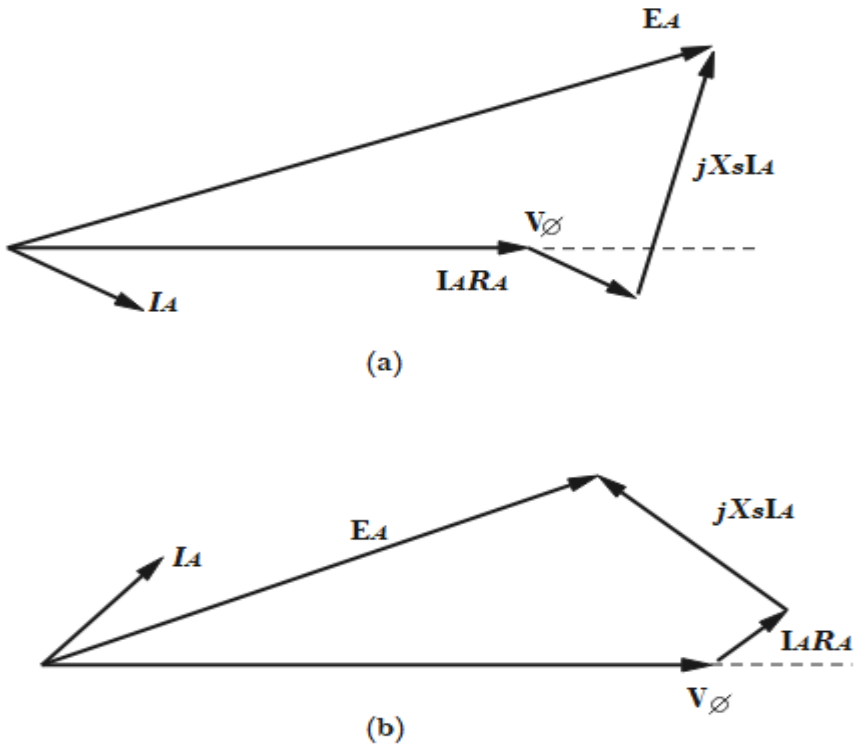

Figure 3.5. The phasor diagram of a synchronous generator at (a) lagging and (b) leading power factor.

For an armature current and phase voltage; a large internally generated voltage, E_A is required for loads that are lagging rather than for loads that are leading. Hence, there is a need for larger field current with lagging loads in order to get E_A. As,

$$E_A = K\emptyset\omega \tag{3.9}$$

ω should be kept constant in order to achieve a constant frequency. Otherwise, the terminal voltage (E_A) is higher for leading loads and lower for lagging loads for a given magnitude of load current and field current. In synchronous generators, the reactance is generally found to be much larger when compared with winding resistance (R_A). Therefore, in the qualitative study regarding the variations in voltage, R_A is neglected. In order to have an accurate numerical result, R_A needs to be considered.

CHAPTER 4

EXPERIMENTAL SETUP

An experimental setup was prepared for automatic control of frequency and voltage by loading the SG having 1 kW power with different loads. The equipment used in the experimental setup was obtained from the Electrical Machines Laboratory of Karabük University Engineering Faculty. The experimental setup consisted of a 1 kW SG, a 4 kW asynchronous motor, a frequency converter (Drive), a PLC, load groups and other auxiliary equipment. In this part of the thesis, the hardware and software used in the experimental setup will be explained briefly. The experimental setup has been shown in Figure 4.1.

Figure 4.1. Experimental Setup.

4.1. EXPERIMENT SETUP EQUIPMENTS

4.1.1. Synchronous Generator

Synchronous generator is a 3 phase, 4 wired, 1 kW, 380V, 2.3 A, 1500 rpm, brushed generator having an excitation voltage of 72V and excitation current of 2.1A. Figure 4.2 shows the synchronous generator.

Figure 4.2. Synchronous generator.

4.1.2. Induction Motor

It is the motor that mechanically connects to the shaft of the SG with a coupling and runs the SG by supplying it the mechanical power. The speed (frequency) control of the asynchronous motor can be performed with the frequency converter. Induction motor is a 3 phase, 4kW, 380V, 8.2 A, 1500 rpm. Figure 4.3 shows the asynchronous motor and its parameters.

Figure 4.3. Asynchronous motor.

4.1.3. Frequency Converter

A 2.2 kW ABB ACS355 brand/model driver was used to drive the asynchronous motor. Although the label value of the motor was noted to be 4 kW, there was no problem with the driver power since it did not draw more than 2.2 kW in the experimental studies.

Figure 4.4. Frequency converter.

4.1.4. PLC

S7-1200 1215C DC/DC/DC type PLC was used in order to control and remotely monitor the systems. The PLC that has been shown in Figure 4.5, has 14 digital inputs (DI), 10 digital outputs (DO), 2 analog inputs (AI), 2 analog outputs (AO), 2 PROFINET ports and 125 KB memory.

Figure 4.5. S7-1200 1215C DC/DC/DC PLC.

4.1.5. AI/AQ Module

In our system, 2 analog outputs were needed to control the frequency converter and voltage clipper card with PLC. The 2 analog outputs (AQs) on the PLC were of current (0-20 mA) type. The analog input (AI) of the voltage card was of voltage (0-5V) type. Both current and voltage type could be selected in case of the driver; however, voltage type AI was selected in this project. For this reason, the AI/AQ module (SM1234) with 2 AOs on it, as seen in Figure 4.6, was added to the PLC.

Figure 4.6. AI/AQ module.

4.1.6. AI Energy Meter

To measure the electrical parameters of the SG, the AI Energy Meter module (SM1238) which is added to the PLC was used. The AI Energy Meter has been shown in Figure 4.7

Figure 4.7. AI Energy meter.

Phase-neutral voltages (U_{L1-N}, U_{L2-N}, U_{L3-N}), phase-to-phase voltages (U_{L1-2}, U_{L2-3}, U_{L3-1}), phase current and neutral current (I_{L1}) of SG , I_{L2}, I_{L3}, I_N), frequency, active powers (P_{L1}, P_{L2}, P_{L3}, P_{total}), reactive powers (Q_{L1}, Q_{L2}, Q_{L3}, Q_{total}) apparent powers (S_{L1}, S_{L2}, S_{L3}, S_{total}), power factors (pF1, pF2, pF3, pF_{total}) and some other parameters can be measured using the Energy Meter module,.

4.1.7. Power Supplies

Two power supplies were used in our system. The first one was used to feed the PLC and the AI/AO module, and the second one was used to feed the excitation winding of the SG. The power supply feeding the PLC was 240W, 220V with AC/24V DC ratings. The power supply feeding the excitation winding was 800W, 220V and AC/0-85V DC output voltage was adjustable. Power supplies are shown in Figure 4.8 and 4.9.

Figure 4.8. 24V DC power supply.

Figure 4.9. 0-85V DC power supply.

4.1.8. PWM DC Voltage Clipper

DC 0-85V, 10A, 800W switched mode power supply was selected to generate the power required for the excitation of the generator. The PWM DC clipper circuit board, which could be driven proportionally with the analog output of the PLC for the voltage/current values required for the excitation of the generator according to the synchronous load of the output voltage of the power supply, and had 0-5 V_{dc} control input, 15 kHz PWM Pulse Amplitude Modulation, maximum input voltage of 90Vdc which could drive loads up to 15A proportionally was selected. PWM DC clipper circuit board has been shown in Figure 4.10,

Figure 4.10. PWM DC voltage clipper circuit board.

4.1.9. Encoder

An encoder mechanically connected to the shaft of the SG was used to measure the speed of the SG and accordingly control the frequency. The encoder is a 1024 ppr, 24V, rotary, incremental type encoder. The encoder can be seen in Figure 4.11.

Figure 4.11. Encoder.

4.1.10. Current Transformers

Electrical connections were made between the SG and the Energy Meter to measure the output voltage of the SG and the current drawn from the SG. According to the datasheet of Energy Meter, it is mandatory to use current transformers (for each phase) in the current circuit. Since the maximum current of the SG is 2.3 A according to the label value, three 5/5 current transformers were used.

Figure 4.12. Current transformers.

4.1.11. Contactors

To connect the load groups to SG, contactors with coil voltage of 24V and contact current of 10A were used. The contactors used have been shown in Figure 4.13.

Figure 4.13. Contactors.

4.2. PLC and SCADA Hardware and Software

PLC and SCADA software was implemented using Simatic Step 7 TIA Portal V16 interface. Siemens S7-1200 1215C DC/DC/DC brand/model PLC was used. The ladder programming language has been preferred for programming. Instead of a real (physical) HMI panel, the computer (PC) screen was used as an operator panel via the SIMATIC HMI Application/Win CC RT Advanced. "Device & Networks" and "Portal View" of the created TIA Portal project have been shown in Figures 4.14 and 4.15, respectively.

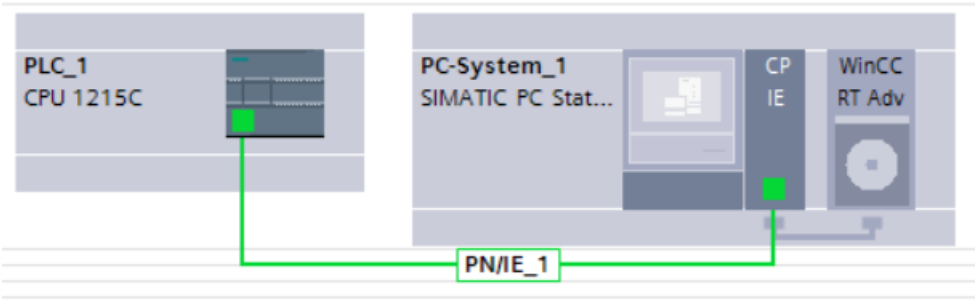

Figure 4.14. Device & Networks view of the project.

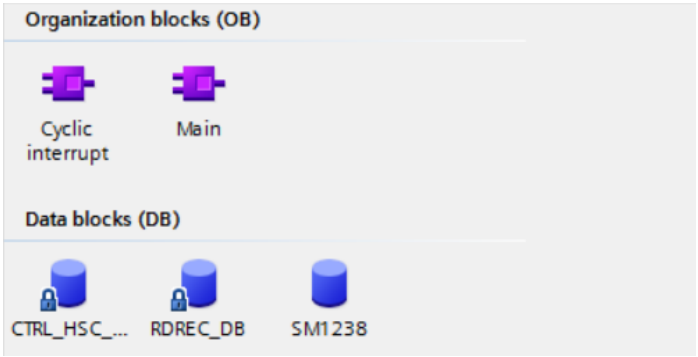

Figure 4.15. Portal View of the project.

There are 2 analog inputs (AI) and 10 digital outputs (DQ) on the PLC used in the project. The "device configuration" of the project is shown in Figure 4.16. 2 analog outputs were needed to control the frequency converter and voltage clipper card with PLC. The 2 analog outputs (AQs) on the PLC were of current (0-20 mA) type. The analog input (AI) of the voltage card was of voltage (0-5V) type. Both current and voltage type AI of the driver could be selected, however, the voltage type AI of the

frequency converter was selected in this project. For this reason, AI/AQ module (SM1234) and AI Energy Meter (1238) seen in Figure 4.16 were added to the PLC. The "device configuration" of the project is shown in Figure 4.16.

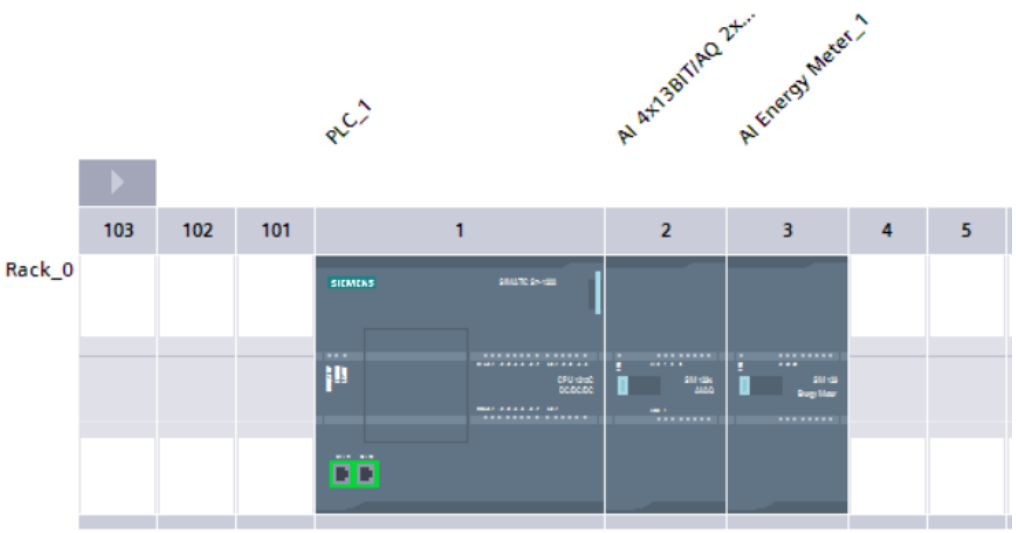

Figure 4.16. Device Configuration view of the project

Analog outputs (QW96 and QW98) were used to control the speed and voltage of the SG. QW96 was connected to AI of frequency converter and QW98 was connected to AI of voltage clipper board. A digital input (I0.0) was connected to the encoder. In addition, HSC (High Speed Counter) hardware configuration was made for the encoder in the software. Seven of the digital outputs (Q0.0-Q0.6) were used. One was used to the start/stop the system, one was used to turn on or turn off the power supply feeding the excitation winding, and five were used to activate and deactivate the load groups. A user_data_type and a data block were created for the Energy Meter. Power connections were made between SG-Energy Meter and Current Transformers-Energy Meter.

Once the digital and analog hardware connections described above were made, the hardware and software configurations required for the project were carried out on the TIA Portal interface.

The general block diagram of the system has been given in Figure 4.17.

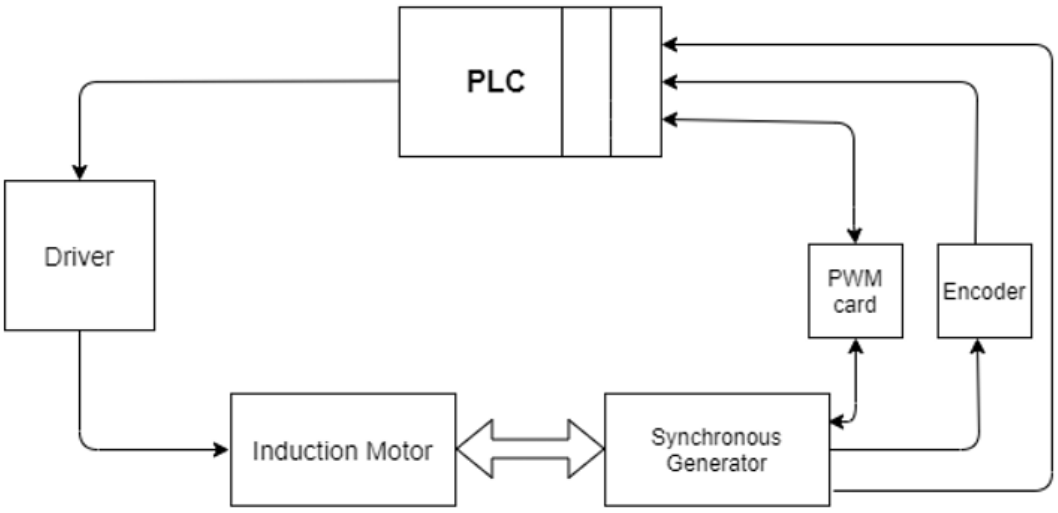

Figure 4.17. Block diagram of the system.

4.2.1. Control System

4.2.1.1. Frequency Control

Frequency control in the experimental setup is performed based on the speed (rpm) value obtained from the encoder. If this value is different from the set value (1500), the frequency of the frequency converter (driver) is either increased or decreased, and the speed of the asynchronous motor is changed accordingly. As a result, the rpm (speed) and the frequency of the SG, which is mechanically connected to the asynchronous motor, is changed and set, respectively. This is accomplished by a proportional 0-10V signal sent from the analog output of the PLC to the analog input of the driver. When the number of revolutions (speed) is 1500 min^{-1}, the frequency of the SG becomes 50 Hz. In Figure 4.18, the frequency setting flow chart of SG is given.

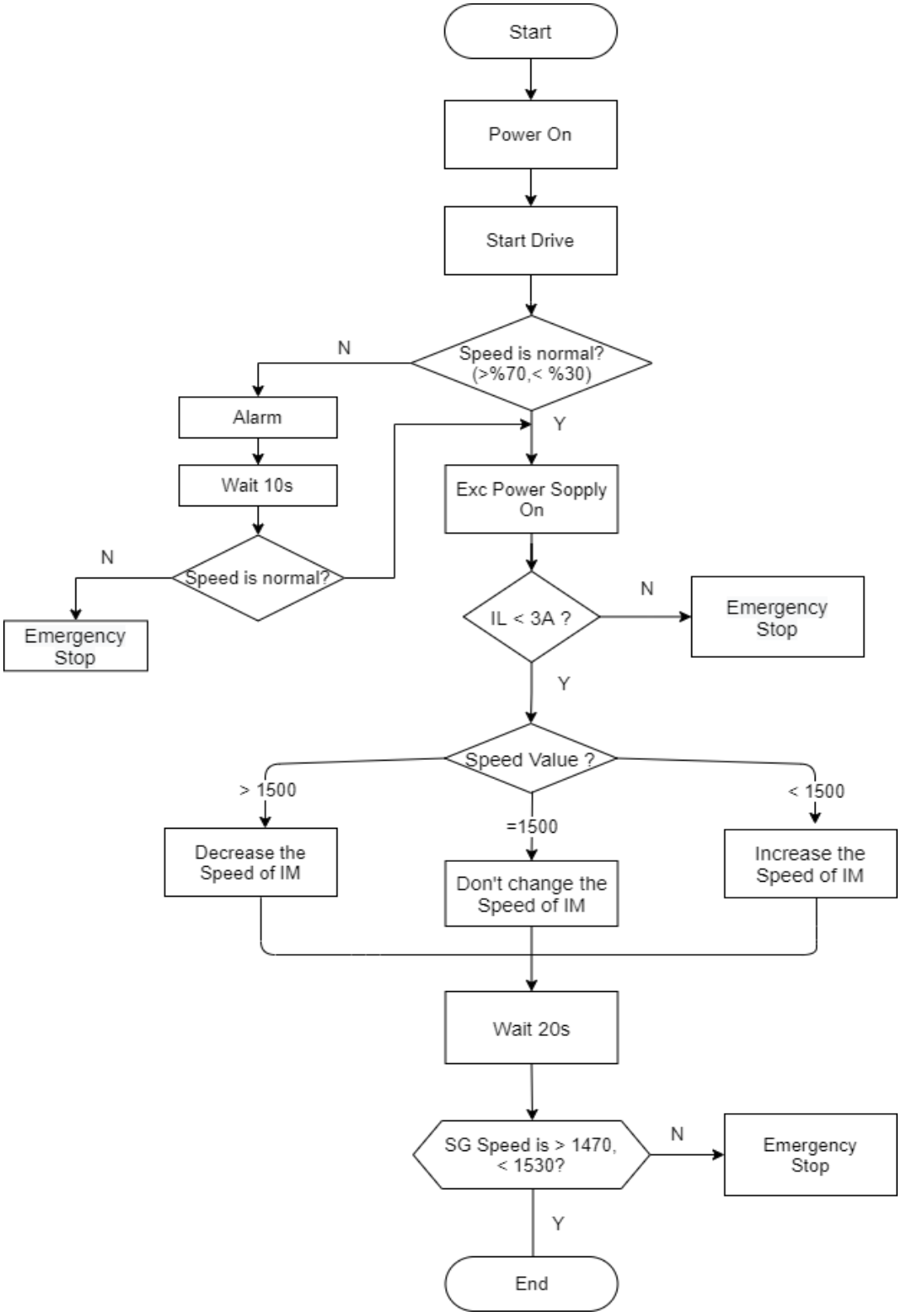

Figure 4.18. Frequency control flow chart.

4.2.1.2. Voltage Control

The control of the voltage produced by SG is based on the phase-neutral (UL2-N) voltage value obtained from the Energy Meter. If this value is different from the set value (220V), the value of the voltage applied to the excitation winding (resultantly, the excitation current value) is proportionally increased or decreased. This is carried out by a 0-5 V analog signal sent from the analog output of the PLC to the 0-5 V DC analog control input of the DC voltage clipper circuit placed at the power supply output. Since the analog output of the PLC (AI/AQ module) is only 10 V, the adjustment has been made in the software to send max.5V analog output. The change in the excitation voltage changes the excitation current at the same rate. The voltage adjustment flow chart of SG is given in Figure 4.19.

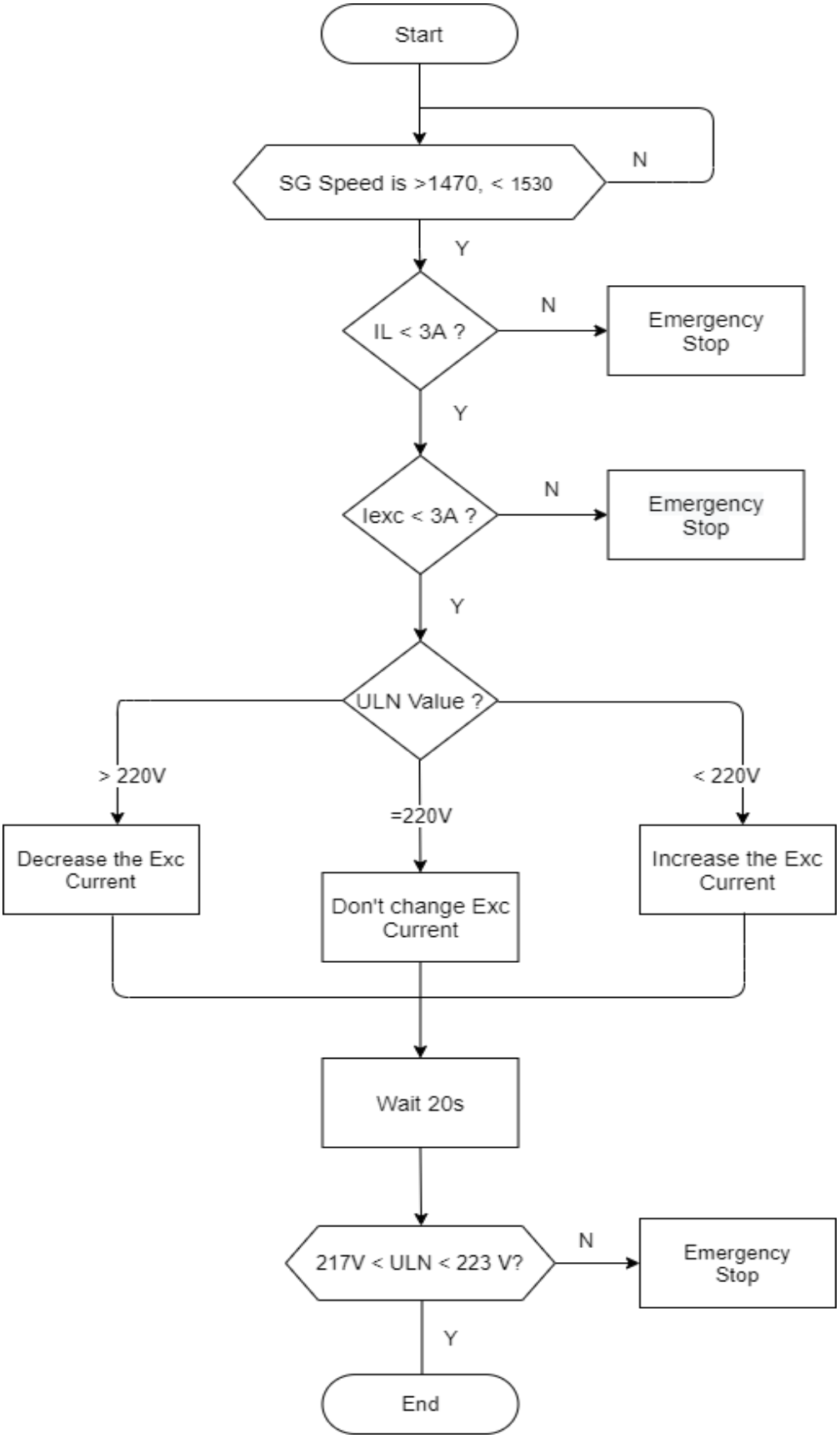

Figure 4.19. Voltage control flow chart.

4.2.2. PID Function

The frequency and voltage values of the SG were adjusted according to the load by using the PID_Compact function of the PLC software. The simple block diagram of the PID_Compact function used in the TIA Portal interface has been shown in Figure 4.20.

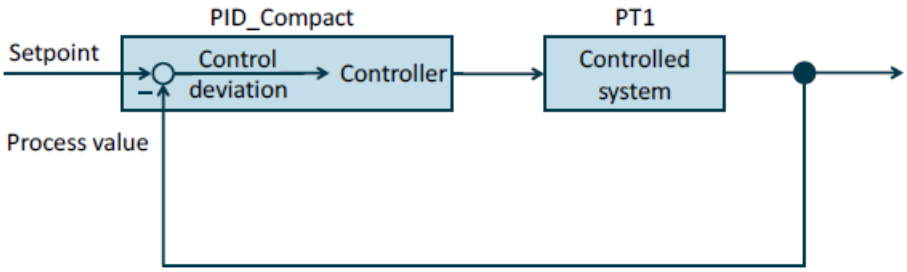

Figure 4.20. Simple block diagram of PID_Compact function [42].

The detailed block diagram is given in Figure 4.21.

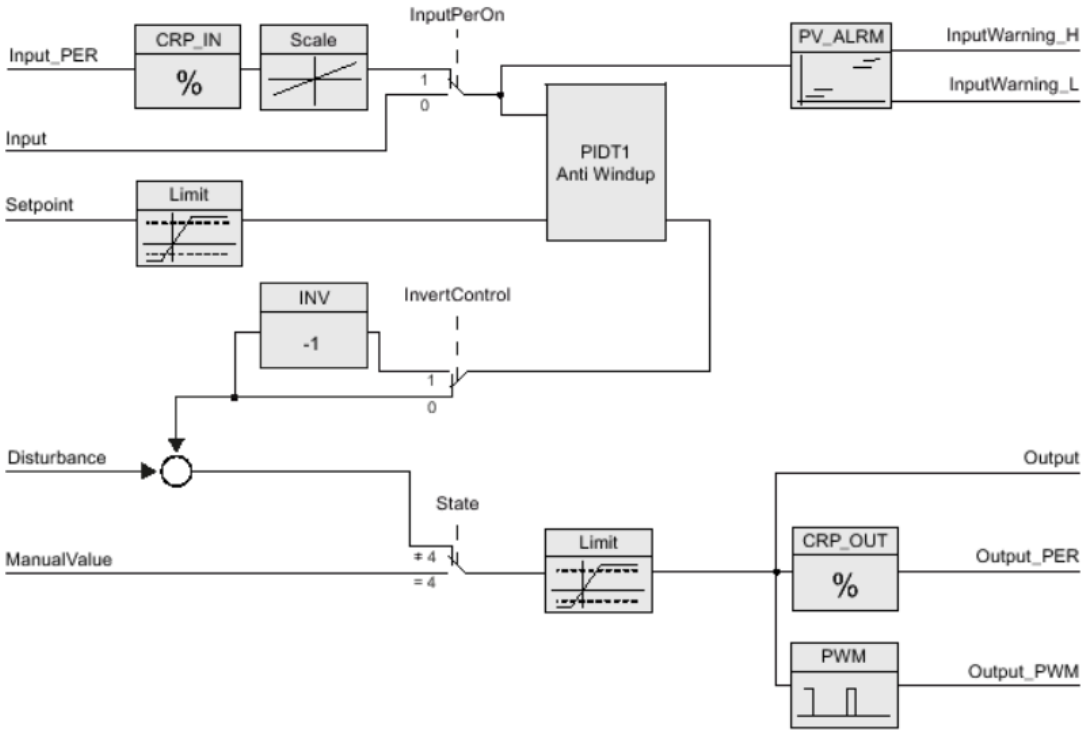

Figure 4.21. Detailed block diagram of PID_Compact function [42].

The PID algorithm works according to the equation given below [42]:

$$y = K_p \left[(b.w - x) + \frac{1}{T_I.s}(w - x) + \frac{T_D.s}{a.T_D.s + 1}(c.w - x) \right] \quad (4.1)$$

Here, y is the output value of the PID algorithm, K_p is the proportional gain, s is Laplace operator, b is proportional action weighting, w is set point, x is process value, T_I is integral action time, T_D is derivative action time, a is the derivative delay coefficient and c is derivative action weighting [37].

The PID block diagrams related to the frequency (speed) and the voltage brought to the set point in the system have been given in Figure 4.22 and Figure 4.23, respectively.

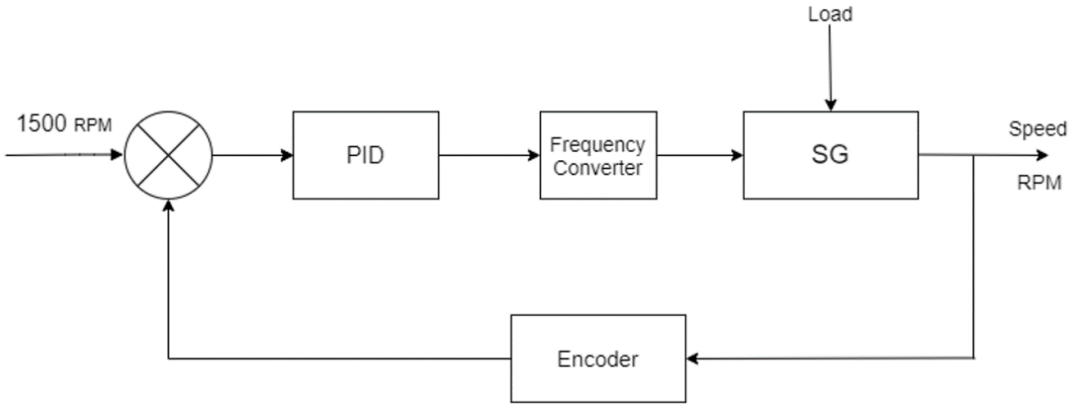

Figure 4.22. PID block diagram of frequency control.

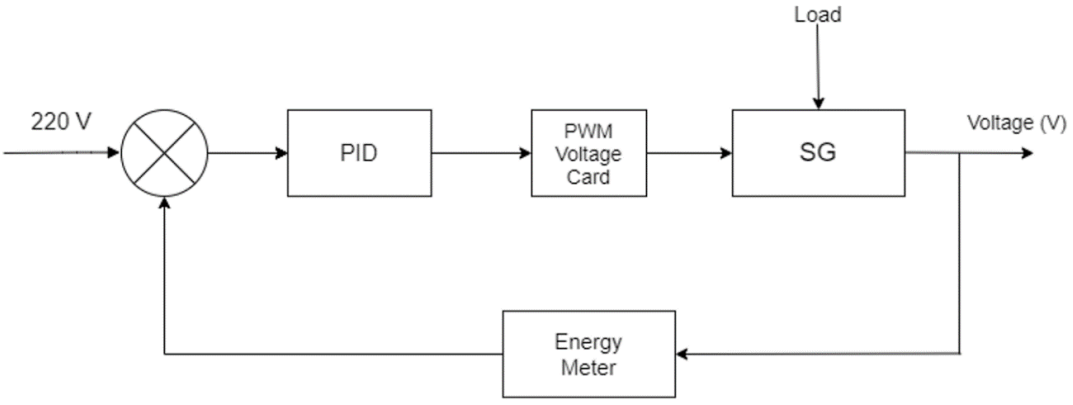

Figure 4.23. PID block diagram of voltage control.

The ladder diagrams of the project are given in section Annotations A.

4.3. SCADA SCREENS

In this thesis, SCADA software was also developed in order to monitor and control the system remotely. PC screen was used as SCADA screen. Three SCADA screens, Main, Values and Alarms, were created accordingly. On the Main Screen, the start-stop function of the system can be performed, the basic parameter values (speed, voltages and currents) can be monitored, load groups can be activated and deactivated, and data logging can be started and stopped. All electrical parameters from the Energy Meter are displayed on the Values Screen. On Screen 3, alarms received from the system are displayed. Main screen and Values screen are shown in Figure 4.24 and 4.25.

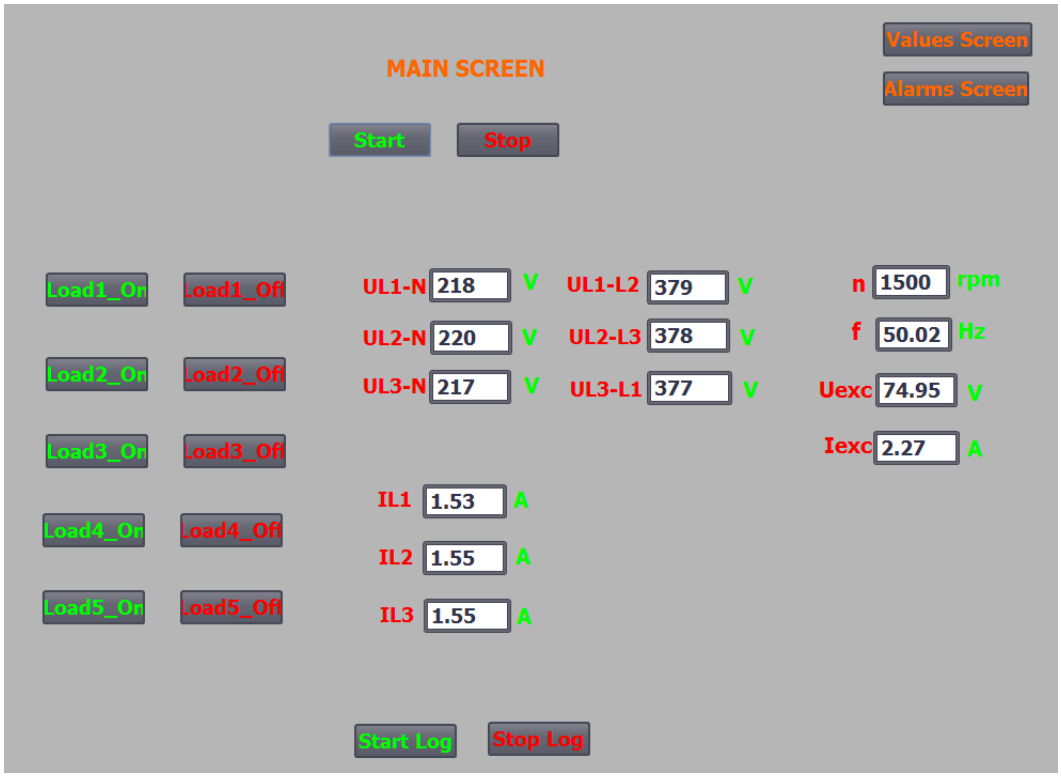

Figure 4.24. Main SCADA screen.

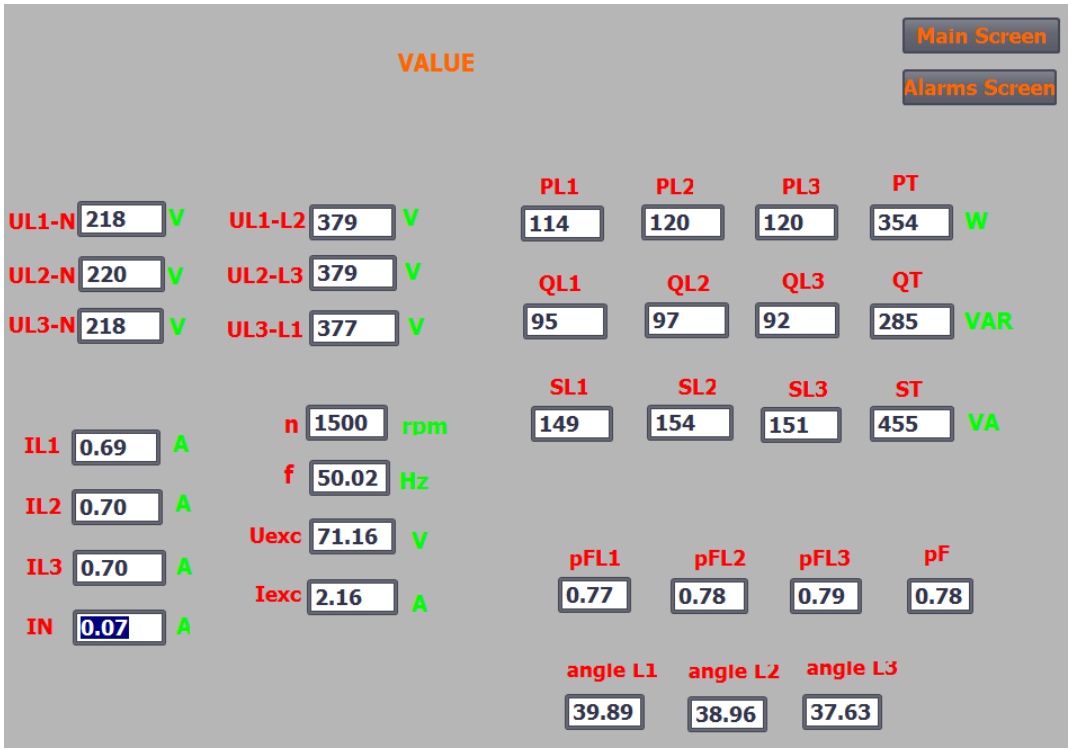

Figure 4.25. Values SCADA screen.

On the Alarms screen, six different alarms are displayed for the SG: overload, over-voltage, under-voltage, over-frequency, under-frequency and over-excitation current. When one of these alarms is encountered, the system is stopped. The alarm screen is shown in Figure 4.26.

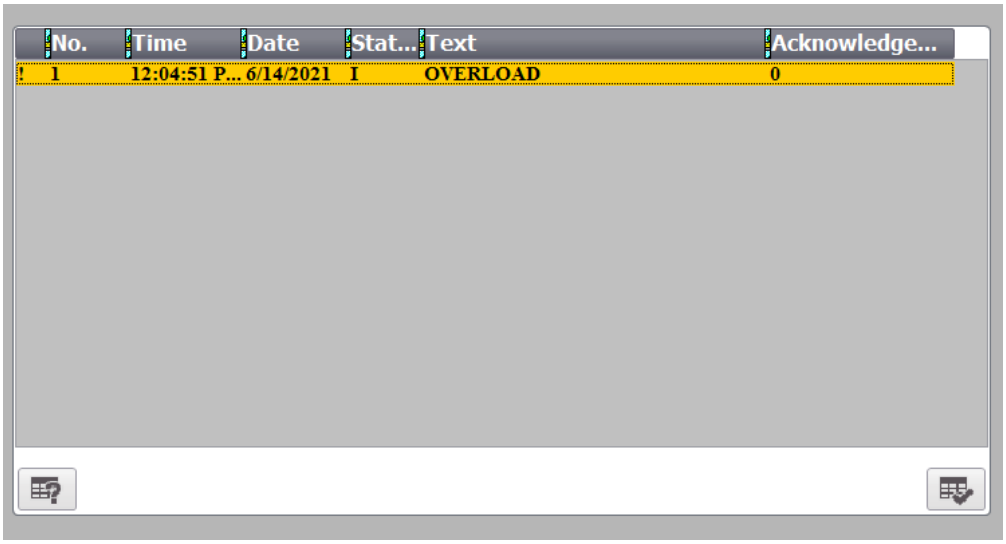

Figure 4.26. Alarms SCADA screen.

4.4. THE EQUIVALENT CIRCUIT OF SG

The per-phase equivalent circuit of the SG used in the experiment was obtained in accordance with the explanations in Chapter 3.6. In order to obtain this, firstly; one phase winding resistance of SG was measured. This value was found to be 9.4Ω. However, after the SG was operated at full load for a while, the measured value was observed to be 10Ω when the windings were hot. This value was used in the equivalent circuit (RA=10Ω).

To find inductive reactance in the equivalent circuit, the excitation current was gradually increased by short-circuiting the output of SG. When the drawn armature current (load current) had reached the rated value (2.2A), the short circuit was removed and a phase voltage was measured at that moment. This value was 260V.

Synchronous impedance is calculated as;

$$Z_S = \frac{U}{I_A} \tag{4.1}$$

$Z_S = \frac{260}{2.2} = 118.18\ \Omega$ olur.

$$Z_S = \sqrt{R_A^2 + X_S^2} \tag{4.2}$$

$$X_S = \sqrt{Z_S^2 - R_A^2} \tag{4.3}$$

$X_S = \sqrt{118.18^2 - 10^2} = 117.75\ \Omega$

The equivalent circuit of SG is obtained as in Figure 4.27.

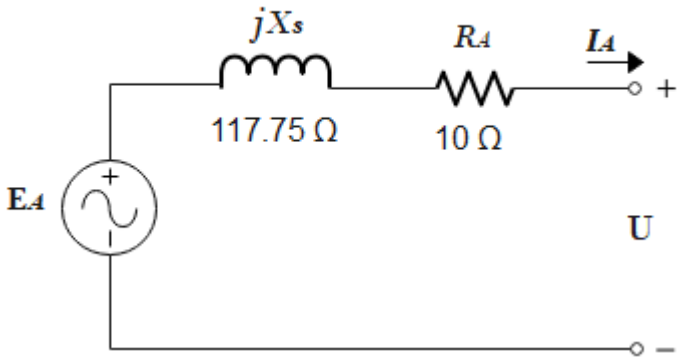

Figure 4.27. The per-phase equivalent circuit of the SG.

4.5. THE PHASOR DIAGRAM OF SG

In accordance with the explanations made in Chapter 3.7, the phasor diagram of SG was obtained. To obtain it, the SG's speed (1500 rpm) and excitation current (1.35A) were kept constant each time, and the SG was loaded with loads of different values and the terminal voltage was measured. The terminal voltages measured at different loads are given in Table 4.1.

Table 4.1. Terminal voltage variation at different load currents.

n (rpm)	I_{exc} (A)	I_A (A)	U (V)
1500	1.35	0	220
1500	1.35	0.46	208
1500	1.35	0.85	186
1500	1.35	1.20	141

For I_A=0.46A, E_A is calculated as;

$$E_A = \mathrm{U} + jX_S I_S + R_A I_A \quad (4.4)$$

$$E_A = 208 + j(117.75x0.46) + (10\mathrm{x}0.46)$$

$$E_A = 208 + \mathrm{j}54.16 + 4.6$$

$$E_A = 212.6 + \mathrm{j}54.16$$

$$E_A = 219.39\angle 14.2\ \mathrm{V}$$

For I_A=0.85 A, E_A is calculated as;

$$E_A = 186 + j(117.75x0.85) + (10x0.85)$$
$$E_A = 186 + j100.0875 + 8.5$$
$$E_A = 194.5 + j100.0875$$
$$E_A = 218.74\angle 27.2 \text{ V}$$

For I_A=1.20 A, E_A is calculated as;

$$E_A = 141 + j(117.75x1.2) + (10x1.2)$$
$$E_A = 141 + j141.3 + 12$$
$$E_A = 153 + j141.3$$
$$E_A = 208.26\angle 42.7 \text{ V}$$

Figure 4.28 depicts the effect of change in SG load on terminal voltage.

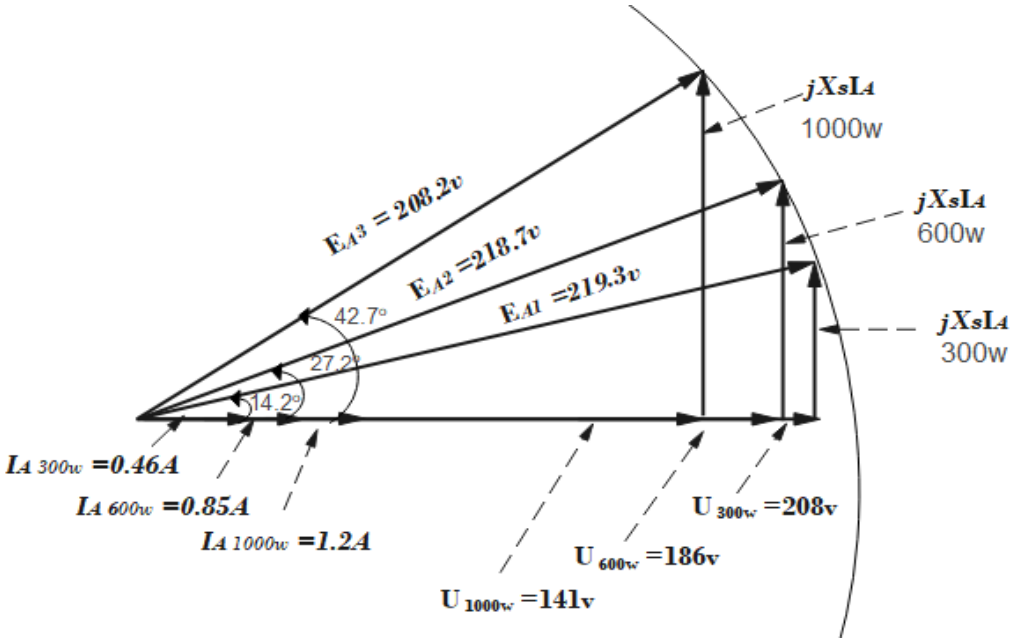

Figure 4.28. Effect of increase in SG load on terminal voltage.

4.6. EXPERIMENT RESULTS

In the experiments, the SG was loaded with different types and values of loads, and the graphs regarding the changes in frequency and voltage were drawn separately for the PID and PI control modes. The experiments were conducted in the form of loading and unloading at 0-300W, 300-0W, 0-540W, 540-0W, 300-700W, 700-300W, 700-1000W, 1000-7000W values for resistive loads, 0-294VA, 294-0VA, 0-455VA, 455-0VA, 0-650VA, 650-0VA, 0-800VA, 800-0VA values for inductive loads, and 0-550VA, 550-0VA, 0-840VA, 840-0VA values for capacitive loads.

During the experiments, the values were recorded in an excel file using the SCADA data log function. As an example, the values taken from the 0-1000W resistive load PID control experiment are given in Table 4.2. All experiments were performed separately for PID and PI control modes.

Table 4.2. 0-300W resistive load experimental values of PID control

VarName	TimeStringt	VarValue
P	14:11:59	0
UL2N	14:11:59	220.3338
FREQUENCY	14:12:00	50
P	14:12:00	347.8588
UL2N	14:12:00	196.4013
FREQUENCY	14:12:01	49.23333
P	14:12:01	612.0941
UL2N	14:12:01	202.4776
FREQUENCY	14:12:02	49.23333
P	14:12:02	718.1877
UL2N	14:12:02	177.1333
FREQUENCY	14:12:03	48.93333
P	14:12:03	852.1408
UL2N	14:12:03	195.046
FREQUENCY	14:12:04	49.13333

P	14:12:04	905.6884
UL2N	14:12:04	204.104
FREQUENCY	14:12:05	49.13333
P	14:12:05	929.4544
UL2N	14:12:05	207.3216
FREQUENCY	14:12:06	49.2
P	14:12:06	948.7386
UL2N	14:12:06	210.4535
FREQUENCY	14:12:07	49.26667
P	14:12:07	962.4073
UL2N	14:12:07	212.7017
FREQUENCY	14:12:08	49.33333
P	14:12:08	975.1258
UL2N	14:12:08	214.2076
FREQUENCY	14:12:09	49.4
P	14:12:09	983.4399
UL2N	14:12:09	215.5574
FREQUENCY	14:12:10	49.46667
P	14:12:10	989.5958
UL2N	14:12:10	216.088
FREQUENCY	14:12:11	49.5
P	14:12:11	996.9326
UL2N	14:12:11	217.4254
FREQUENCY	14:12:12	49.5
P	14:12:12	1000.326
UL2N	14:12:12	217.7546
FREQUENCY	14:12:13	49.6
P	14:12:13	1005.432
UL2N	14:12:13	218.6532

4.6.1. Resistive Load Experiments

5 groups of incandescent lamps with different powers were used as resistive loads. Since the used SG was a 3-phase 4 wired generator, the load connections were balanced accordingly. In Figure 4.29, resistive load groups (incandescent lamps) have been shown.

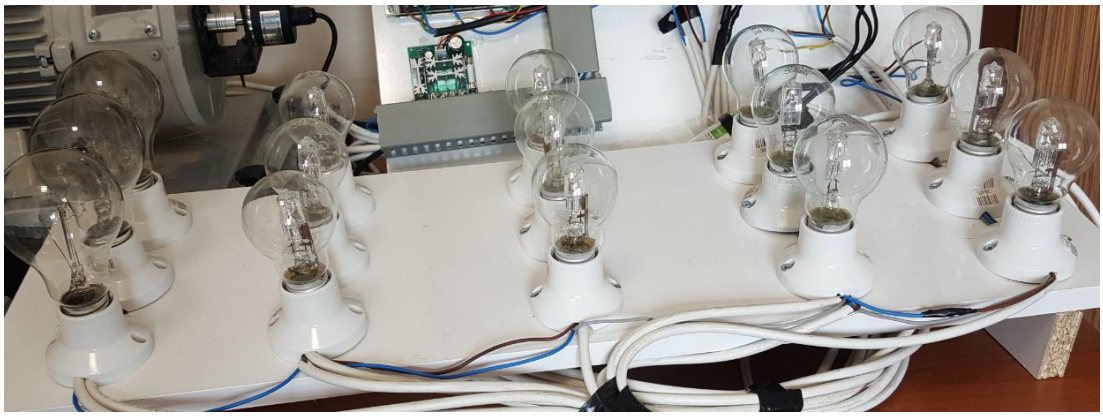

Figure 4.29. Resistive load groups.

After the resistive load experiments were made to reach set values of SG, PID and PI control for 0-300W, 300-0W, 0-540W, 540-0W, 300-700W, 700-300W, 700-1000W, 1000-700W values in the form of loading and unloading were performed for different modes. Set (reference) values were determined as 220V (phase-neutral voltage) for voltage and 1500 for speed (rpm). Speed data was taken from the encoder, whereas, the voltage data was taken from the Energy Meter. Frequency-time and voltage-time graphs are given in Figures 4.30-4.45.

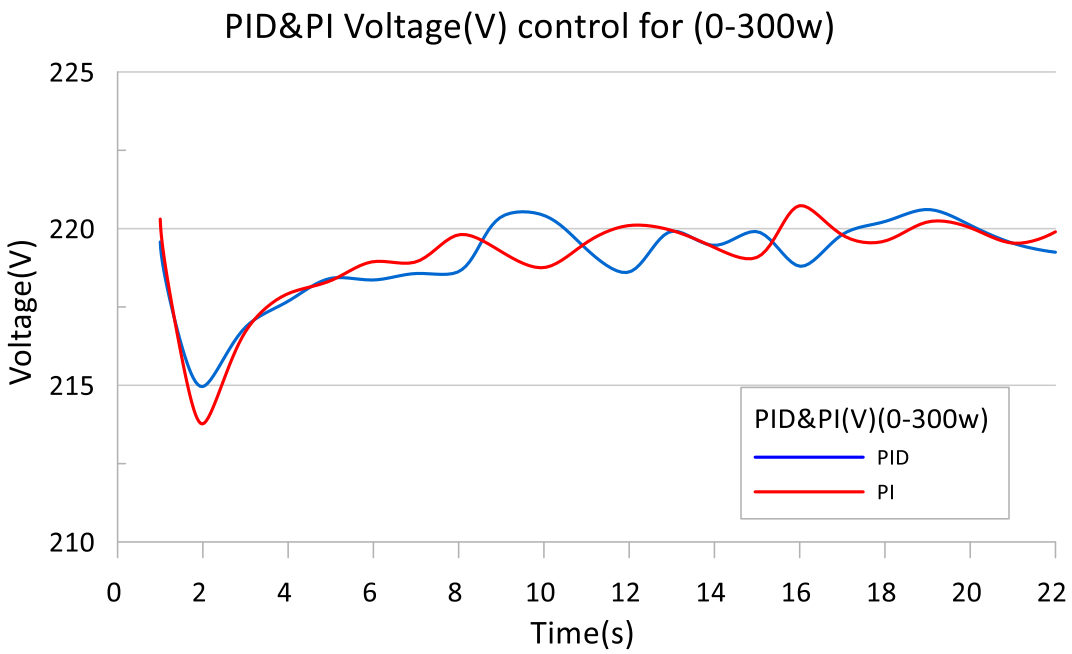

Figure 4.30. 0-300W V-t graph.

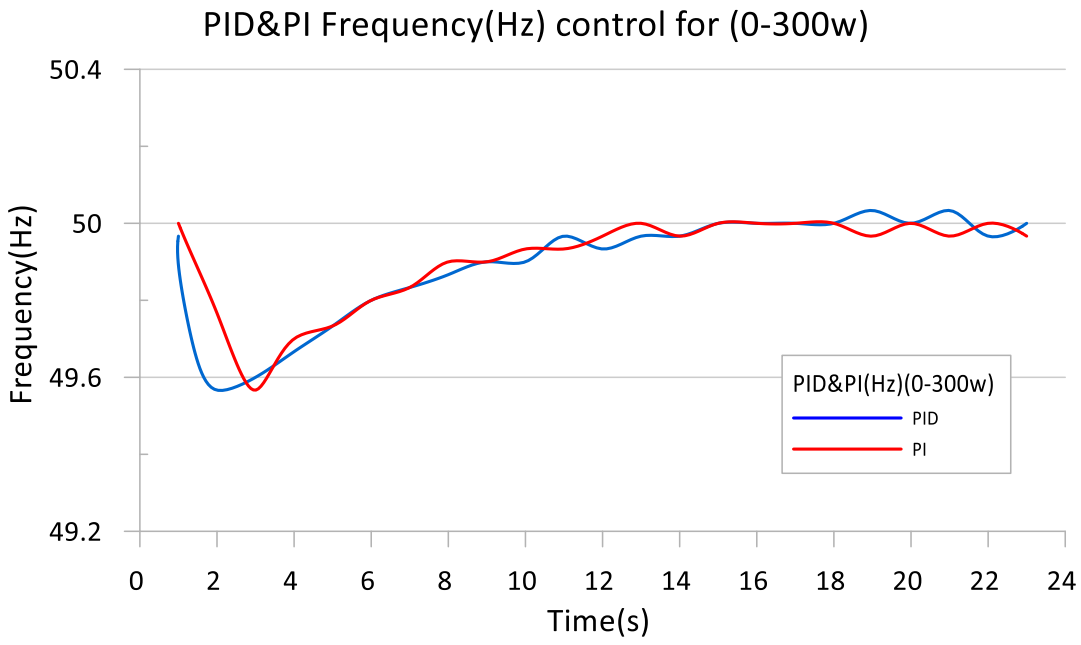

Figure 4.31. 0-300W f-t graph.

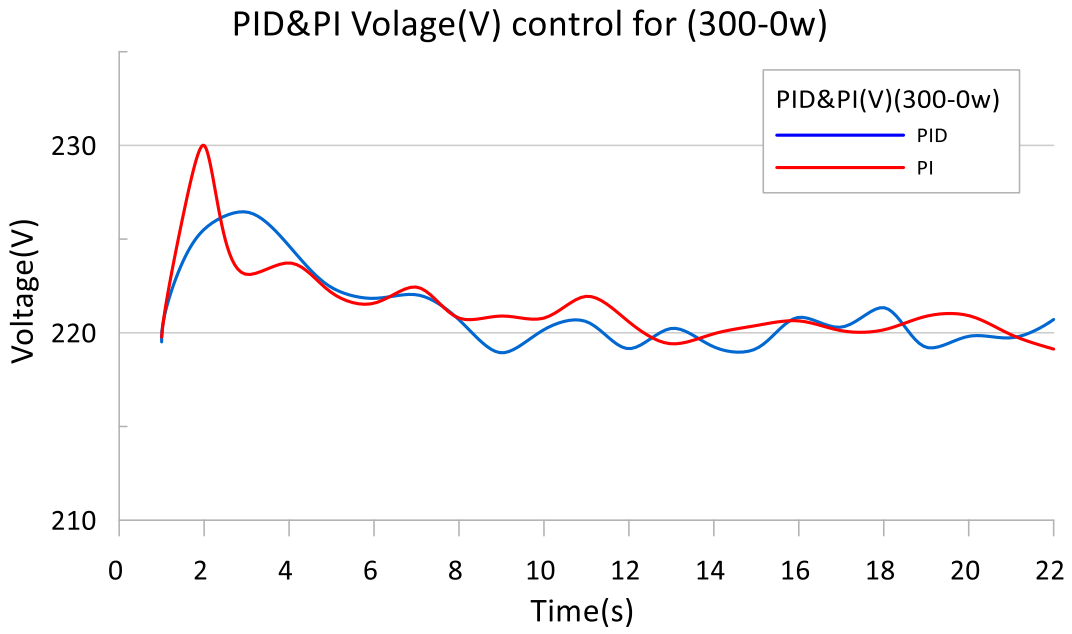

Figure 4.32. 300-0W V-t graph.

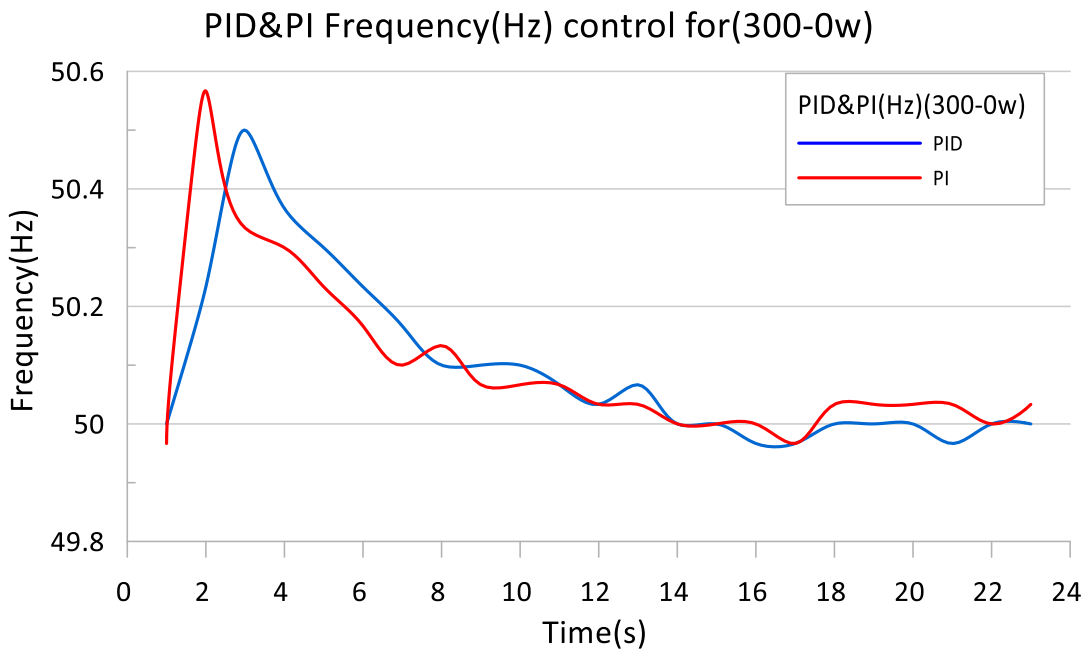

Figure 4.33. 300-0W f-t graph.

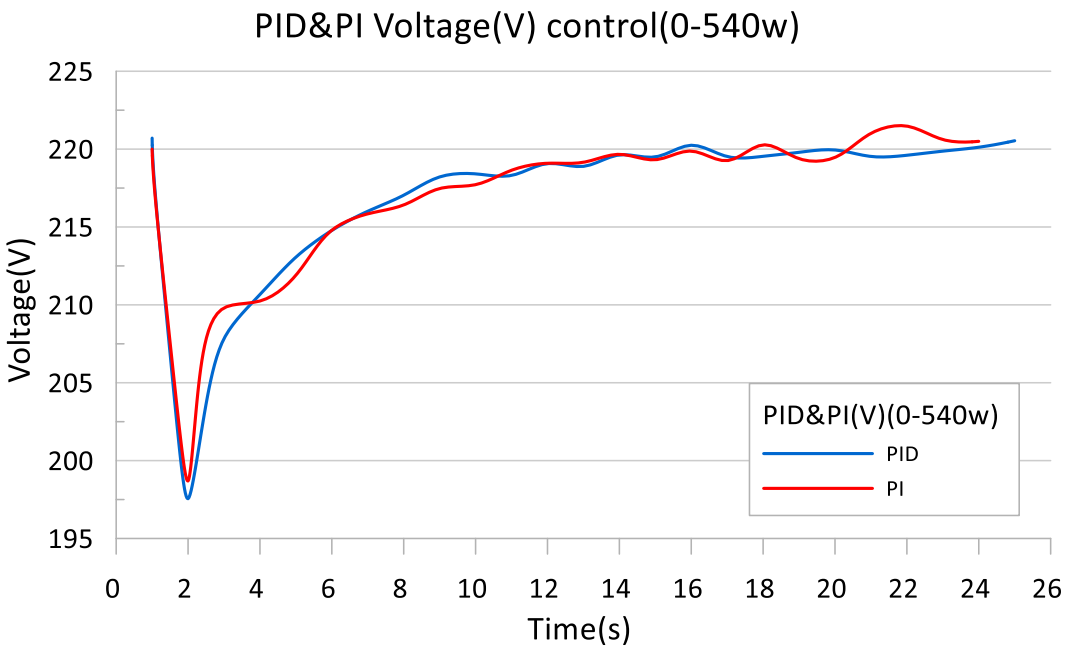

Figure 4.34. 0-540W V-t graph.

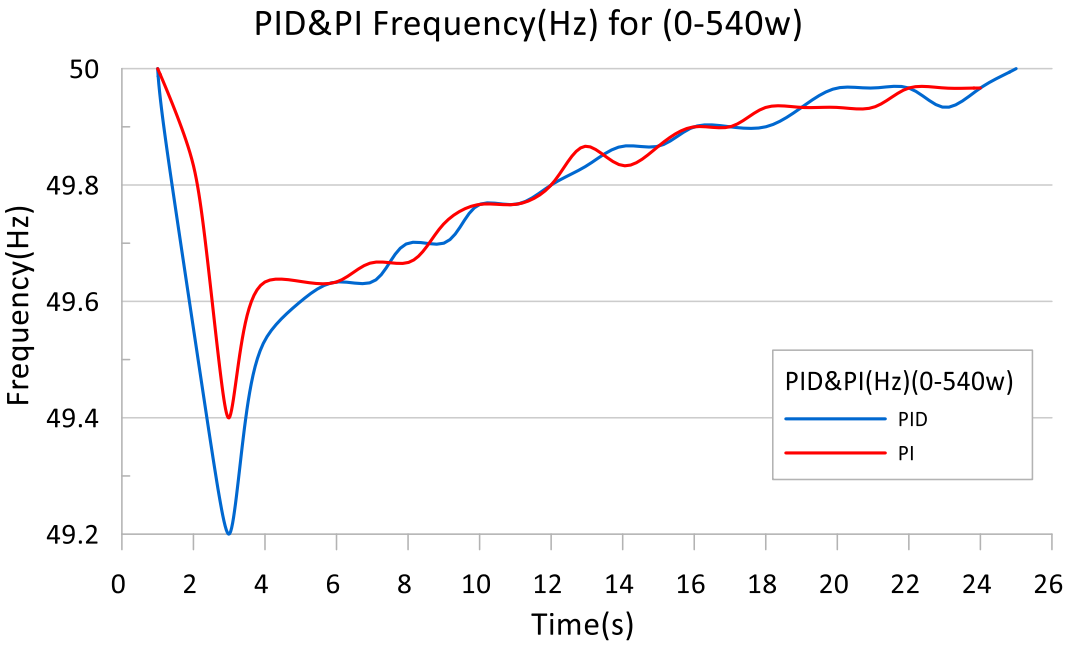

Figure 4.35. 0-540W f-t graph.

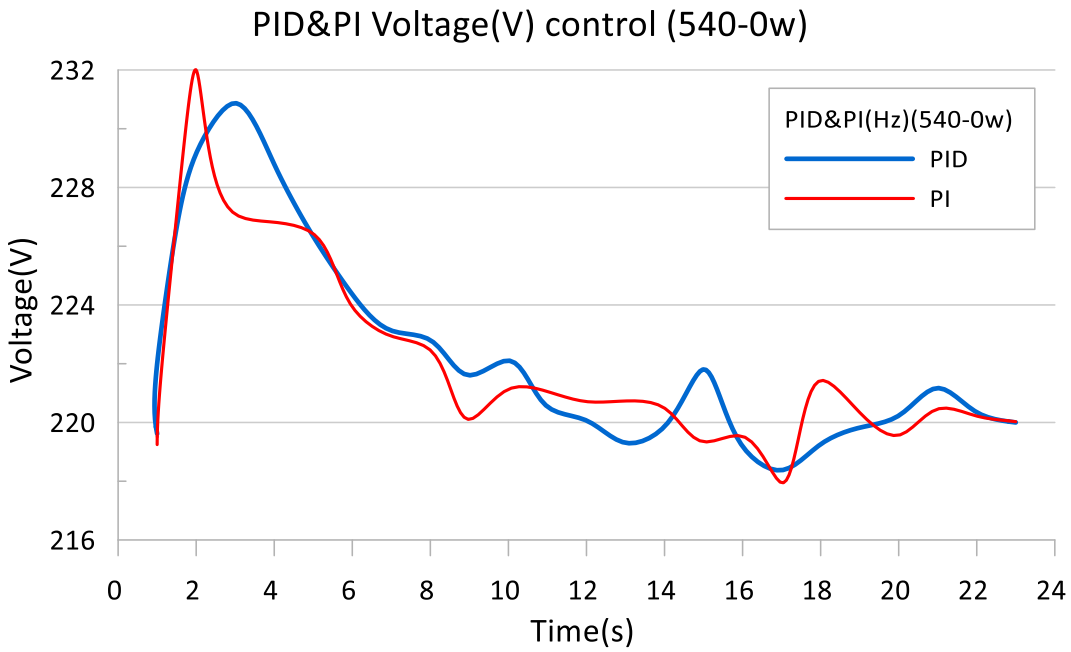

Figure 4.36. 540-0W V-t graph.

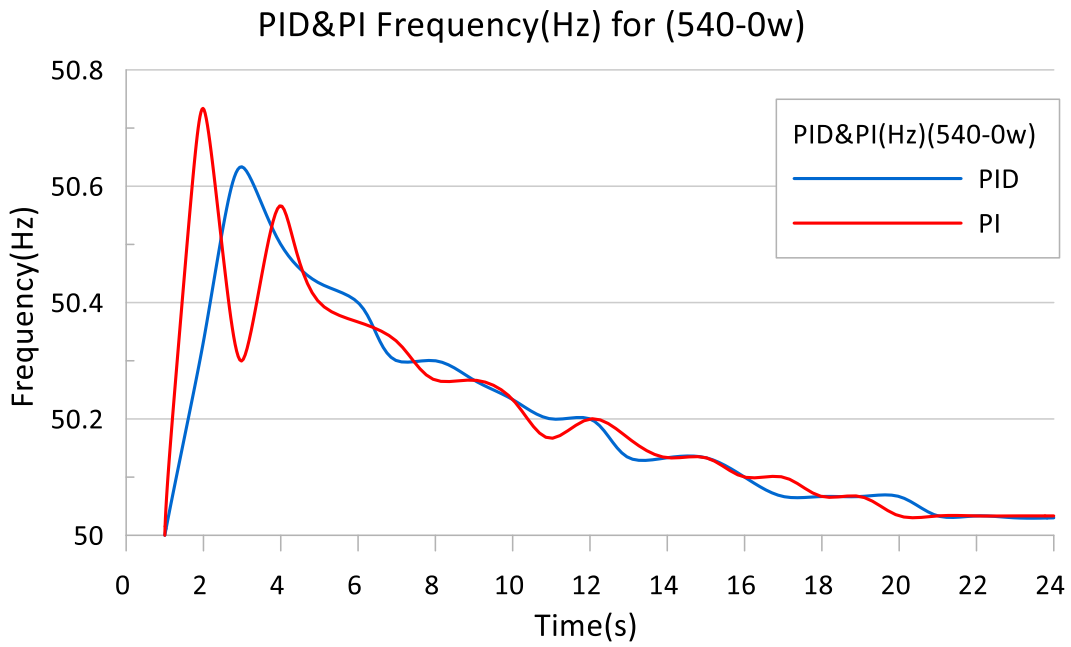

Figure 4.37. 540-0W f-t graph.

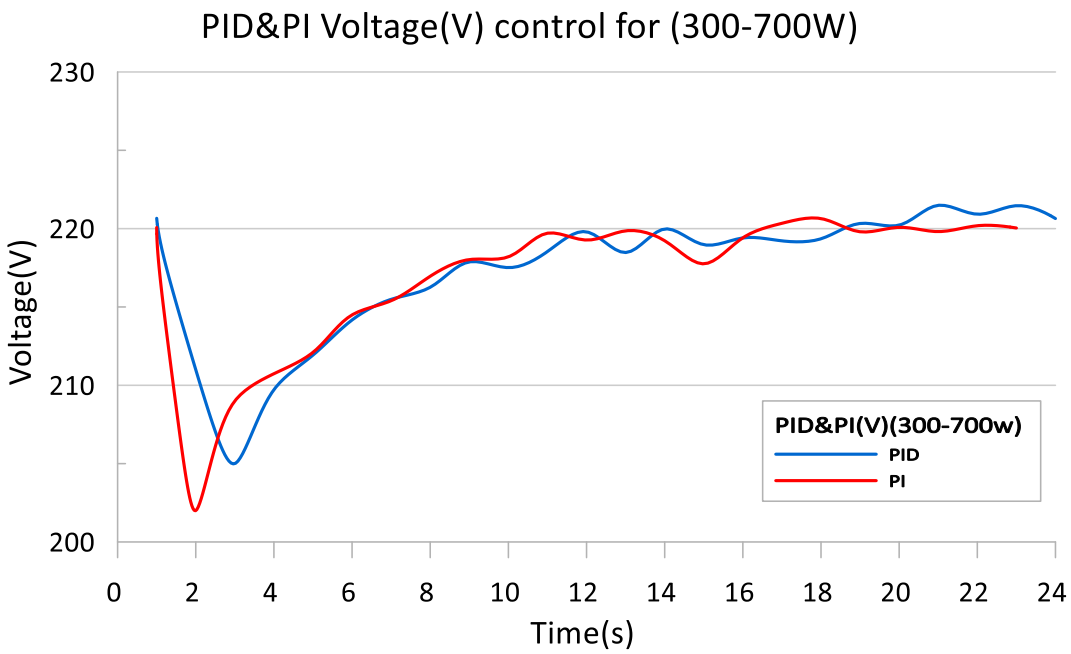

Figure 4.38. 300-700W V-t graph.

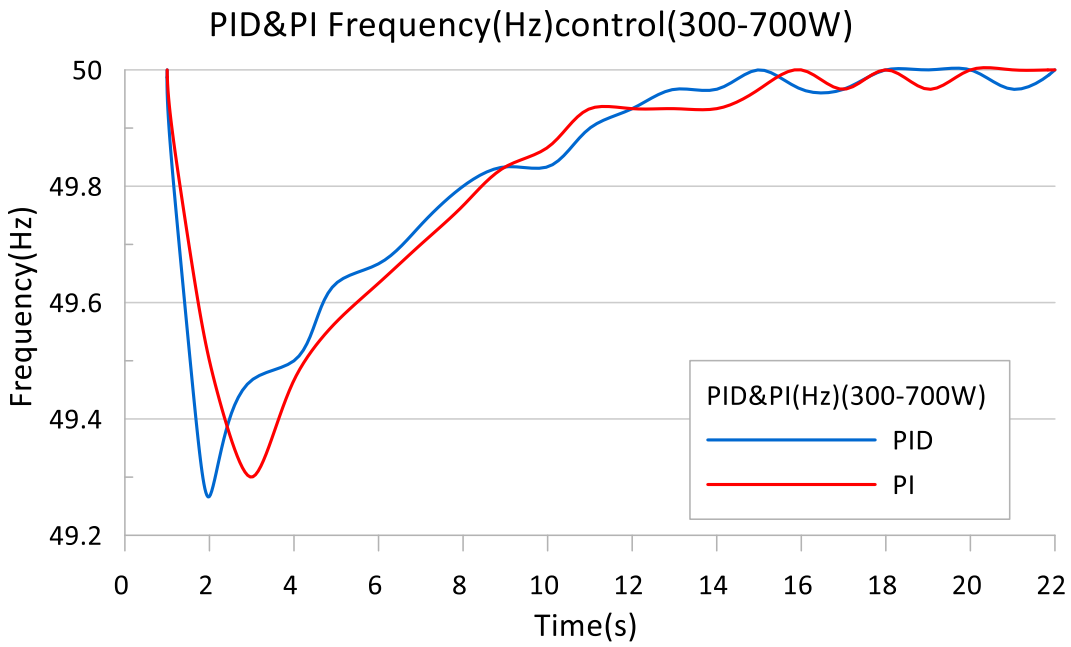

Figure 4.39. 300-700W f-t graph.

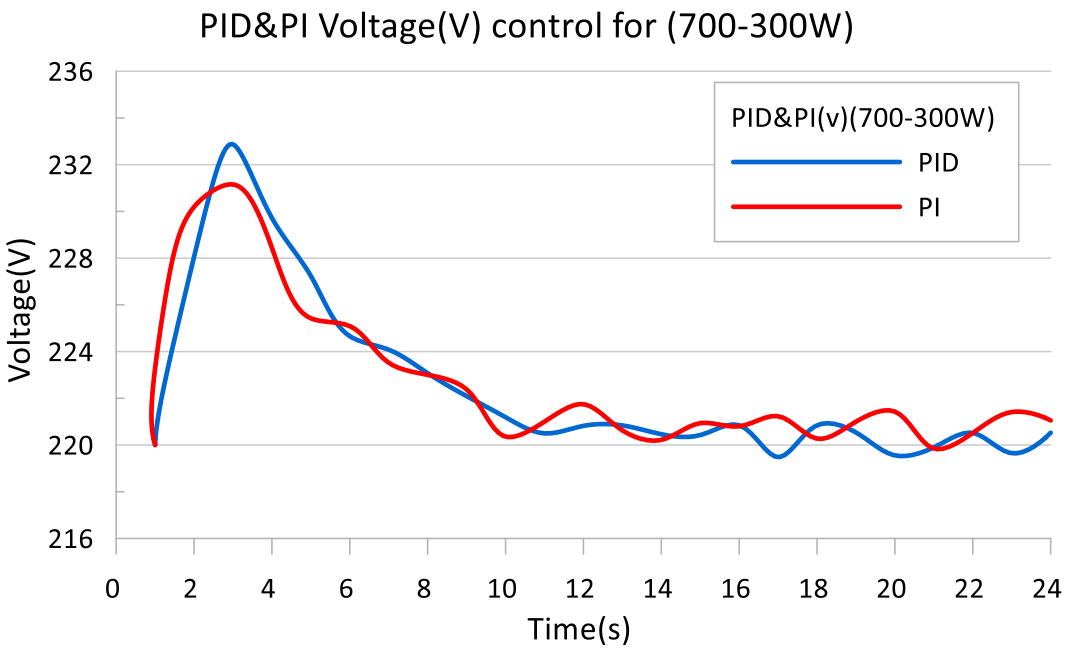

Figure 4.40. 700-300W V-t graph.

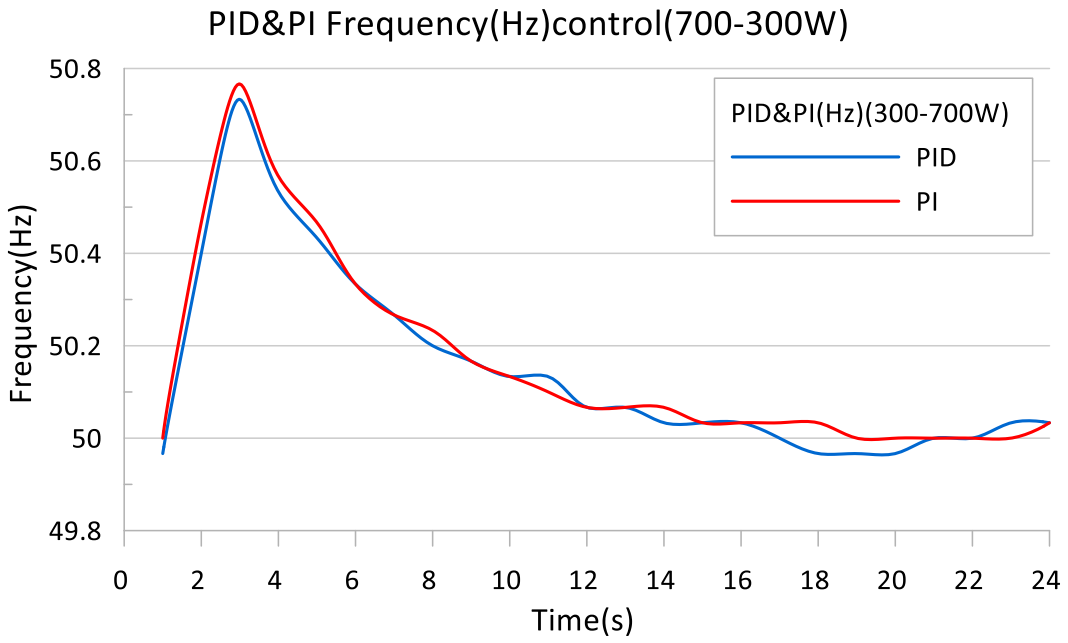

Figure 4.41. 700-300W f-t graph.

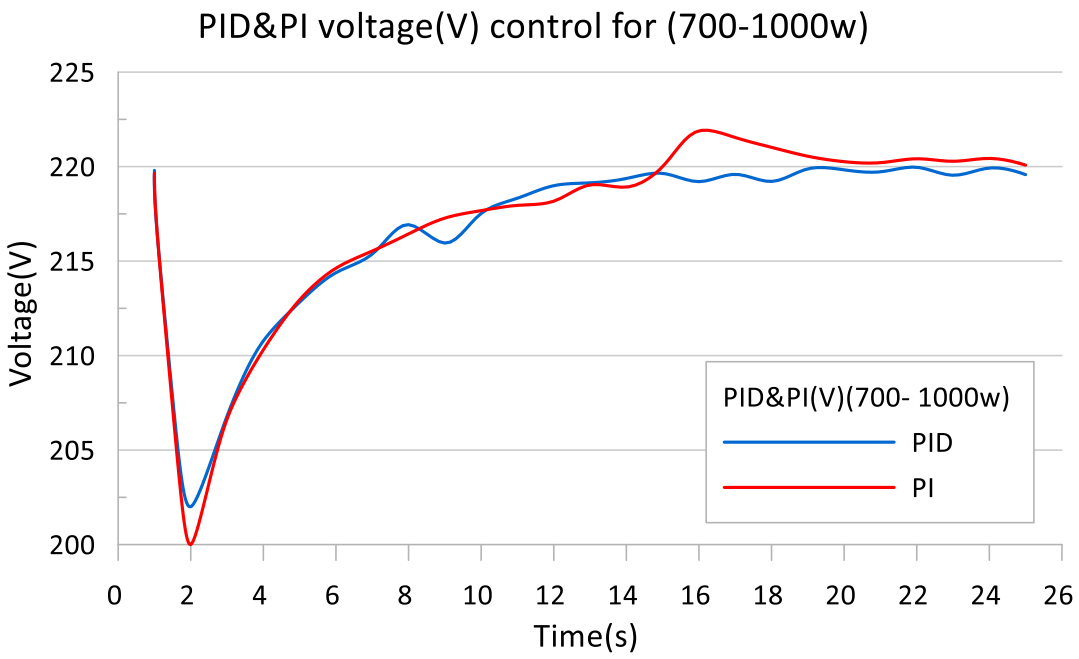

Figure 4.42. 700-1000W V-t graph.

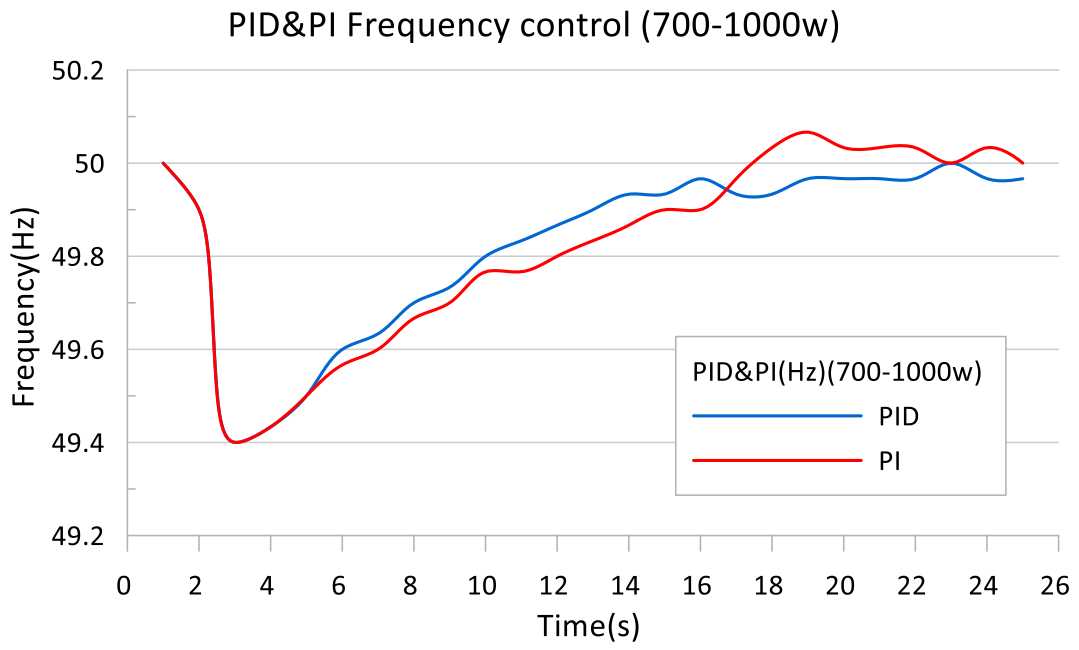

Figure 4.43. 700-1000W f-t graph.

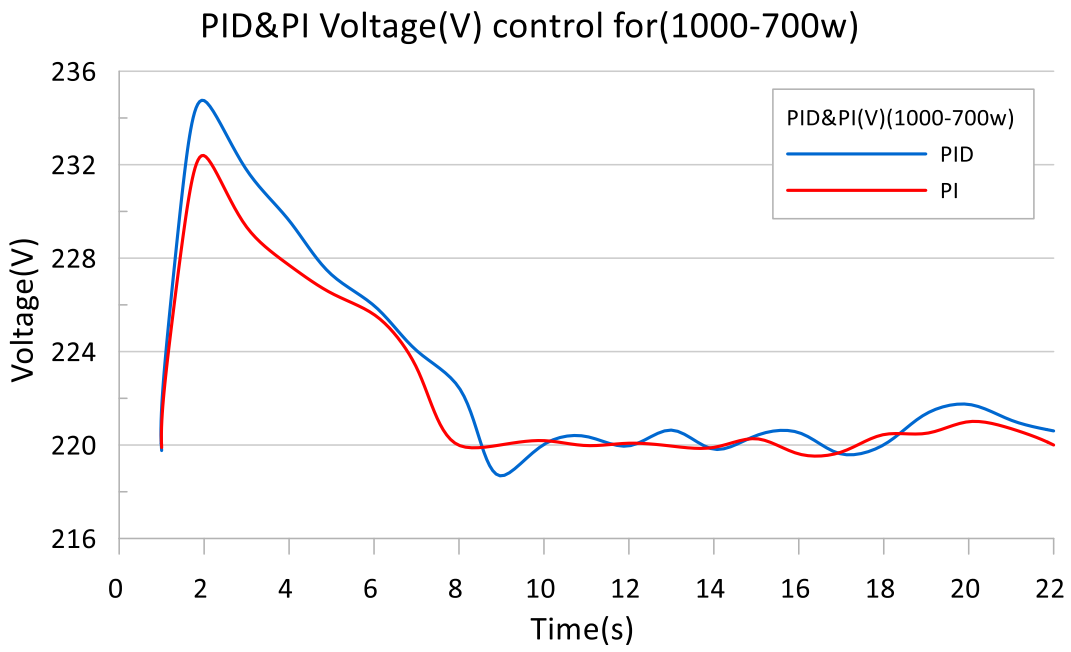

Figure 4.44. 1000-700W V-t graph.

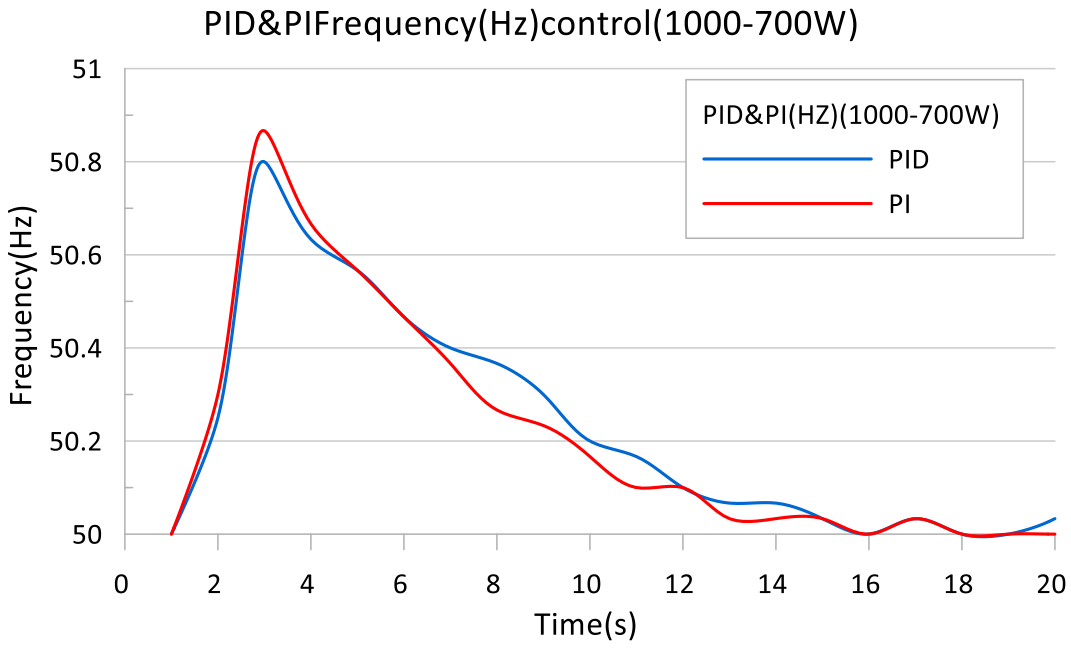

Figure 4.45. 1000-700W f-t graph.

The experiments were conducted in the form of loading and unloading the SG once the frequency and voltage were brought to the set values (50Hz, 220V) when the SG was unloaded. The graphs of the experiments with resistive loads were examined and

as expected, while the amount of load was increased, the frequency and voltage values were observed to be moving further away from the set value at first. It was seen that the frequency and voltage were brought to the acceptable value range of (49-51Hz, 217-223V) within 5-10 seconds. Set values were reached in maximum 20 seconds.

PID and PI control modes gave close results in our experiments. It was observed that the amount of overshoot and undershoot in the first loading and unloading of the SG was found to be higher in the PI control mode as compared to the PID control mode. The settling times for PID and PI control modes were found to be very close to each other. Steady-state error was zero or small enough to be accepted as zero for both control modes.

4.6.2. Inductive Reactive Load Experiments

As inductive reactive load, an induction motor of 0.18kW having cosφ value of 0.69 and an asynchronous motor of 1kW, having cosφ value of 0.80 were used as seen in Figure 4.46. Frequency and voltage control for 4 different inductive reactive loads at 0-294VA (pF=0.20), 294-0VA (pF=0.20), 0-455VA (pF=0.78), 455-0VA (pF=0.78), 0-650VA (pF=0.19), 650-0VA (pF=0.19) and 0-800VA (pF=0.94), 800-0VA (pF=0.94) values were carried out separately for PID and PI control types, by operating the motors alone and together with lamp groups.

Figure 4.46. Inductive loads.

Graphs obtained from inductive reactive load experiments are given in Figure 4.47-4.62.

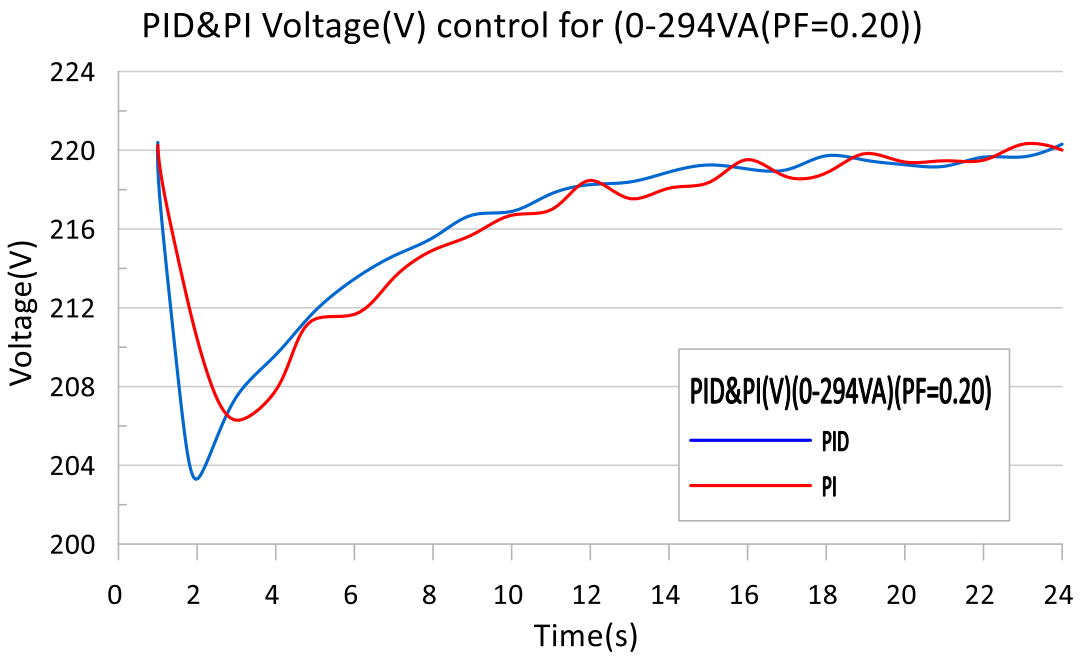

Figure 4.47. 0-294VA V-t graph.

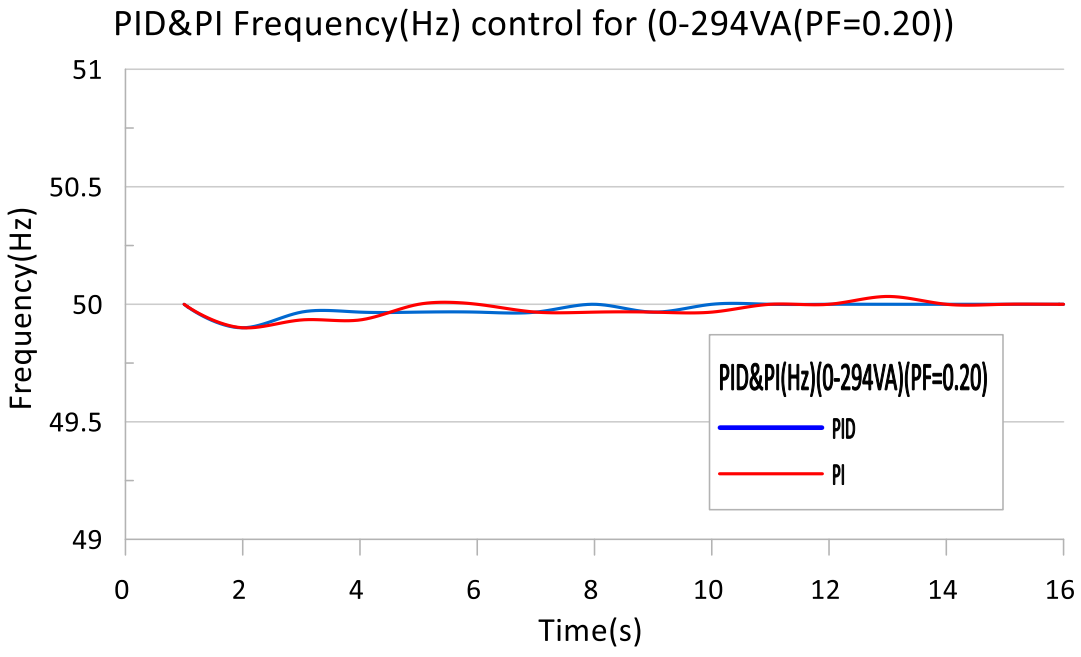

Figure 4.48. 0-294VA f-t graph.

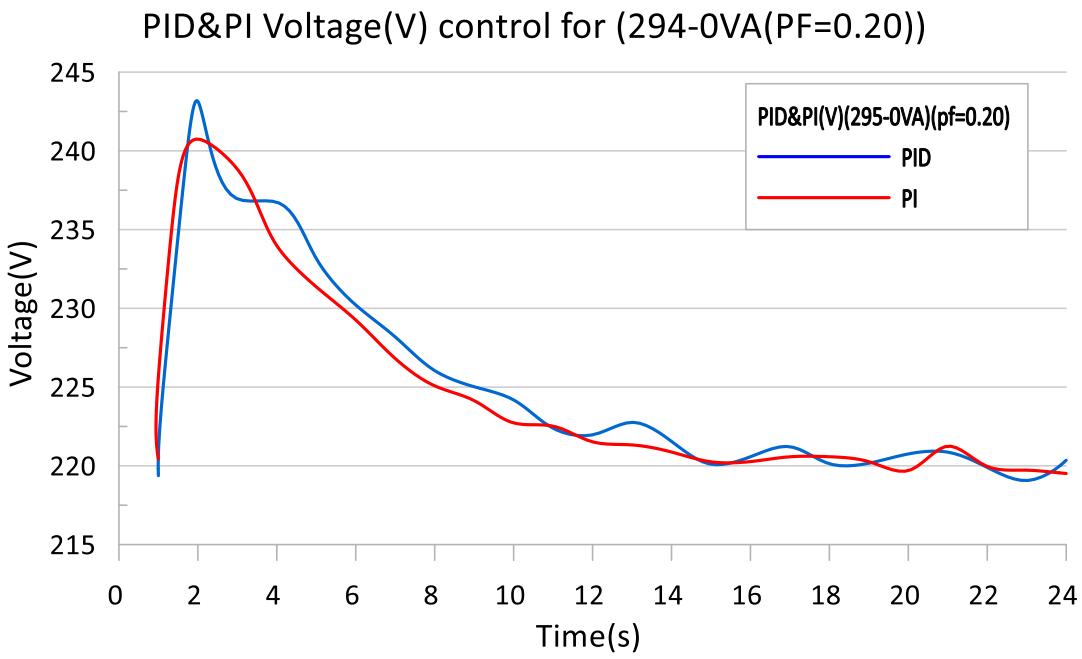

Figure 4.49. 294-0VA V-t graph.

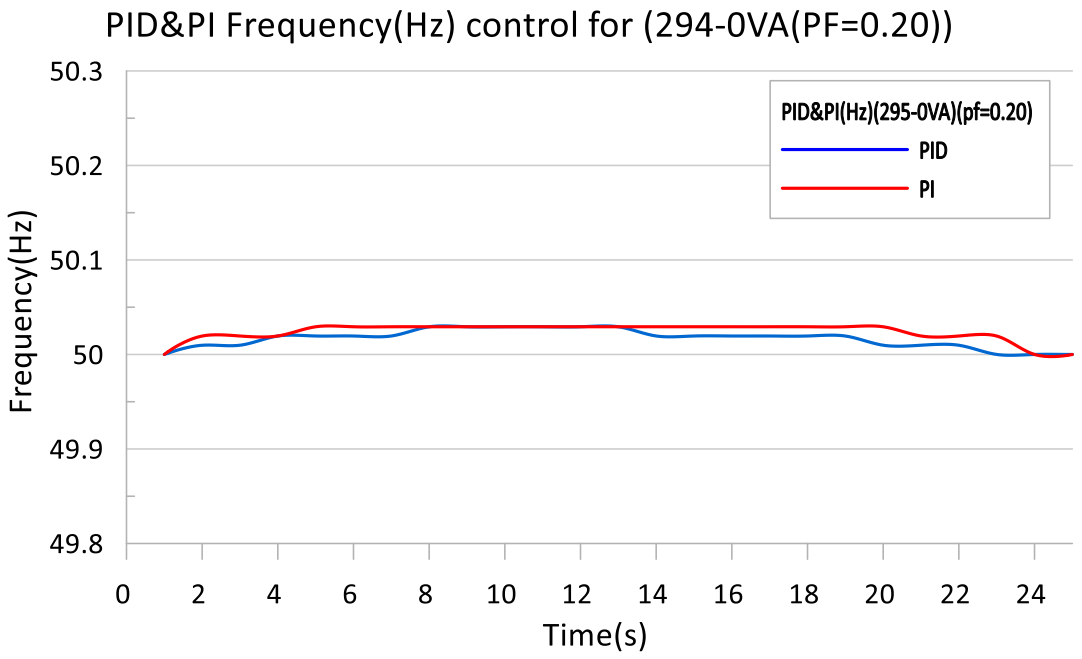

Figure 4.50. 294-0VA f-t graph.

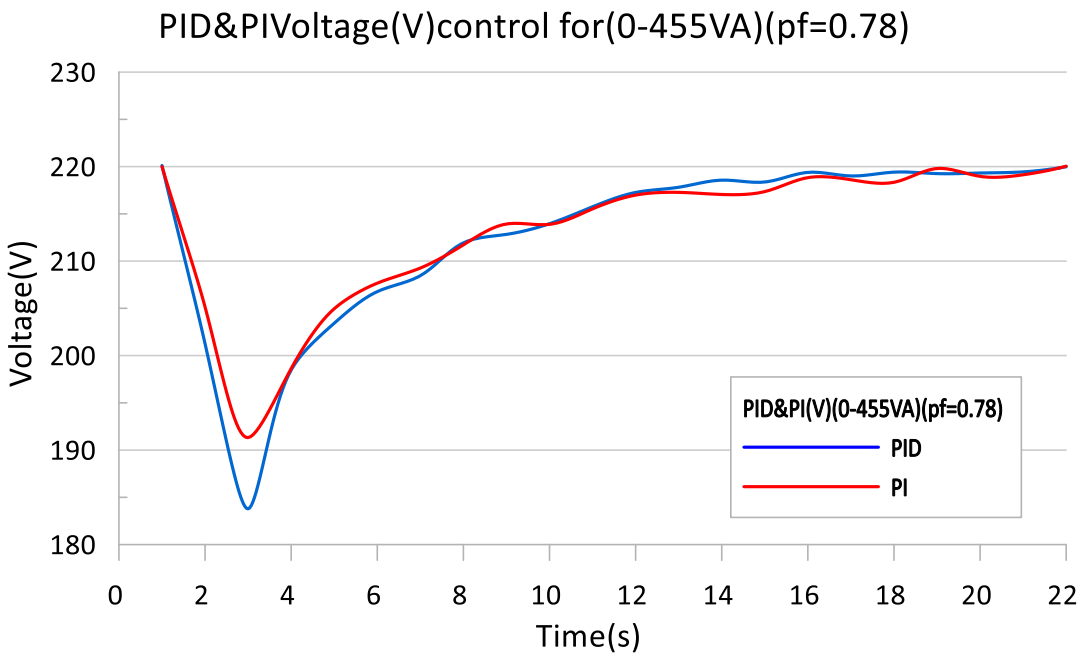

Figure 4.51. 0-455VA V-t graph.

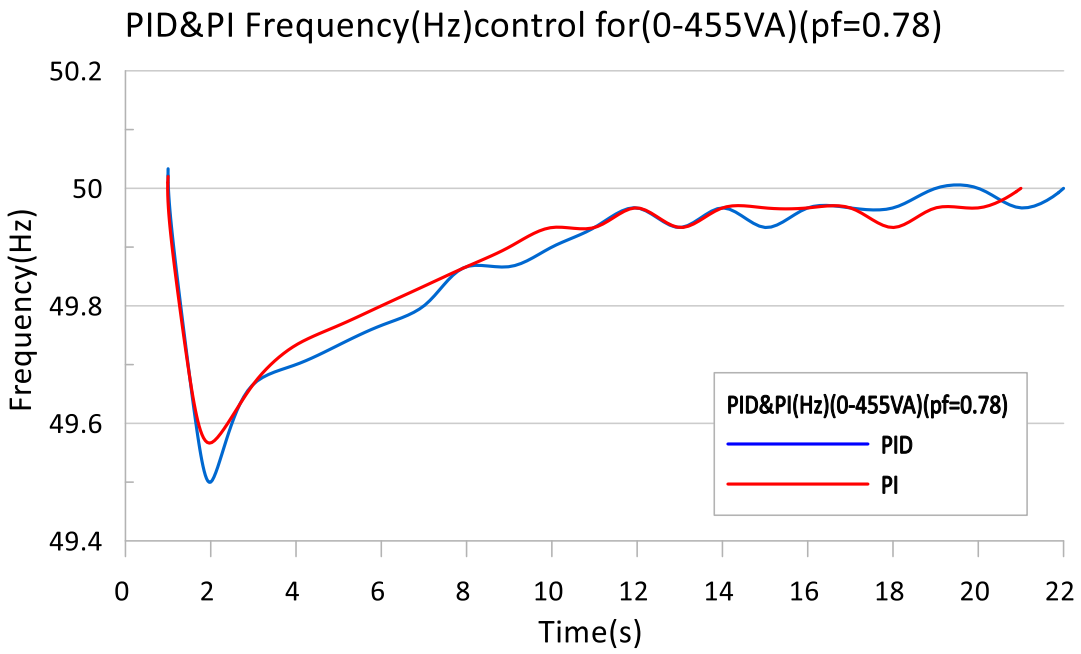

Figure 4.52. 0-455VA f-t graph.

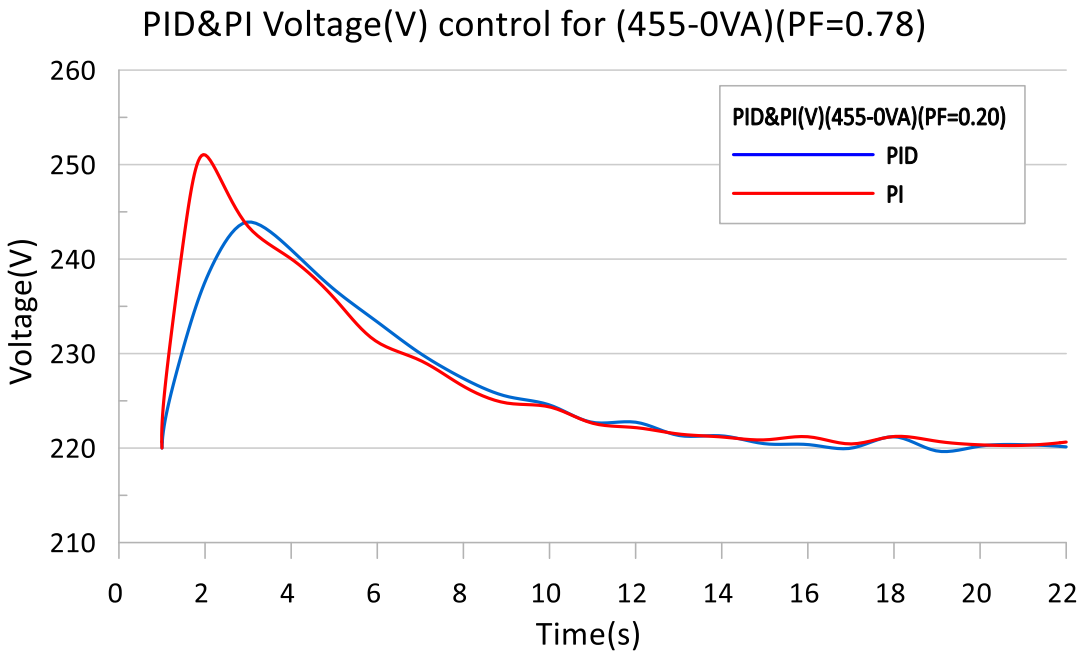

Figure 4.53. 455-0VA V-t graph.

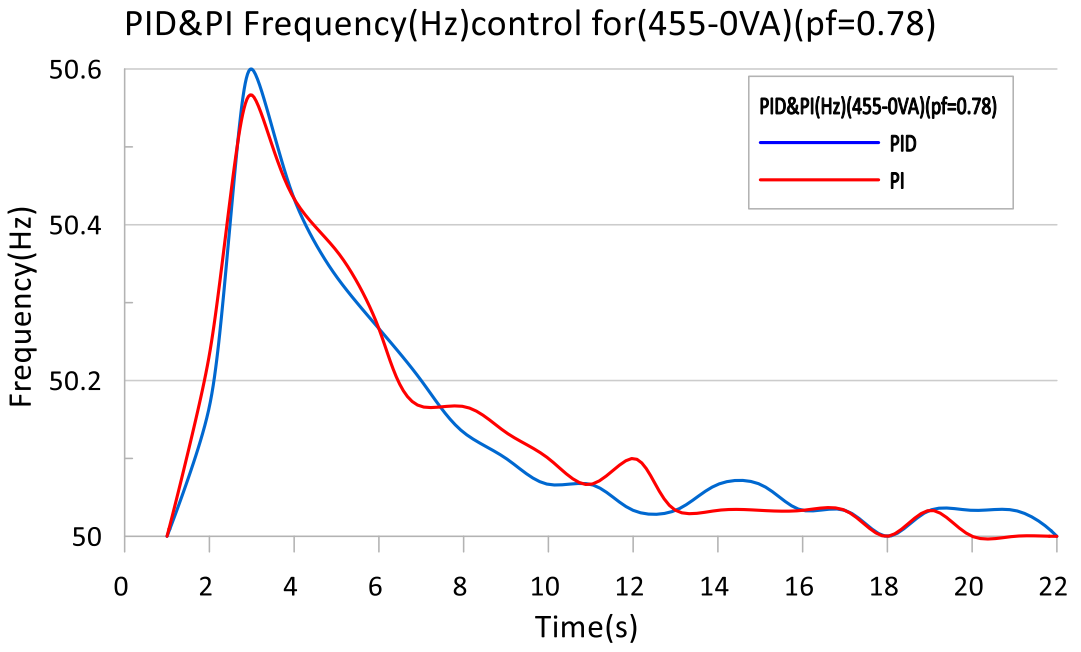

Figure 4.54. 455-0VA f-t graph.

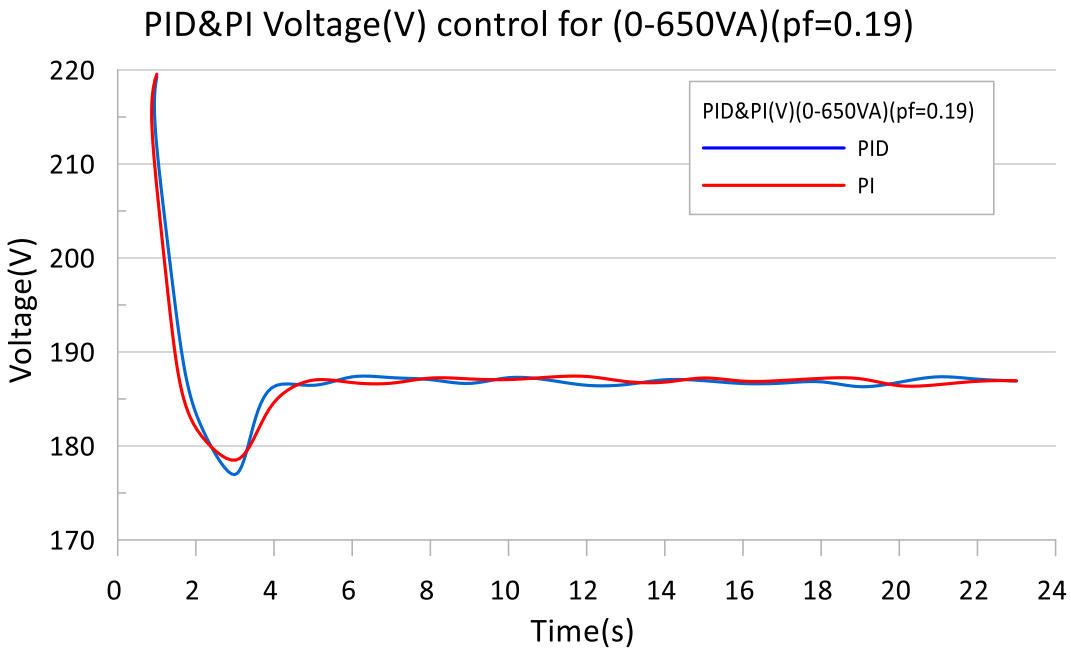

Figure 4.55. 0-650VA V-t graph.

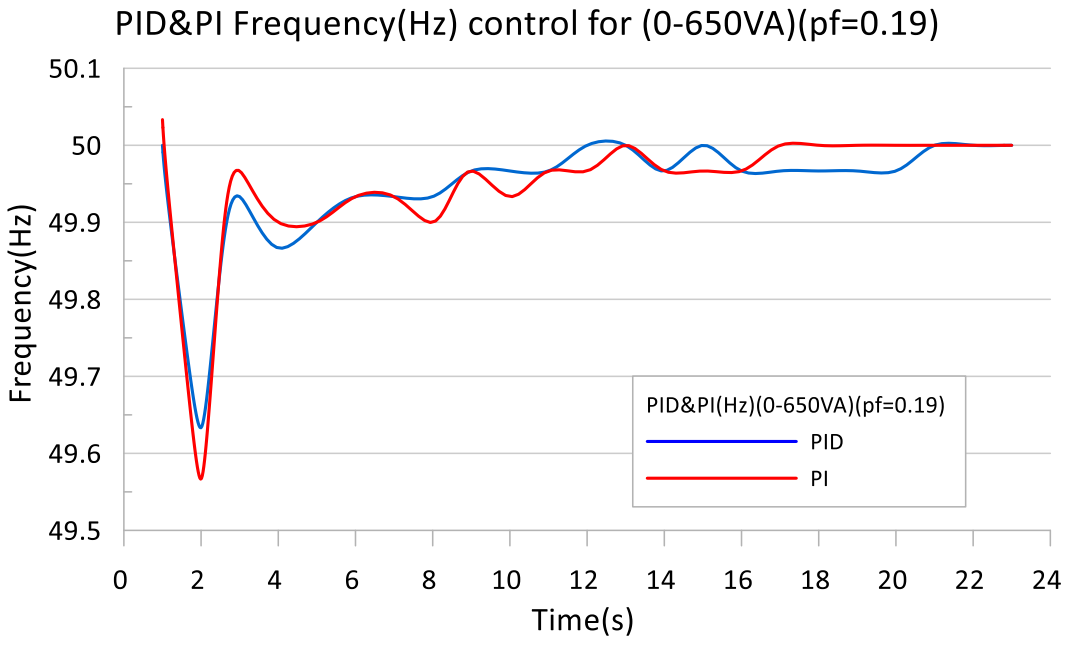

Figure 4.56. 0-650VA f-t graph.

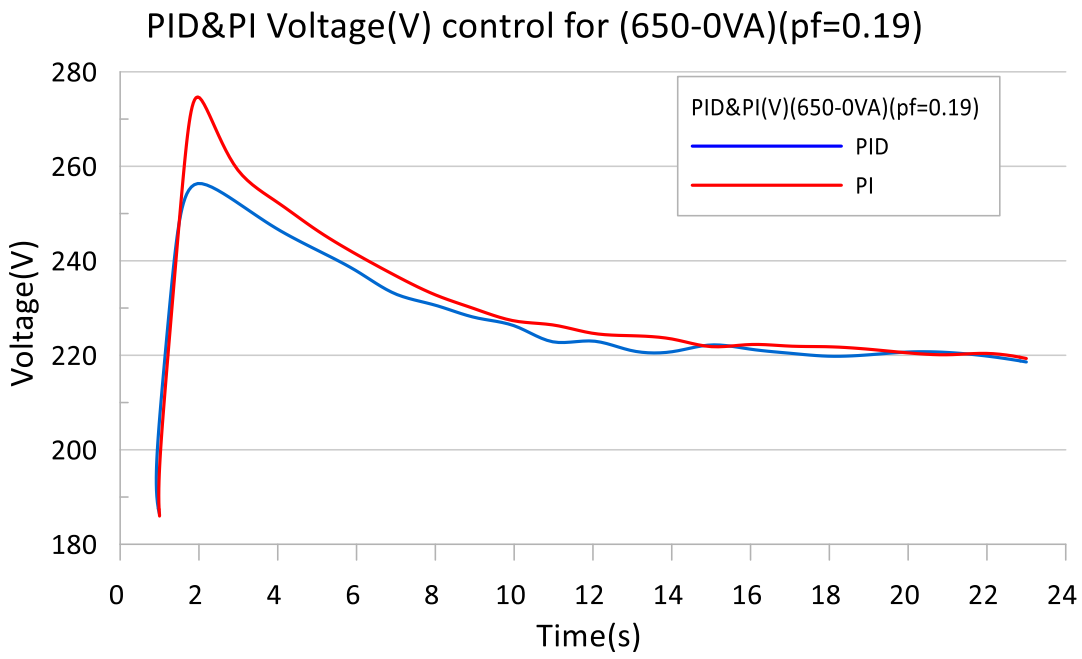

Figure 4.57. 650-0VA V-t graph.

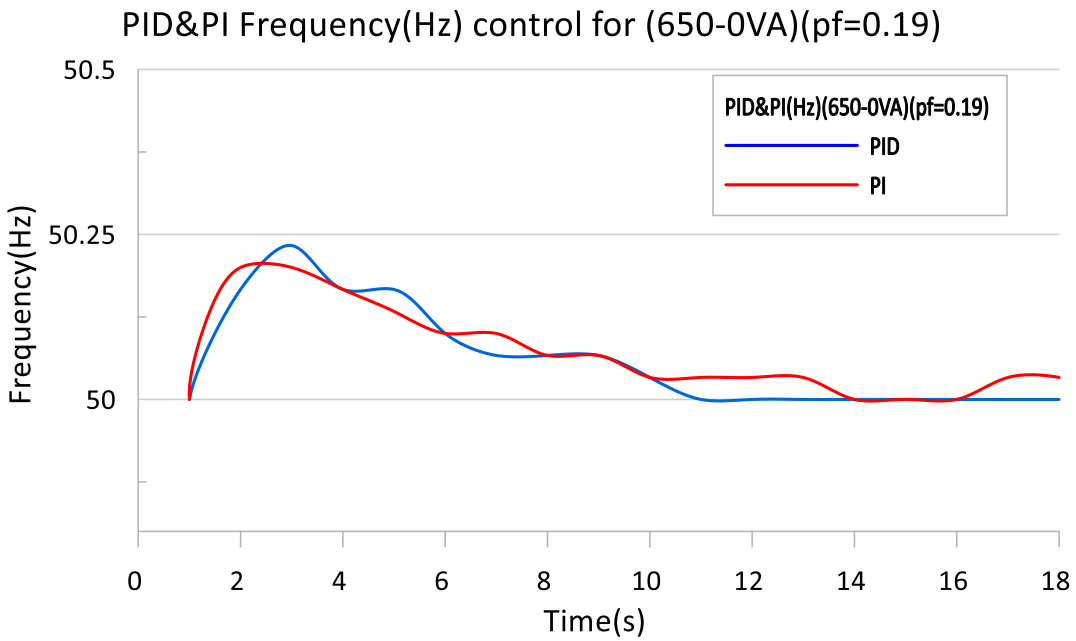

Figure 4.58. 650-0VA f-t graph.

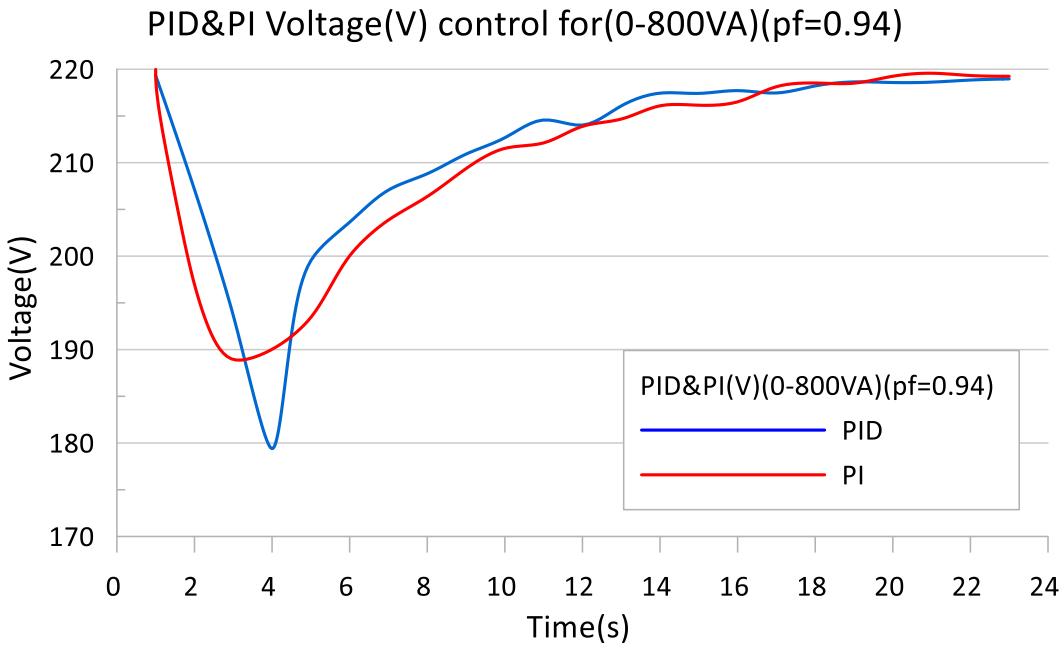

Figure 4.59. 0-800VA V-t graph.

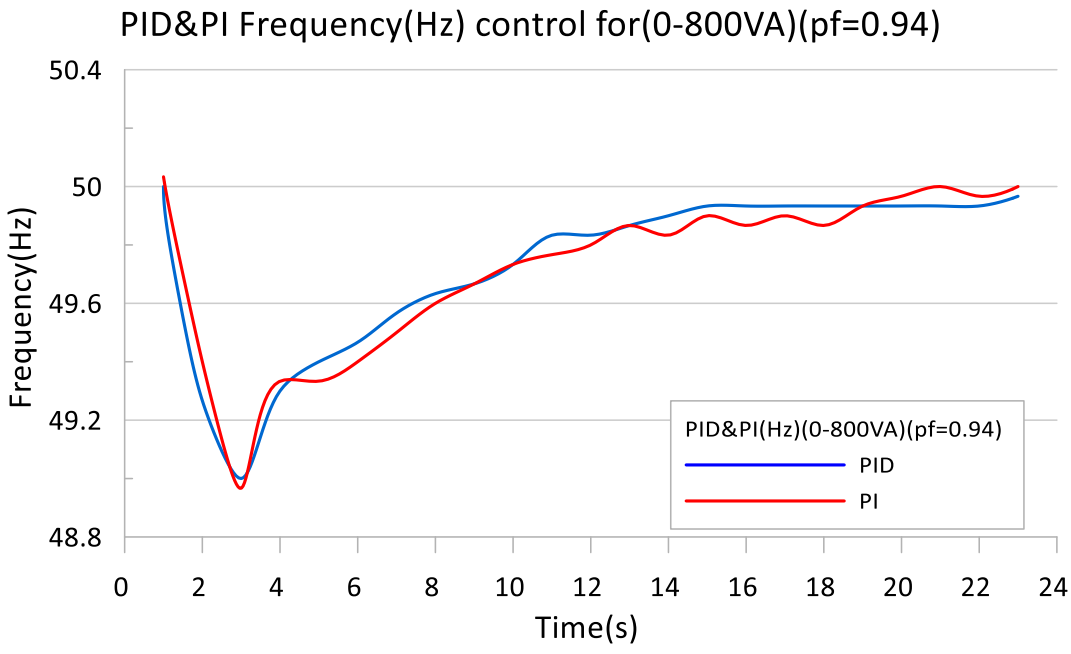

Figure 4.60. 0-800VA f-t graph.

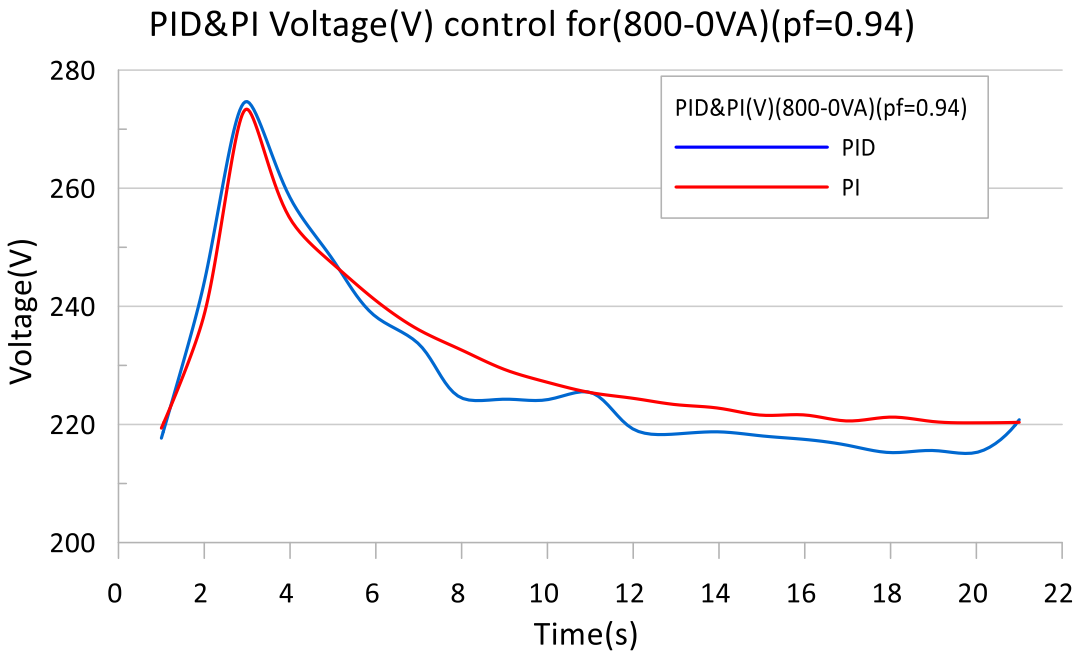

Figure 4.61. 800-0VA V-t graph.

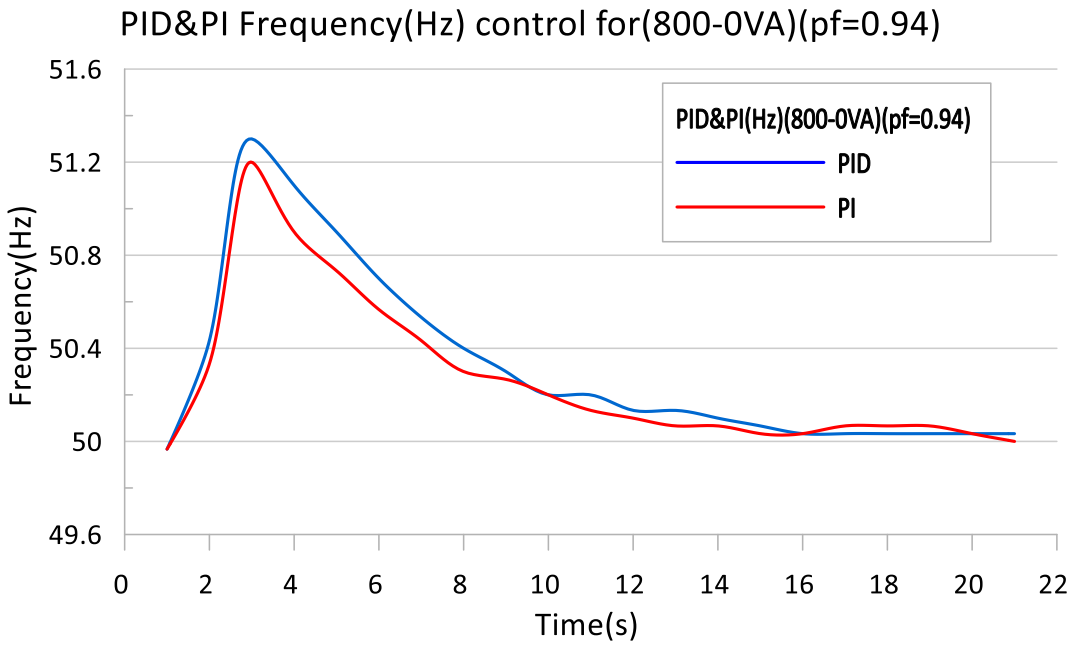

Figure 4.62. 800-0VA f-t graph.

As in resistive load experiments, inductive-reactive load experiments were carried out as loading and unloading of SG after being brought to frequency and voltage set values of 50Hz, 220V when SG was unloaded.

In the inductive reactive load experiments as well, similar results to the resistive load experiments were obtained for PID and PI control modes in terms of overshoot, undershoot, settling time and steady state.

In the 0-650VA (pF=0.19) experiment, the voltage could not reach the set value and a steady state occurred at 186V. Because, as the inductive reactive load increases, which is explained in Chapters 3.4 and 3.5, more excitation current must be drawn in order to bring the voltage to its nominal value. Although the excitation current was drawn 25% more than the nominal value, the terminal voltage of the SG could not exceed 186 V. This is because the power factor of the load was very small.

4.6.3. Capacitive Reactive Load Experiments

0.5 kVAR and 1 kVAR capacitors seen in Figure 4.63 were used as capacitive reactive load. The frequency and voltage control were conducted separately for PID and PI control types for 2 different inductive reactive loads at 0-550VA (pF=0.54), 550-0VA (pF=0.54) and 0-840VA (pF=0.83), 840-0VA (pF=0.83) values by operating capacitors together with lamp groups.

Figure 4.63. Capacitive loads.

Graphs obtained from capacitive-reactive load experiments are given in Figure 4.64-4.71.

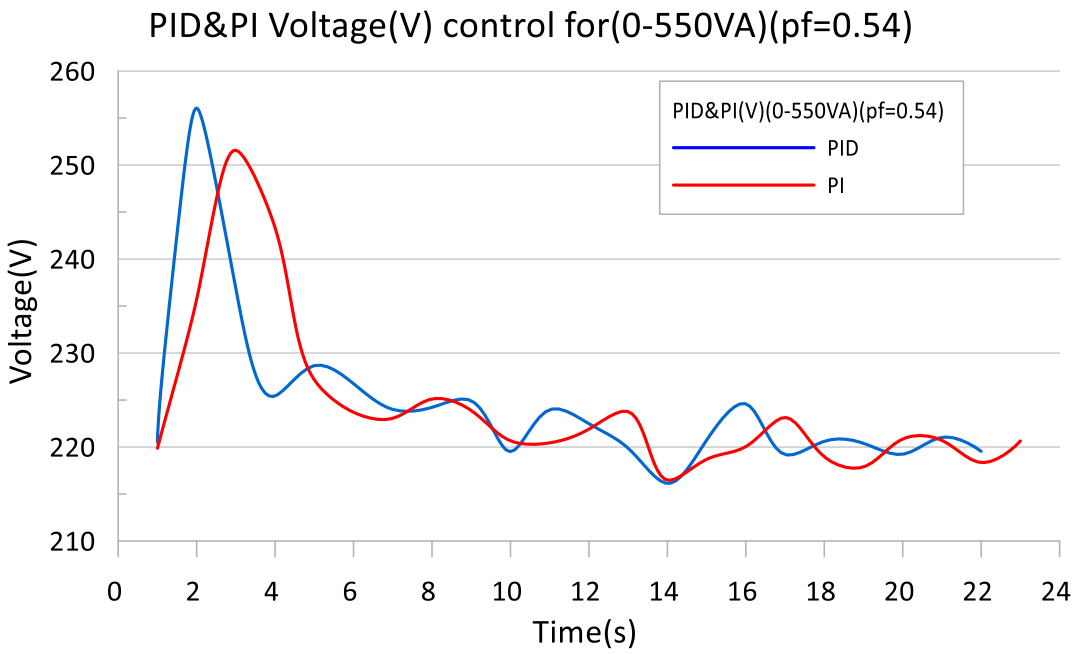

Figure 4.64. 0-550VA V-t graph.

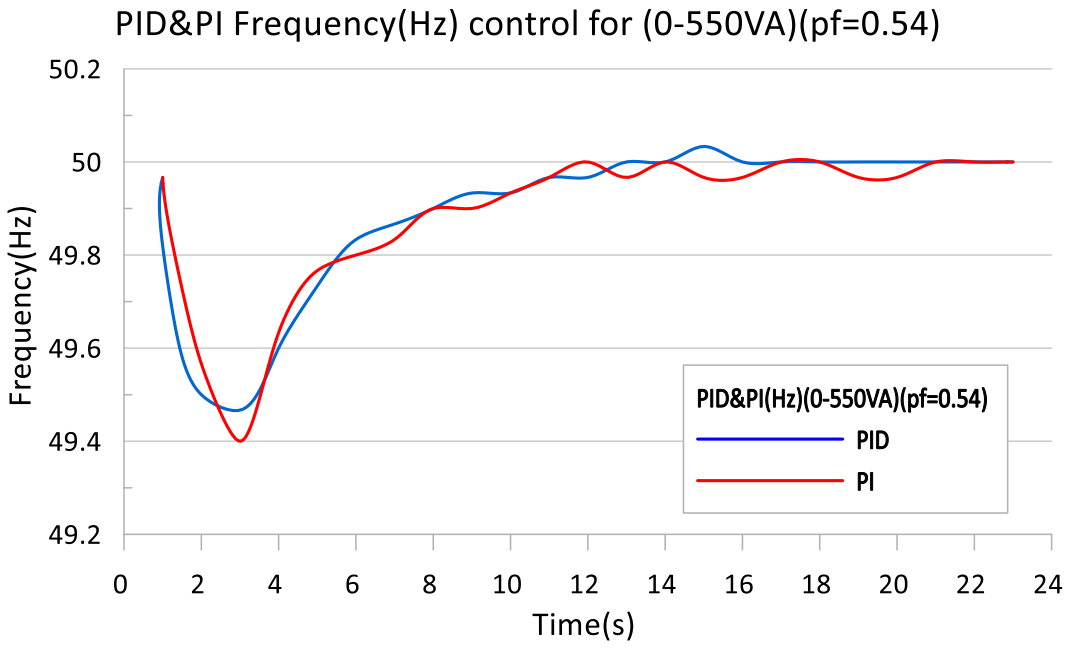

Figure 4.65. 0-550VA f-t graph.

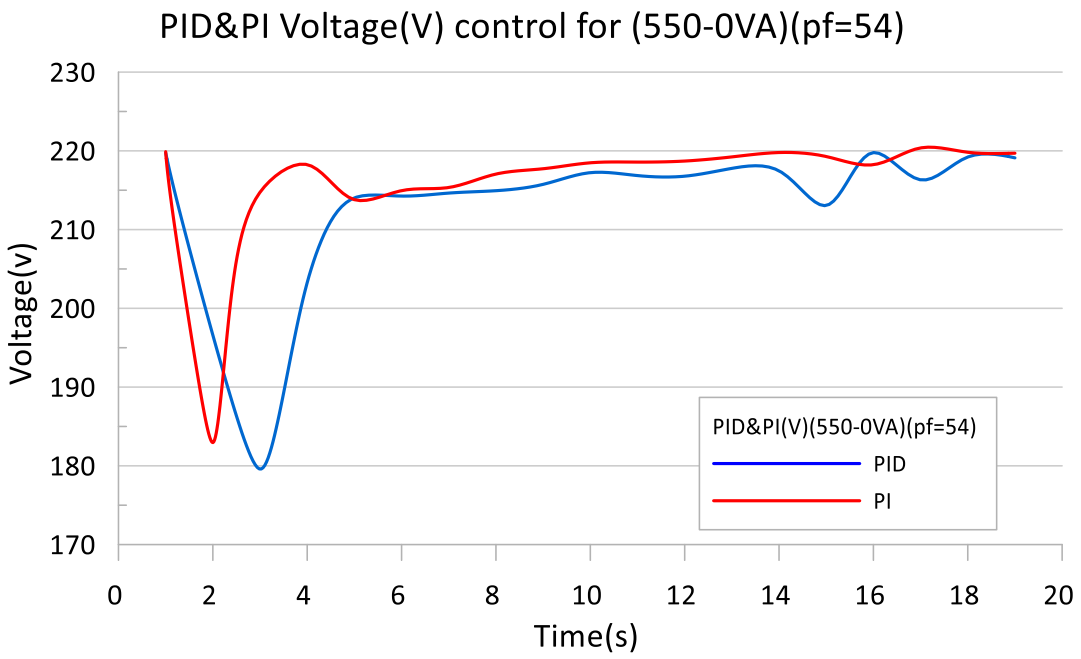

Figure 4.66. 550-0VA V-t graph.

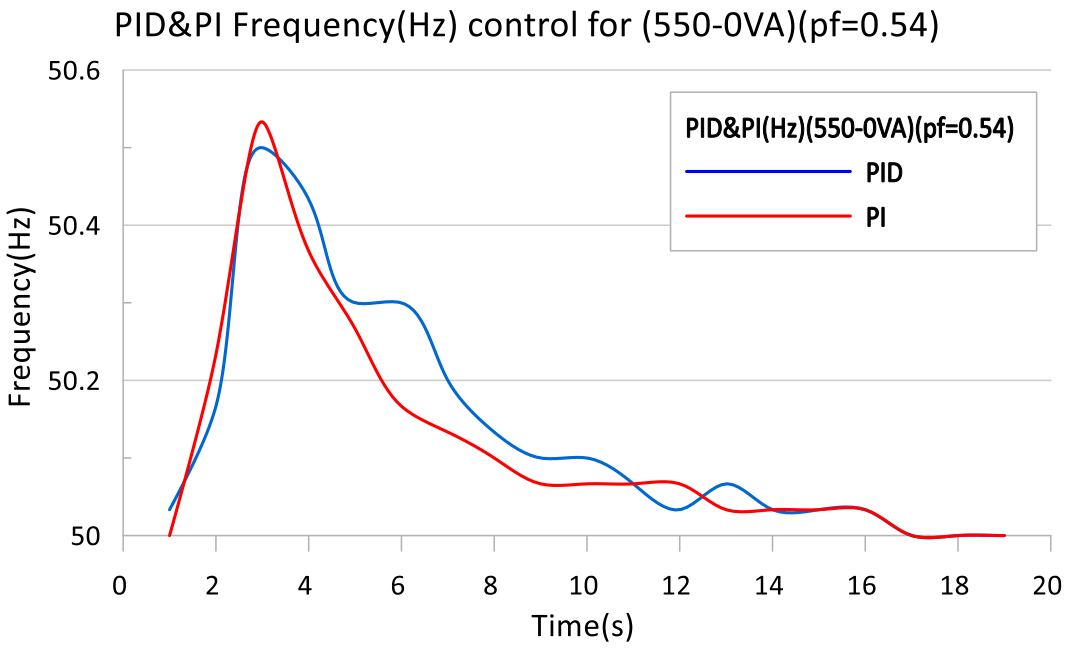

Figure 4.67. 550-0VA f-t graph.

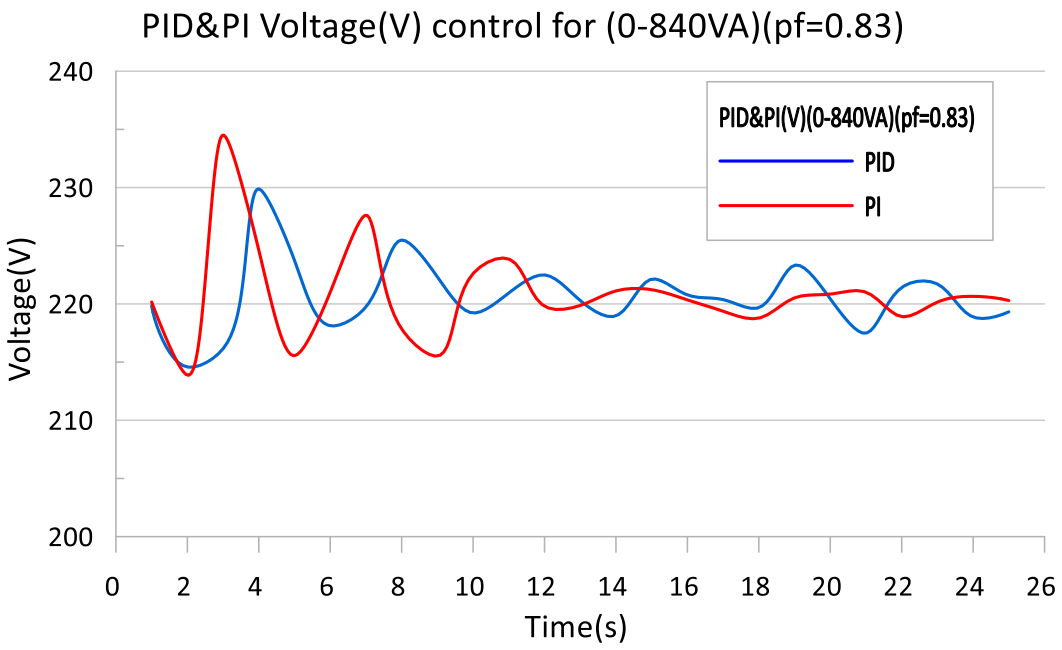

Figure 4.68. 0-840VA V-t graph.

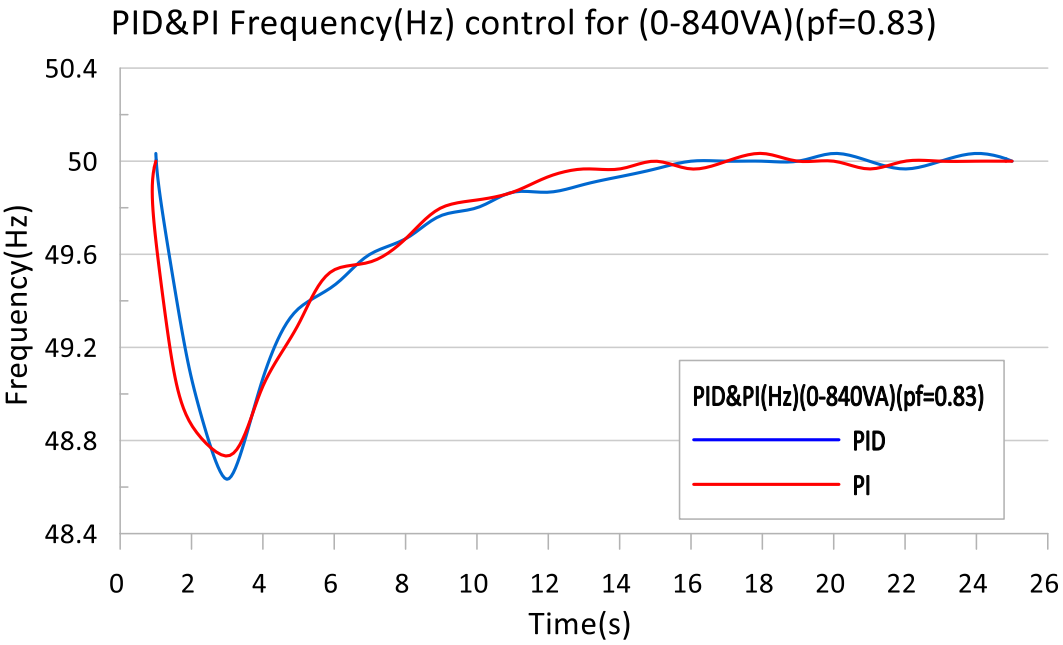

Figure 4.69. 0-840VA f-t graph.

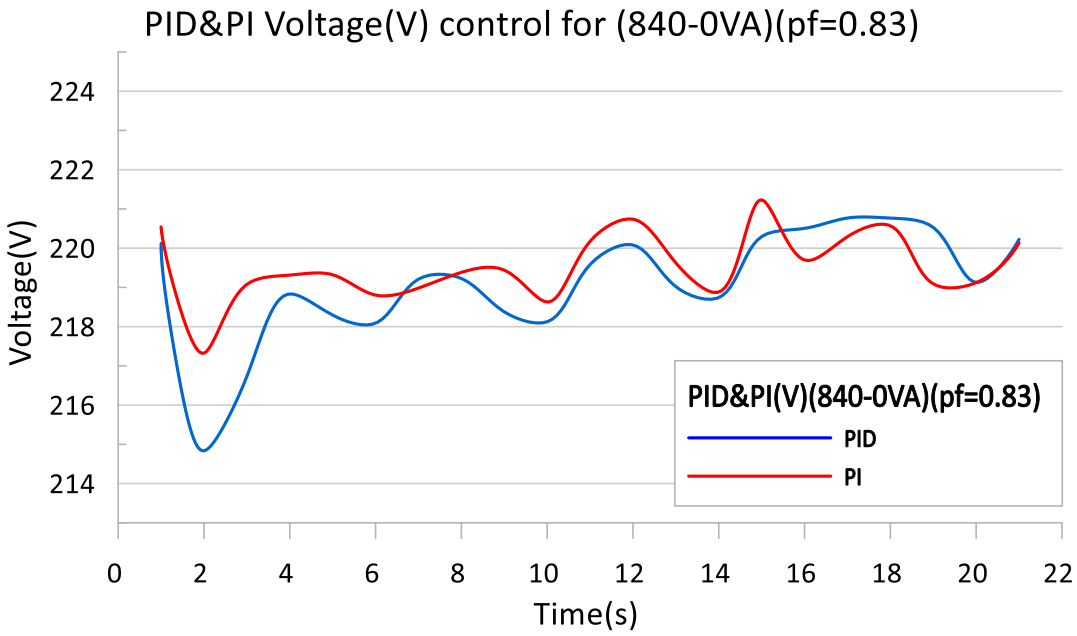

Figure 4.70. 840-0VA V-t graph.

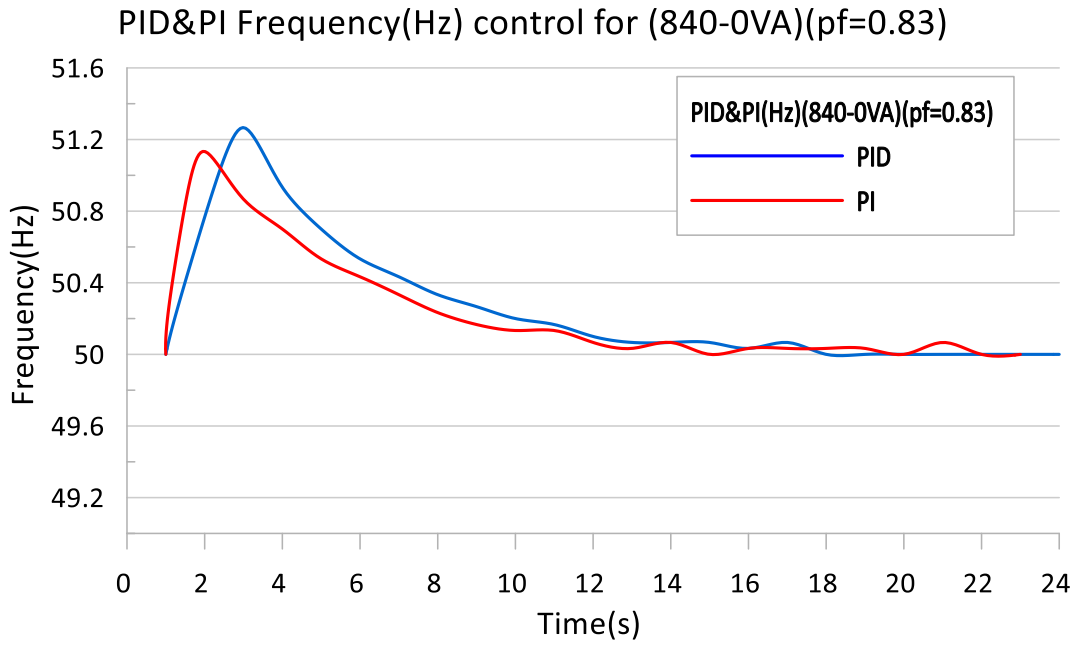

Figure 4.71. 840-0VA f-t graph.

Capacitive-reactive load experiments, as in resistive load and inductive-reactive load experiments, were performed as loading and unloading of SG after being brought to frequency and voltage set values of 50Hz, 220V when SG was unloaded.

As in resistive and inductive reactive load experiments, similar results were obtained in capacitive reactive load experiments in terms of overshoot, undershoot, settling time and steady state for PID and PI control modes.

Voltage stabilization could not be achieved when a pure capacitive load (0.5 kVAR or 1 kVAR) was connected to the SG. This can be explained by the equivalent circuit and phasor diagrams described in Chapters 3.6 and 3.7. For this reason, pure capacitive load graphs are not included here. Capacitive reactive loads at different cosφ values were used by charging the lamp groups together with the capacitors.

CHAPTER 5

CONCLUSIONS AND SUGGESTIONS

In this thesis, the frequency and voltage control of a stand-alone SG has been carried out. Frequency-time and voltage-time graphs were obtained for PID and PI control modes for resistive, inductive-reactive and capacitive-reactive loads with different values. In addition, experiments were carried out to derive the equivalent circuit of SG.

The experiments were conducted in the form of loading and unloading at 0-300W, 300-0W, 0-540W, 540-0W, 0-700W, 700-0W, 0-1000W, 1000-0W values for resistive loads, 0-294VA, 294-0VA, 0-455VA, 455-0VA, 0-650VA, 650-0VA, 0-800VA, 800-0VA values for inductive loads, and 0-550VA, 550-0VA, 0-840VA, 840-0VA values for capacitive loads, respectively.

It is seen that the frequency and voltage were brought to the acceptable value range (49-51Hz, 217-223V) within 5-10 seconds. Set values were reached in maximum 20 seconds, and PID and PI control modes gave close results. It is observed that the amount of overshoot and undershoot in the first loading and unloading moments of the SG was higher in the PI control mode as compared to the PID control mode. Settling times for PID and PI control modes were very close to each other. Steady-state error was zero or small enough to be accepted as zero for both control modes.

In the 0-650VA (pF=0.19) experiment, the voltage could not reach the set value and a steady state occurred at 186V. Voltage stabilization could not be achieved when a pure capacitive load (0.5 kVAR or 1 kVAR) was connected to the SG.

The thesis was initially planned to be conducted as the application of fuzzy-PID, fuzzy-

PI, ANN-PID and ANN-PI control modes using fuzzy logic (FL) and artificial neural network (ANN) together with traditional PID and PI control modes. However, FL and ANN could not be included in the study due to difficulties faced due to pandemic conditions and time constraints. In future studies, FL and ANN can also be included in the study and the results obtained from traditional PID and fuzzy-PID and/or ANN-PID can be compared. More data can be obtained by increasing the number of experiments. The obtained data can be used not only for frequency and voltage control, but also for estimating some parameters of SG, a non-linear machine, with artificial intelligence techniques.

REFERENCES

1. Kroposki B, Johnson B, Zhang Y, Gevorgian V, Denholm P, Hodge B-M, et al. Achieving a 100% renewable grid: Operating electric power systems with extremely high levels of variable renewable energy**.** ***IEEE Power Energy Magazine*** ; 15:61–73 (2017).

2. El-Hameed MA, Elkholy MM, El-Fergany AA. Efficient frequency regulation in highly penetrated power systems by renewable energy sources using stochastic fractal optimiser**.** ***IET Renew Power Generation*** ; 13:2174–2183 (2019).

3. Cagnano A, De Tuglie E, Mancarella P. Microgrids: Overview and guidelines for practical implementations and operation. ***Applied Energy***;258:114039 (2020).

4. Meng J, Wang Y, Peng J, Xu L, Yin J. Flexible virtual synchronous generator control for distributed generator with adaptive inertia. ***Electric Power Compon System***.;1–13 (2019).

5. Li W, Wang H, Jia Y, Yang S, Liu H. Frequency control strategy of grid-connected PV system using virtual synchronous generator. ***IEEE Innovative Smart Grid Technologies-Asia (ISGT Asia)***, 1618–1622 (2019).

6. Quan X, Zhao X, Zhang L, Xu R, Lei Y, Huang AQ. Novel power control of voltage- controlled inverters for grid inertia support. ***IEEE Applied Power Electronics Conference and Exposition (APEC)***, 927–931 (2019).

7. Alsiraji HA, El-Shatshat R. Comprehensive assessment of virtual synchronous machine based voltage source converter controllers. ***IET Generation, Transmission Distrib***,11:1762–1769 (2017).

8. J. Liu, Y. Miura, H. Bevrani, and T. Ise, "Enhanced Virtual Synchronous Generator Control for Parallel Inverters in Microgrids***," IEEE Transactions on Smart Grid***, 8(5): 2268-2277 (2017).

9. C.Andalib-Bin-Karim, X. Liang, and H. Zhang, "Fuzzy-Secondary-Controller-Based Virtual Synchronous Generator Control Scheme for Interfacing Inverters of Renewable Distributed Generation in Microgrids***," IEEE Transactions on Industry Applications,*** 54 (2):1047-1061(2018).

10. J. Gonzalez and W. Yu, “Non-linear system modelling using LSTM neural networks,” ***IFAC-PapersOnLine***, 51(13):485–489 (2018).

11. X. Meng, and W. Li, “An incremental neuronal-activity- based RBF neural network for nonlinear system modeling,” ***Neurocomputing,*** 302: 1–11 (2018).

12. S. B. Cooper and D. Di Maio, “Static load estimation using artificial neural network: Application on a wing rib,” ***Advances in Engineering Software***, 125:113–125 (2018).

13. P. Melin, I. Miramontes, and G. Prado-Arechiga, “A hybrid model based on modular neural networks and fuzzy systems for classification of blood pressure and hypertension risk diagnosis,” ***Expert Systems with Applications***, 107:146–164 (2018).

14. Q. Xu, X. Zhuo, C. Jiang, and Y. Liu, “An artificial neural network for mixed frequency data,” ***Expert Systems with Applications***,118: 127–139 (2019).

15. . Yang and J. Ma, “Feed-forward neural network training using sparse representation,” ***Expert Systems with Applications***,116:255–264 (2019).

16. B. Pournazarian, P. Karimyan, G.B. Gharehpetian, M. Abedi, and E. Pouresmaeil,“Smart participation of PHEVs in controlling voltage and frequency of island microgrids,” ***International Journal of Electrical Power & Energy Systems***.,110:510-522 (2019).

17. A. Gencer, "Modelling of operation PMSG based on fuzzy logic control under different load conditions," 2017 ***10th International Symposium on Advanced Topics in Electrical Engineering (ATEE), Bucharest***, 736-739 (2017).

18. A. Gencer., Modelling and control of permanent magnet synchronous generator based on three level NPC using fuzzy PI, ***Balkan Journal Of Electrıcal & Computer Engıneerıng***,6(3):171-177 (2018).

19. S. Bhamu, T.S. Bhatti “Coordinated Control Strategy of Distributed Energy Resources based Hybrid System for Rural Electrification,” ***International Journal of Renewable Energy Research***, 8(2):1189-1199 (2018).

20. S. Ekinci, A. Demiroren, H.L. Zeynelgil, S. Kaya, “Design of PID Controller for Automatic Voltage Regulator System through Kidney- inspired Algorithm,” ***GU J Sci, Part C***, 7(2):383-398 (2019).

21. Gungor B, Kaplan O ve Yalcın S.S., Artificial Neural Network Based Automatic Voltage Regulator for a Stand-Alone Synchronous Generator***, 8th International Conference on Renewable Energy Research and Applications***, 1032-1035 (2019).

22. A. Uysal, S. Gökay, E. Soylu, T. Soylu, S. Çaşka Fuzzy proportional-integral speed control of switched reluctance motor with MATLAB/Simulink and

programmable logic controller communication ***Measurement and Control***, 52(7-8) :1137–1144 (2019).

23. Hadžiselimović, M., Srpčič, G., Brinovar, I., Praunseis, Z., Seme, S., & ŠTumberger, B.. A novel concept of linear oscillatory synchronous generator designed for a stirling engine. ***Energy***, 180:19–27 (2019). **https://doi.org/10.1016/j.energy.2019.04.187**

24. Shengji, G. .An Excitation Control Strategy of Synchronous Generator Based on Fuzzy PID. ***13th International Conference on Measuring Technology and Mechatronics Automation (ICMTMA)***. (2021).**https://doi.org/10.1109/icmtma52658.2021.00092**

25. Hirase, Y., Abe, K., Sugimoto, K., Sakimoto, K., Bevrani, H., & Ise, T. A novel control approach for virtual synchronous generators to suppress frequency and voltage fluctuations in microgrids. ***Applied Energy***, 210:699–710 (2018). **https://doi.org/10.1016/j.apenergy.2017.06.058**

26. Geraldi, E. L., Fernandes, T. C., Piardi, A. B., Grilo, A. P., & Ramos, R. A. Parameter estimation of a synchronous generator model under unbalanced operating conditions. ***Electric Power Systems Research***, 187: 106487 (2020). **https://doi.org/10.1016/j.epsr.2020.106487**

27. Huda, J. K., Afandi, A. N., & Putranto, H. Analysis of Load Fluctuation Effect on the Excitation Current of the Three-Phase Synchronous Generator at the Diesel Power Plant. ***International Conference on Information and Communications Technology (ICOIACT)*** (2019). **https://doi.org/10.1109/icoiact46704.2019.8938560**

28. Sudjoko, R. I., & Darwito, P. A. Design and simulation of synchronous generator excitation system using buck converter at motor generator trainer model LEM-MGS. ***International Conference on Advanced Mechatronics, Intelligent Manufacture, and Industrial Automation (ICAMIMIA)*** (2017). **https://doi.org/10.1109/icamimia.2017.8387554**

29. Muñoz-Aguilar, R. S., Dòria-Cerezo, A., & Fossas, E. Extended SMC for a stand-alone wound rotor synchronous generator. ***International Journal of Electrical Power & Energy Systems***, 84:25–33 (2017). **https://doi.org/10.1016/j.ijepes.2016.04.052**

30. G, S. J., D, M. M., & K, T. (2021). Fuzzy logic based load frequency control of power system. Materials Today: ***Proceedings***, 45: 8170–8175. **https://doi.org/10.1016/j.matpr.2021.02.536**

31. Sanampudi, N., & Kanakasabapathy, P. Integrated voltage control and frequency regulation for stand-alone micro-hydro power plant. ***Materials Today***: (2021). **https://doi.org/10.1016/j.matpr.2020.10.403** ***Published***

32. da Silva, G. S., de Oliveira, E. J., de Oliveira, L. W., de Paula, A. N., Ferreira, J. S., & Honório, L. M.. Load frequency control and tie-line damping via virtual synchronous generator. ***International Journal of Electrical Power & Energy Systems***, 132: 107-108 (2021). **https://doi.org/10.1016/j.ijepes.2021.107108**

33. Wang, Y., Wang, H., Liu, W., & Wang, Q. Modeling and Analysis of a New Voltage Regulation Method for Surface-Mounted Permanent Magnet Synchronous Generator. ***IEEE 18th International Power Electronics and Motion Control Conference (PEMC),*** (2018).**https://doi.org/10.1109/epepemc.2018.8521986**

34. Fogli, G. A., de Almeida, P. M., & Barbosa, P. G. Modelling and control of an interface power converter for the operation of small diesel gen-sets in grid-connected and stand-alone modes. ***Electric Power Systems Research***, 150: 177–187 (2017). **https://doi.org/10.1016/j.epsr.2017.05.016**

35. Sang-Hoon Park, Jae-Sung Yu, Sang-Seuk Lee, Su-Won Lee, & Chung-Yuen Won. Output voltage control of synchronous generator for ships using a PMG type digital AVR. ***IEEE Energy Conversion Congress and Exposition*** (2009). **https://doi.org/10.1109/ecce.2009.5316195**

36. Mocanu, R., & Onea, A.. Simple adaptive voltage control of permanent magnet synchronous machine. 21st International Conference on System Theory, ***Control and Computing (ICSTCC)***, (2017). **https://doi.org/10.1109/icstcc.2017.8107027**

37. ShangGuan, X. C., He, Y., Zhang, C. K., Jin, L., Jiang, L., Wu, M., & Spencer, J. W. Switching system-based load frequency control for multi-area power system resilient to denial-of-service attacks. ***Control Engineering Practice***, 107: 104678 (2021). **https://doi.org/10.1016/j.conengprac.2020.104678**

38. Kassem, A. M., & Yousef, A. M. Voltage and frequency control of an autonomous hybrid generation system based on linear model predictive control. ***Sustainable Energy Technologies and Assessments***, 4: 52–61 (2013). **https://doi.org/10.1016/j.seta.2013.09.002**

39. Chang, Y.-C., Chang, H.-F., Dai, W.-F., & Wu, C.-W. Voltage regulation and maximum output power tracking of a 4.5kW permanent-magnet synchronous generator. ***International Power Electronics Conference (IPEC-Hiroshima 2014 - ECCE ASIA)*** (2014)**. https://doi.org/10.1109/ipec.2014.6869602**

40. Bevrani, H., Golpîra, H., Messina, A. R., Hatziargyriou, N., Milano, F., & Ise, T. Power system frequency control: An updated review of current solutions and new challenges. ***Electric Power Systems Research***, 194: 107_114 (2021). **https://doi.org/10.1016/j.epsr.2021.107114**

41. Chapman S. J., "Electric Machinery Fundamentals 4th ed.", ***Mc Graw Hill***, 267-290 (2005).

42. Internet: **https://hbogm.meb.gov.tr/MTAO/1ElektrikMakLab/unite7.pdf**

43. Internet**:https://support.industry.siemens.com/cs/document/100746401/pid-control-with-pid_compact-for-simatic-s7-1200-s7-1500?dti=0&lc=en-WW.**

APPENDIX A.

PARTS OF LADDER DIAGRAM

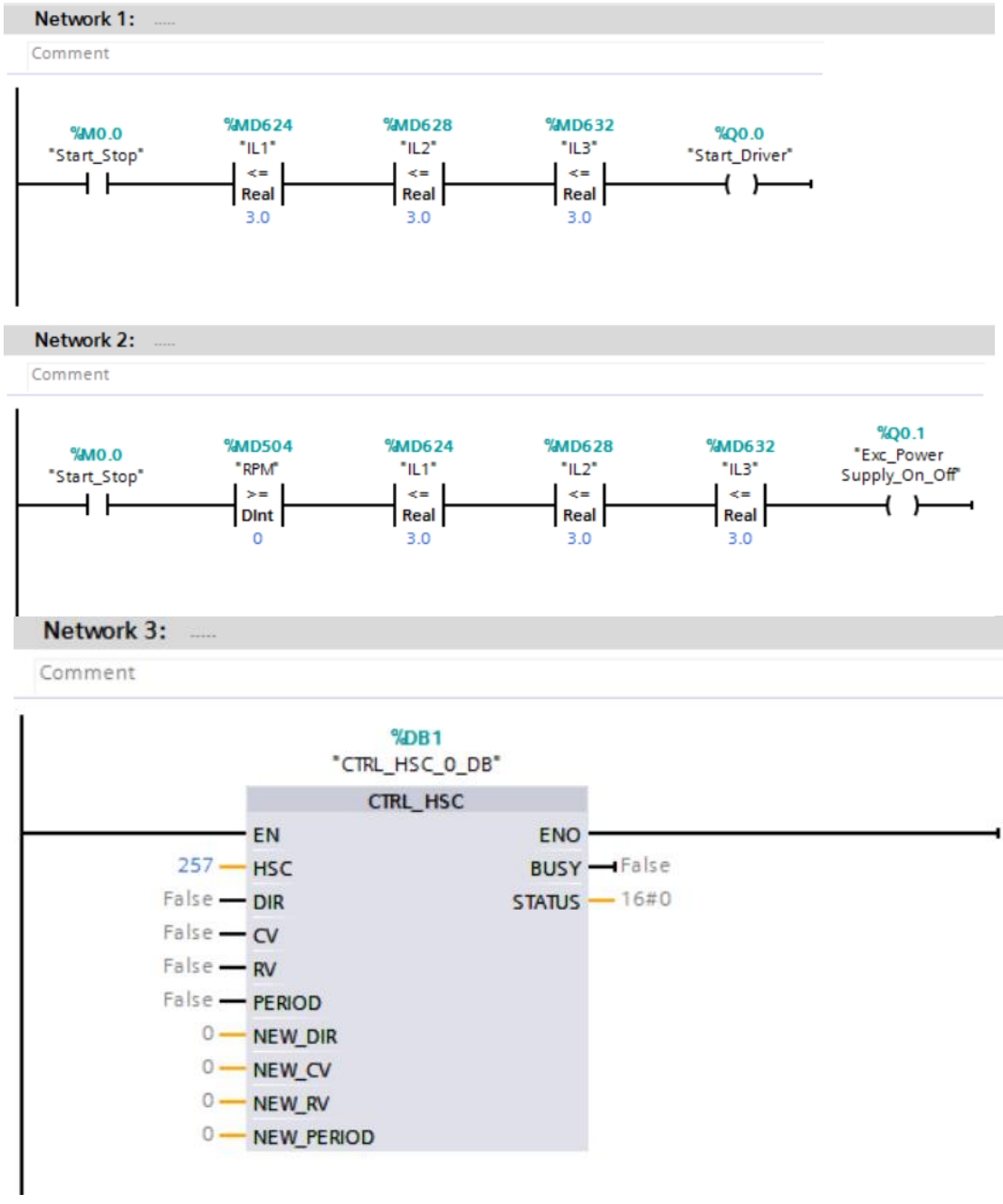
Network 1:
Comment
%M0.0
"Start_Stop"
%MD624
"IL1"
<=
Real
3.0
%MD628
"IL2"
<=
Real
3.0
%MD632
"IL3"
<=
Real
3.0
%Q0.0
"Start_Driver"
Network 2:
Comment
%M0.0
"Start_Stop"
%MD504
"RPM"
>=
DInt
0
%MD624
"IL1"
<=
Real
3.0
%MD628
"IL2"
<=
Real
3.0
%MD632
"IL3"
<=
Real
3.0
%Q0.1
"Exc_Power
Supply_On_Off"
Network 3:
Comment
%DB1
"CTRL_HSC_0_DB"
CTRL_HSC
EN
ENO
257
HSC
BUSY
False
False
DIR
STATUS
16#0
False
CV
False
RV
False
PERIOD
0
NEW_DIR
0
NEW_CV
0
NEW_RV
0
NEW_PERIOD

Network 4: .....

Comment

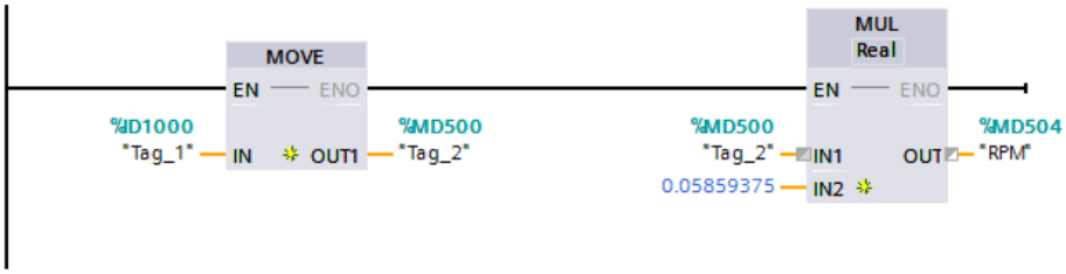

Network 5: .....

Comment

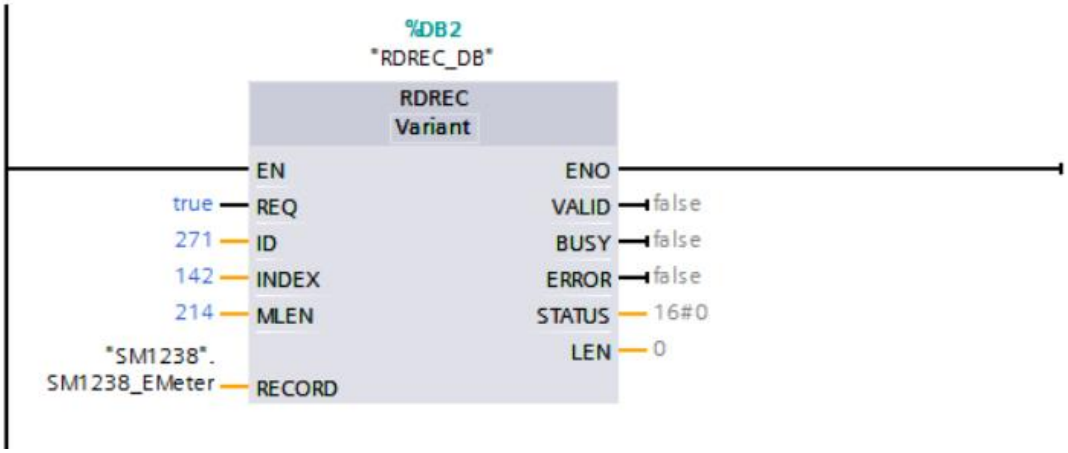

Network 13: .....

Comment

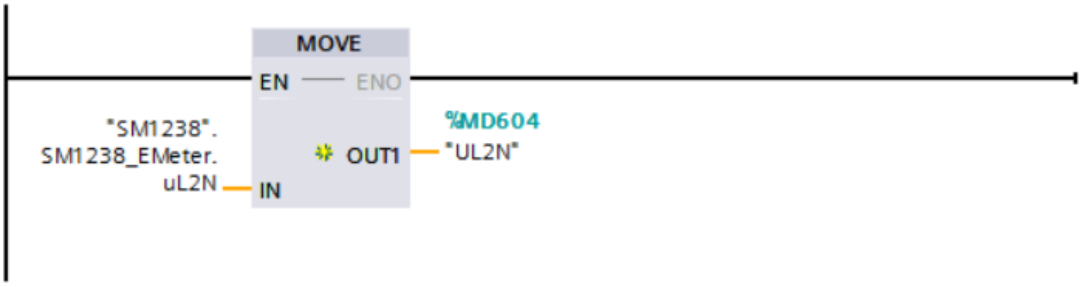

Network 14: .....

Comment

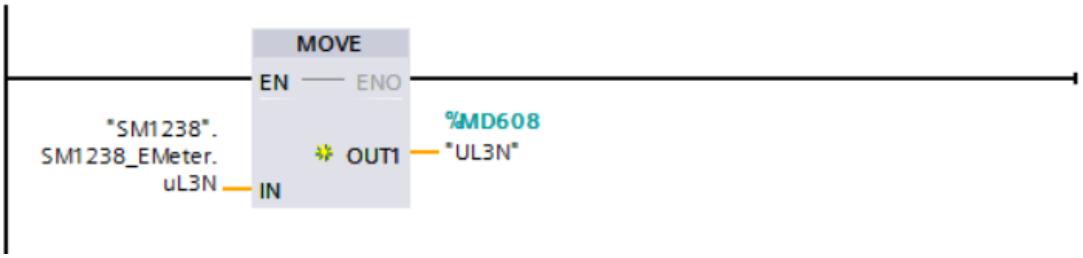

Network 15: .....

Comment

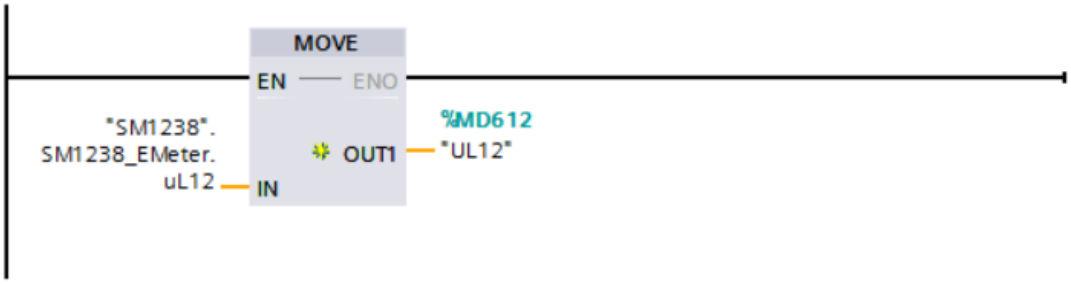

Network 16: .....

Comment

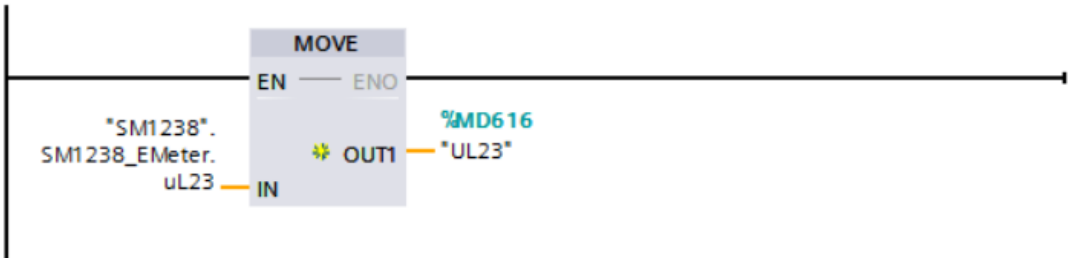

Network 27: .....

Comment

Network 28: .....

Comment

Network 29: .....

Comment

Network 30: .....

Comment

SM1238_EM

	Name	Data type	Default value	Accessible f...	Writa...	Visible in ...
1	version	Bool	false	☑	☑	☑
2	reserved	Bool	false	☑	☑	☑
3	uL1N	Real	0.0	☑	☑	☑
4	uL2N	Real	0.0	☑	☑	☑
5	uL3N	Real	0.0	☑	☑	☑
6	uL12	Real	0.0	☑	☑	☑
7	uL23	Real	0.0	☑	☑	☑
8	uL31	Real	0.0	☑	☑	☑
9	iL1	Real	0.0	☑	☑	☑
10	iL2	Real	0.0	☑	☑	☑
11	iL3	Real	0.0	☑	☑	☑
12	pfL1	Real	0.0	☑	☑	☑
13	pfL2	Real	0.0	☑	☑	☑
14	pfL3	Real	0.0	☑	☑	☑
15	pftotal	Real	0.0	☑	☑	☑
16	frequency	Real	0.0	☑	☑	☑
17	amplitudeUnbalanceForVolta..	Real	0.0	☑	☑	☑
18	amplitudeUnbalanceForCurre..	Real	0.0	☑	☑	☑
19	sL1	Real	0.0	☑	☑	☑
20	sL2	Real	0.0	☑	☑	☑
21	sL3	Real	0.0	☑	☑	☑
22	sTotal	Real	0.0	☑	☑	☑
23	qL1	Real	0.0	☑	☑	☑

SM1238

	Name	Data type	Start value	Retain	Accessible f...	Writa...	Visible in
1	Static			☐	☐	☐	☐
2	SM1238_EMeter	"SM1238_EM"		☐	☑	☑	☑
3	version	Bool	false	☐	☑	☑	☑
4	reserved	Bool	false	☐	☑	☑	☑
5	uL1N	Real	0.0	☐	☑	☑	☑
6	uL2N	Real	0.0	☐	☑	☑	☑
7	uL3N	Real	0.0	☐	☑	☑	☑
8	uL12	Real	0.0	☐	☑	☑	☑
9	uL23	Real	0.0	☐	☑	☑	☑
10	uL31	Real	0.0	☐	☑	☑	☑
11	iL1	Real	0.0	☐	☑	☑	☑
12	iL2	Real	0.0	☐	☑	☑	☑
13	iL3	Real	0.0	☐	☑	☑	☑
14	pfL1	Real	0.0	☐	☑	☑	☑
15	pfL2	Real	0.0	☐	☑	☑	☑
16	pfL3	Real	0.0	☐	☑	☑	☑
17	pftotal	Real	0.0	☐	☑	☑	☑
18	frequency	Real	0.0	☐	☑	☑	☑
19	amplitudeUnbalan...	Real	0.0	☐	☑	☑	☑
20	amplitudeUnbalan...	Real	0.0	☐	☑	☑	☑
21	sL1	Real	0.0	☐	☑	☑	☑
22	sL2	Real	0.0	☐	☑	☑	☑
23	sL3	Real	0.0	☐	☑	☑	☑

Network 1: .....

Comment

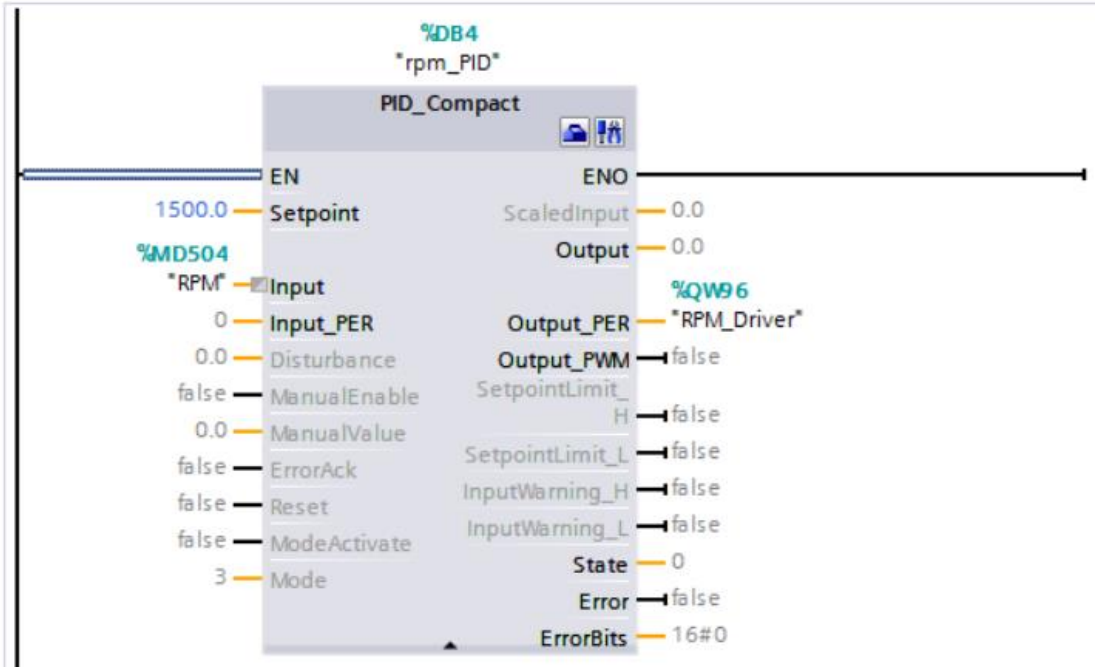

Network 4: .....

Comment

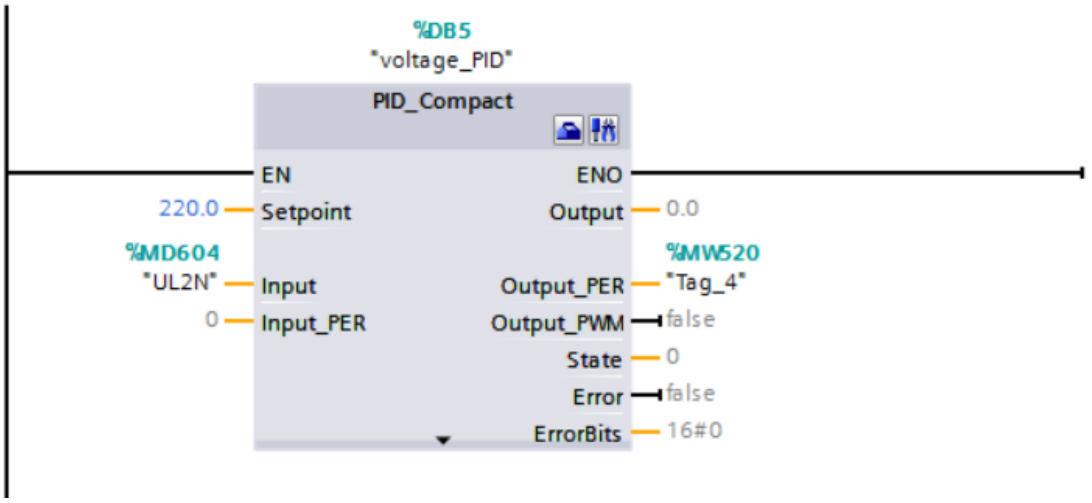

RESUME

Masoud Mohamed Masoud ELHAWAT completed his primary and secondary education in Khoms city in Libya. He pursued his undergraduate degree in High Institute for Comprehensive Professions-Khoms Department of Electrical and Electronics in 2009. As of 2018, he is pursuing his master degree at Karabük university.